The Development and Use of a Novel Finite Element For the Evaluation of Embedded Fluid Dampers Within Light- Frame Timber Structures with Seismic Loading

By

Ying Du

A dissertation submitted in partial fulfillment of
the requirement for the degree of

DOCTOR OF PHILOSOPHY IN CIVIL ENGINEERING

WASHINGTON STATE UNIVERSITY
Department of Civil & Environmental Engineering

December 2003

To the Faculty of Washington State University:

The members of the Committee appointed to examine the dissertation of Ying Du find it satisfactory and recommend that it be accepted.

_____

Chair

_____

_____

_____

ACKNOWLEDGEMENT

The completion of this dissertation was made possible with the support and guidance of many individuals. Thanks to my advisors, William F. Cofer, who provided close supervision and encouragement through out what seemed to be a never-ending process. Thanks also to Dr. David Pollock, Dr. Cole McDaniel, and Dr. Robert Dillon for serving on my committee. I would like to thank Dr. Michael Symans for working closely with me on the CUREE project.

Finally, this dissertation dedicates to my husband Mark for constant support through out all these years and to my parents, my sisters, and my brother. Without the close relationship to them, this dissertation will not exist.

The Development and Use of a Novel Finite Element For the Evaluation of Embedded Fluid Dampers Within Light- Framed Timber Structures with Seismic Loading

ABSTRACT

By Ying Du, Ph.D.
Washington State University
December 2003

Chair: William F. Cofer

There are two main objectives in this research. One is to develop modeling techniques by which the dynamic, nonlinear response of wood structures may be assessed. The method considers dissipated energy, collapse, and demand on structural components, and it is based on the principles of mechanics. The proposed method is simple compared to models that consider all components in detail in terms of number of elements and nodes, computer storage, and computing time. In addition, the method does not require calibrations with full-size tests as long as the properties of sheathing-to-frame connectors are known. The other objective is to use these modeling techniques to evaluate the effectiveness of viscous fluid dampers for improving the seismic performance of wood structures.

A new five-node finite element for modeling timber shear wall behavior was developed. A shear wall model using this element successfully predicted the load capacity and drift ratio observed in a set of experiments and those resulting from a detailed, calibrated shear wall model and a simplified braced-wall model developed for comparison purposes. The analytical modeling of the wall was developed within the commercially available finite element software, ABAQUS.

An analytical study was performed to evaluate the effect of the addition of viscous fluid dampers on the performance of shear walls and complete two-story buildings using actual ground motions, scaled to represent both code anticipated ground motion levels and more frequent events. A detailed nonlinear shear wall model and a two-story building model with symmetric and asymmetric configurations were used for cases with and without fluid dampers to evaluate their effect on performance. The study shows significant effectiveness of fluid dampers in dissipating energy, reducing drift, and increasing strength both to shear walls and buildings when subjected to earthquakes.

TABLE OF CONTENTS

LIST OF TABLES

LIST OF FIGURES

1. INTRODUCTION

1.1 Problem Statement

In the past, considerable attention has been focused on static analysis of light-frame structures. The reason for the lack of dynamic studies is partially due to the high cost of building and testing full-scale structures. In addition, wood frame structures are generally considered to perform exceedingly well in terms of life safety and damage due to their high strength-to-weight ratio and redundancy of nonload-bearing elements when proper procedures are followed by designers, builders. However, the 1994 Northridge, California earthquake confirmed several weaknesses in the current construction practice for the seismic design of residential wood frame buildings, especially for the connections between structural elements (Filitrault, 1994). The 1995 Hyogo-ken Nanbu, Japan earthquake resulted in 150,000 housing units of timber structures fully or partially destroyed (Filitrault, 1996). These serious consequences call for improvements in the theoretical understanding of the seismic response of light-frame building that will benefit not only the design and construction communities, but also homeowners.

Multi-story wood-frame building systems consist of multiple components, such as walls, floors, foundation, and roof joined by intercomponent connections such as nails or metal plates. The contribution to the performance of wood buildings from each component varies significantly. It is necessary to incorporate all components into a model of a building system to fully understand the entire behavior of the structure. There are two common problems in the numerical analysis of wood structural systems, however. One is the limitation of computer storage; the other is the significant amount of computer time required for dynamic analysis. Thus, simplified equivalent models become necessary for modeling structures consisting of

many substructures. The effort of this research was focused on the development of numerical modeling techniques for shear walls, equivalent shear walls, and multi-story building systems for wood structures when subjected to static and dynamic loading. The improved simplified shear wall model consists of fewer nodes and elements, and does not require calibration against shear wall experimental results as long as nail connection properties are known.

In general, the life-safety performance of light-frame structures during earthquakes is considered satisfactory. However, as the design community shifts the design philosophy from life safety to one of performance level, different standards are used for life safety criteria than those for economic loss. Supplemental damping is one way that has been proposed to achieve both higher strength and reduced damage compared to unprotected structures. Because of their potential value in increasing safety and decreasing damage in wood structures, the effectiveness of viscous fluid dampers was investigated using the new techniques developed for seismic modeling. The numerical analyses were performed to evaluate seismic response with and without dampers in both shear walls and building systems. The effectiveness of dampers in reducing seismic demand was evaluated by comparing peak drift ratios and energy time histories for cases with and without dampers. The dissipation of a significant amount of seismic input energy by dampers resulted in a dramatic reduction in inelastic strain energy demand on the building systems considered.

1.2 Objectives

There are two main objectives. One is to develop modeling techniques by which the dynamic, nonlinear response of wood structures may be assessed. The method should consider dissipated energy, collapse, and demand on structural components, and it should be based on the

principles of mechanics. The proposed method is simple compared to models that consider all components in detail in terms of number of elements, nodes, computer storage, and computing time. In addition, the method does not require calibrations with full-size tests as long as the properties of sheathing-to-frame connectors are known. The other objective is to use these modeling techniques to evaluate the effectiveness of viscous fluid dampers for improving the seismic performance of wood structures.

1.3 Scope

The scope of the research involves two tasks. First, a detailed study of the dynamic behavior of wood shear walls and the effectiveness of using fluid dampers to dissipate seismic energy and reduce damage was performed. Then, special nonlinear finite elements were developed that can be used to model wood shear walls with a very coarse mesh. The ability of these elements to effectively represent the important mechanisms of nonlinear cyclic behavior was verified by comparing with shear wall tests.

1.4 Dissertation Organization

A thorough state-of-the-art literature review on sheathing-to-frame connections, shear walls, and building systems from experimental and analytical points of view is presented in Chapter Two.

In Chapter Three, the detailed formulation of sheathing-to-frame connections and their verification with experimental data is described.

The detailed formulation of a nonlinear finite element model of an 8 ft x 8 ft shear wall and the verification of the model with experimental data is given in Chapter Four.

The derivation of a simplified equivalent shear wall element and its calibration with respect to experimental data and the detailed shear wall model of Chapter Four is presented in Chapter Five. A full-scale house model formed of these elements was then used to evaluate the effectiveness of fluid dampers in wood structures in Chapter Six. A five-node simplified shear wall model was developed and presented in Chapter Seven. Conclusions were drawn in Chapter Eight.

2. Literature Review

2.1 Introduction

Wood-framed building systems consist of multiple interacting components, such as walls, floors, foundation, and roof joined by intercomponent connections such as nails, bolts, steel straps, and metal plates. Figure 2-1 shows a typical light-frame building. Normally, such structures incorporate a set of shear walls that resist the lateral loads from earthquakes and wind. The highly indeterminate nature of the three-dimensional system and the sensitivity of the material properties and connections to the load rate and duration make the theoretical structural analysis complicated. In addition, the influence on the integrity of the system from each component varies significantly. Thus, current structural evaluation and design for seismic loading is performed with little more than a qualitative understanding of the system behavior.

It is well recognized that wood joints are the major cause of the hysteretic behavior in shear walls, and thus, the overall performance of the structure. This section presents a state-of-the-art literature review with emphases on wood joints, shear walls, and wood structures. The review shows that to efficiently model building systems, the use of calibrated simplified equivalent component elements is desirable.

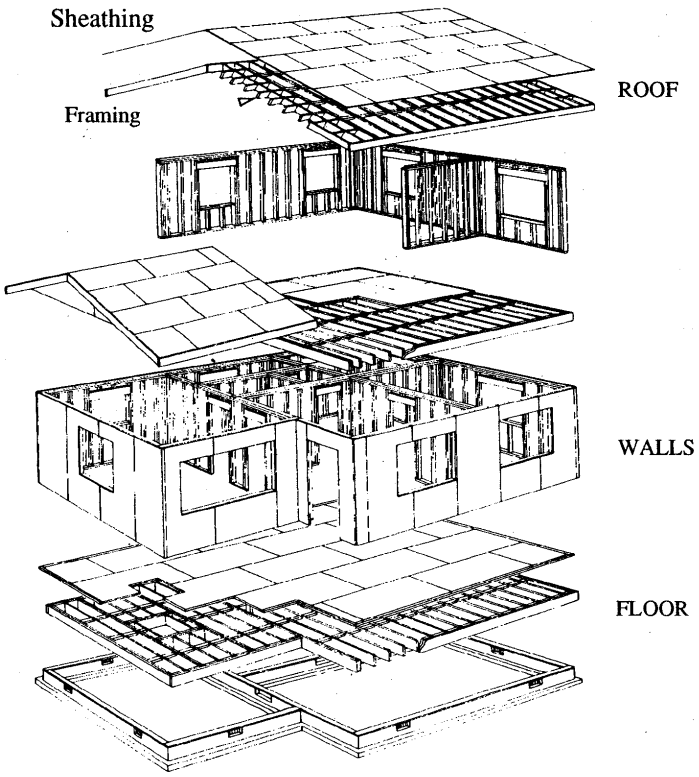

Figure 2-1 - Components of a light-frame building

(From Tarabia, 1994)

2.2 Behavior of Nailed Wood Joints

2.2.1 Introduction

Nailed wood joints are the most common connections in a wood-framed structure. It is well recognized that the connections in a building system dominate the integrity of the structure. A true hysteretic constitutive model of connections is essential in obtaining the accurate dynamic response of the building system. It is observed that the hysteretic behavior of a shear wall is

dominated by the in-plane behavior of sheathing connections; the out-of-plane behavior of connections and the bending stiffness of the wall covering are relatively insignificant when shear walls are subjected to lateral loading. Therefore, a 2-D sheathing to frame connection model is sufficient for modeling shear walls while still enabling the analysis to capture the dominant characteristic behavior of shear walls under lateral loading, which is consistent with their design.

2.2.2 Experimental Observations of Shear Stiffness of Nailed Wood Joints

Much experimental data are available on wood joints (e.g., Easley et al (1982), Dolan (1989), Cruz et al (1991), Ceccotti (1995), Chui and Ni (1997)). Figure 2-2 shows a typical hysteretic loop of a nailed connection (Dolan (1989)). Foliente (1995) summarized the characteristic features of typical hysteretic behavior of nailed wood joints as follows: (1) it is a nonlinear, inelastic load-displacement relationship without a distinct yield point; (2) there is progressive loss of lateral stiffness in each loading cycle (stiffness degradation); (3) there is degradation in strength when cyclically loaded in the same displacement level (strength degradation); and (4) it is composed of hysteresis loops with a pinching zone.

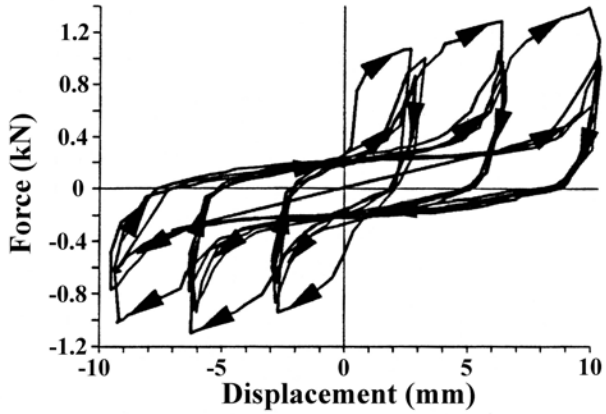

Figure 2-2 - Experimental Test Data (From Dolan, 1989).

2.2.3 Analytical Simulations of Shear Stiffness of Nailed Wood Joints

Easley et al (1982), Dolan (1989), Kasal and Leichti (1994), and He et al (2001) have all developed analytical nonlinear wood joint models based on monotonic verification. In addition, Kasal and Leichti (1992), Foliente (1995), Tarabia et al (1997), and Chui et al (1998) have presented nonlinear hysteretic constitutive models. Few publications deal with connectors evaluated under both static and dynamic loading, however (Dolan (1989), Tarabia and Itani (1997)).

Easley et al (1982) derived load-slip curves for single fasteners, as shown in Figure 2-3, which are defined as follows:

$$F_S = C_1(1 - e^{-C_2 \Delta_S}) \qquad \text{when } (Fs < Fso) \qquad (2\text{-}2)$$

$$F_S = C_3 \Delta_S + C_4 \qquad \text{when } (Fs > Fso) \qquad (2\text{-}3)$$

Coefficients C_1, C_2, C_3, C_4 and Fso were considered as parameters adjustable to fit different test data for a specific case. Δ_S is the total localized deformation at each side fastener.

Equation (2-2) was used to represent the nonlinear part of the model, below the point designated as *Fso*. Equation (2-3) represents the linear part of the model beyond the *Fso* point.

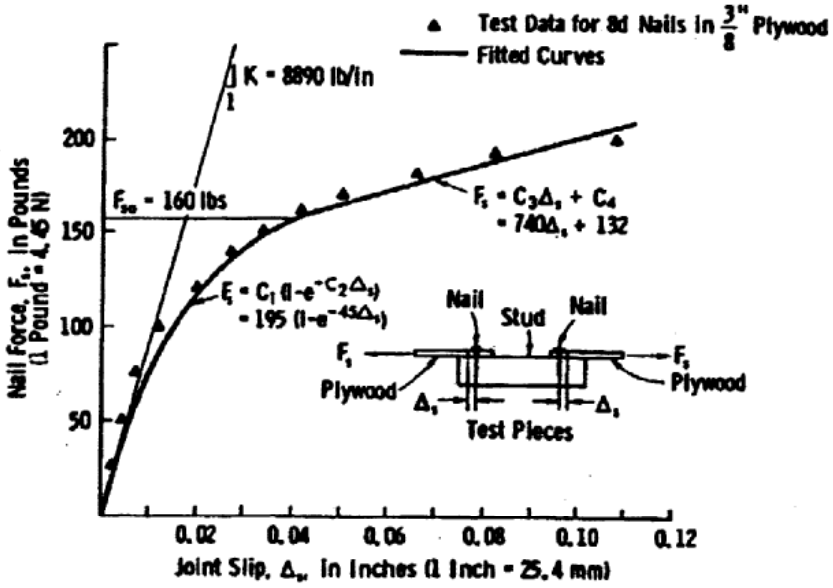

Figure 2-3– Load – Slip Curve for Nail Joint

(From Easley et al,1982)

To verify that the mathematical formulas reasonably predict forces in fasteners, Finite Element models of wood fasteners using special linkage elements were developed. These elements had two nodes and allowed springs extending parallel and perpendicular to the axes of the frame members. These elements were of zero length since they connected coincident nodes on the panel and frame where the fasteners were located. A proper constant stiffness *K* was assumed for spring elements in linear static analysis and 20 straight-line segments along the envelope curves were used in defining the static nonlinear load-slip relationship.

Dolan (1989) presented a detailed sheathing-to-framing connector model taking the out-of-plane motion into account and predicting the ultimate strength under reversed loading. Figure 2-4 shows four exponential segments with four boundary conditions that were idealized to represent the empirical hysteretic model. Three independent non-linear springs provided an accurate representation of sheathing-to-framing connectors. Equation (2-4) represents the backbone curves of the connectors. The area enclosed by hysteretic loops is a direct measure of energy dissipation capability, while the displacement at failure is a direct measure of ductility in the load-slip relationship (Ni, 1993).

$$P = \left(P_o + K_2 u\right)\left[1 - \exp\left(\frac{-K_o u}{P_o}\right)\right] \qquad (2\text{-}4)$$

where the parameters defining the hysteretic behavior are given by (see Figure 2-5):

P_o = force intercept corresponding to slope of the backbone curve at ultimate displacement

P_1 = force intercept within the pinching region

u_{ult} = ultimate displacement corresponding to ultimate force (i.e., displacement at which stiffness degradation initiates)

K_o = initial elastic stiffness of the connection (i.e., initial slope of the backbone curve)

K_2 = stiffness of the connection at ultimate displacement (i.e., slope of backbone curve at ultimate displacement)

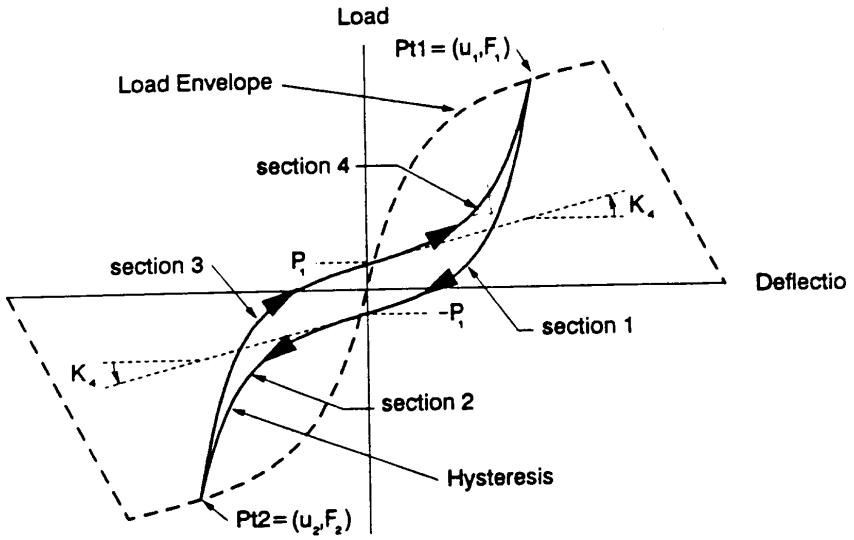

Figure 2-4 – Idealized Hysteretic Loop for Sheathing Connection Element

(From Dolan, 1989)

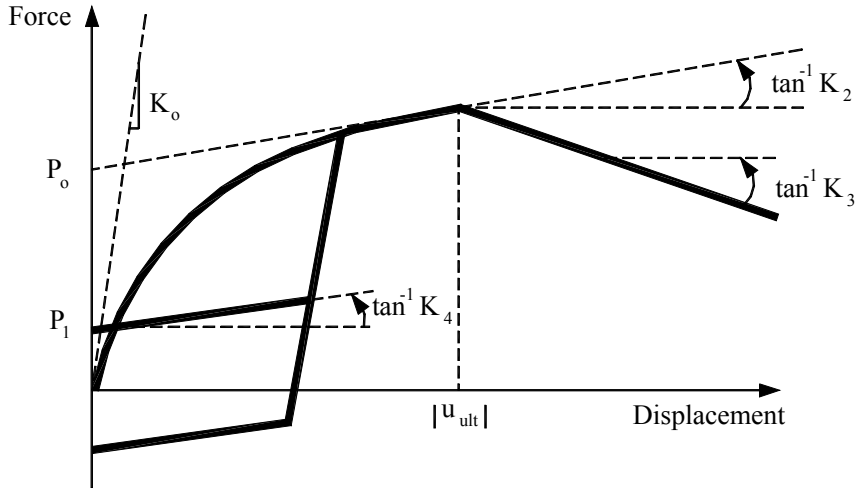

Figure 2-5- Illustration of sheathing connection parameters defining the monotonic and cyclic load-displacement behavior.

Kasal and Leichti (1992) also used spring elements in three directions to represent the fasteners. One spring was used for withdrawal and one was used for shear resistance in each coordinate direction within the plane of the wall. In addition, they pointed out that tensile and compressive spring stiffness could be different, which enabled the proper withdrawal and compressive deformation. Spring behavior was non-conservative, with unloading always following the first defined slope.

Chui et al (1998) modeled nailed wood joints and tested them under cyclic loading. This model included the cyclic response of the fastener material, shear deformation in the fastener, friction between the fastener and the wood, and the withdrawal effect of the fastener. It was a large-displacement finite element model. It predicted the response of a single-shear nailed joint to an arbitrary reversed cyclic loading. The model consisted of several components, in which the nail was represented by a beam element, the load-embedment characteristics of the wood surrounding the nail were represented by two-node spring elements, and the friction between nail and wood was represented by linkage elements. In this model, the total Lagrangian formulation was used. Also, strain hardening was considered. The numerical results were in favorable agreement with experimental results.

The load-withdrawal displacement relationship has been neglected in most nail applications. However, it is essential for the finite element modeling of the out-of-plane action of nailed wood joints (Groom and Leichti, 1992).

2.2.5 Summary

The ductility of timber structures is heavily influenced by connections containing mechanical fasteners, such as nails and bolts. The primary energy is dissipated through fastener deformation. The wood material, itself, has only a limited ability to dissipate energy compared to fasteners (Ni, 1993).

The hysteretic behavior of connections consists of several primary characteristics, namely, nonlinear inelastic behavior, stiffness degradation, strength degradation and pinching. Analytical models need to incorporate the hysteretic behavior accurately in order to obtain the proper response of the structural systems under dynamic or cyclic loading, such as those from earthquakes or hurricanes. There are hundreds of combinations of materials and fasteners in wood systems. The variations in material properties, sheathing types, nail strength, and structural layouts will all impact the parameters used to define the hysteretic model.

2.3 Wood Frame Shear Walls

2.3.1 Introduction

A typical shear wall consists of a wood frame that is composed of a number of studs, a header, sill, and sheathing of 4 ft x 8 ft panels of plywood or other materials (Easley et al, 1982). The header and sill connect the studs to form a frame and the sheathing panel is attached to the frame members by nails or other types of discrete fasteners. Figure 2-6 illustrates typical two-panel shear wall construction details.

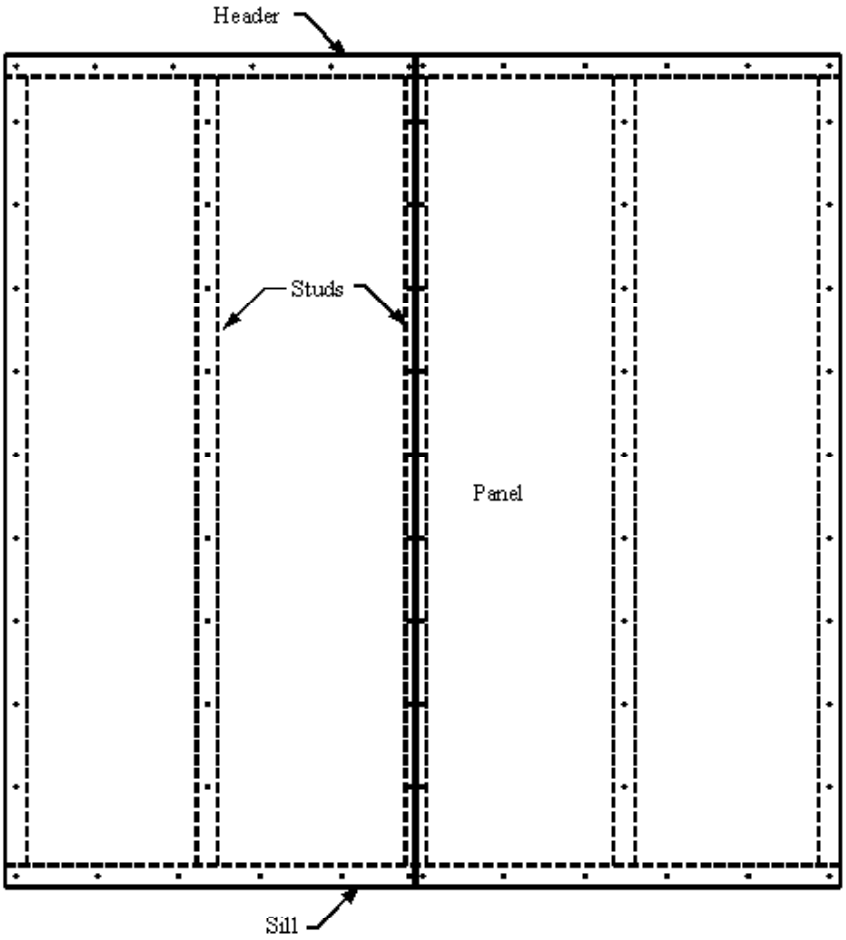

Figure 2-6– Typical Shear Wall Construction Details

A shear wall is designed mainly to resist in-plane loads caused by wind or earthquakes. Literature shows that, in the past, considerable attention has been focused on methods and procedures for predicting shear wall strength and stiffness under racking loads and reversed cyclic loads in the form of both experiments and numerical analysis. In-plane racking loads tend to cause the shear wall frame to undergo distortion into a parallelogram shape while sheathing panels remain rectangular. In-plane reversed cyclic loads create a hysteretic response caused by

discrete sheathing-to-frame connections, such as nails or fasteners along framing members of shear walls.

2.3.2 Racking Response of Wood Frame Shear Walls

Closed-form equations were proposed by Tuomi and McCutcheon (1978) for predicting the racking behavior of timber shear walls based on a linear nail load-slip relationship. McCutcheon (1985) revised this method by taking into account the nonlinear behavior of the nails.

Easley et al (1982) derived simple closed-form formulas for predicting fastener forces in a loaded shear wall based on force equilibrium and moment equilibrium. These formulas can predict the maximum fastener forces and their location within a wall. The side fastener force, *Fs*, was defined as:

$$F_S = \frac{Nb}{\beta} \tag{2-5}$$

where:

$$\beta = n_s + \frac{4I_e + 2n_{si}I_s}{\omega^2} \tag{2-6}$$

$$I_e = \sum_1^{n_e} x_{ei}^2 \text{ and } I_s = \sum_1^{m} x_{si}^2 \tag{2-7}$$

Here, n_s is the number of the side fasteners; n_e is the number of end fasteners; n_{si} is the number of fasteners in each interior stud; m is the number of interior studs; and N is shear force per unit length of shear wall. Dimensions W and b are shown in Figure 2-7.

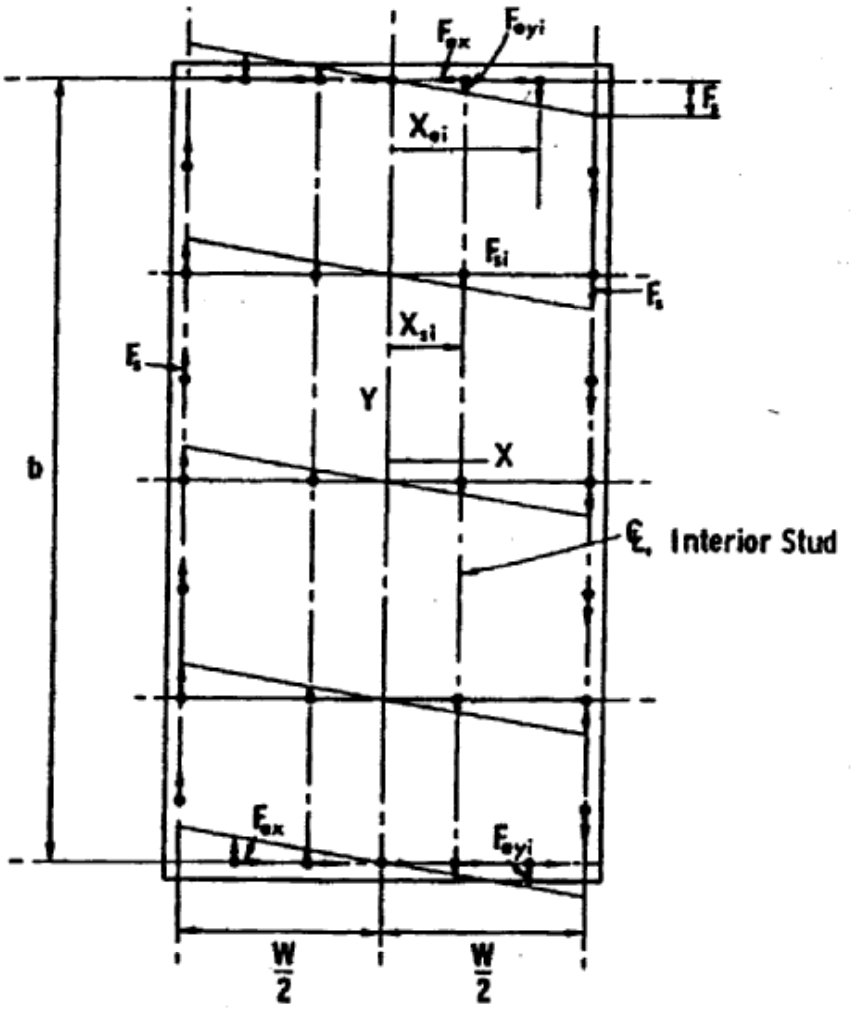

Figure 2-7– Typical Shear Wall Construction Details

(From Easley et al, 1982)

The resultant of the end fastener forces, F_{ei} is the vector sum of F_{ex} and F_{eyi}, the two components in the x- and y- directions along the framing members:

$$F_{ei} = \sqrt{F_{ex}^2 + F_{eyi}^2} = N\left[\left(\frac{\omega}{n_e}\right)^2 + \left(2x_{ei}\frac{b}{\omega\beta}\right)^2\right]^{\frac{1}{2}} \qquad (2\text{-}8)$$

Based on the above equation, the maximum fastener forces are applied to the two fasteners on each end at the greatest distance from the panel centerline. Then, the interior fastener forces were found to be:

$$F_{si} = 2 x_{si} b \frac{N}{\omega \beta} \tag{2-9}$$

Equations (2-5), (2-8), and (2-9) give fastener force values when located at the side, end, and interior of sheathing panels. They predicted that the maximum values occurred in end fasteners of either side for a given loading case. Results from a finite element model, experimental tests, and the numerical formulas were in close agreement.

With the intention of deriving simple and rational equations rather than closed-form formulas for predicting racking strength, Gupta and Kuo (1985) presented a relatively simple method that included 4 dof's in a single wall and the assumption that studs deform in a sine-wave shape. The method is also applicable to multi-panel walls with the flexibility of reducing degrees of freedom by adding horizontal constraints to vertical studs. Close agreement between test data and finite element results was achieved.

A power curve, similar to that of the sheathing connector was used to predict racking strength by Dolan (1989). The parameters used to define the monotonic response were calibrated against the experimental results.

2.3.3 Reversed Cyclic Response of Wood Shear Walls

Dolan (1989) originally developed the finite element program WALSEIZ with the ability to simulate shear wall behavior using plate, framing, and connector elements, but the program lacked the capability to calculate forces or stress. White and Dolan (1995) modified WALSEIZ for monotonic and dynamic nonlinear analysis. Four elements were included: a two-dimensional, linear-elastic six-degree-of-freedom beam element to model framing of walls; an eight-degree-of-freedom, orthotropic, linear-elastic, rectangular, plane stress element with two degrees of freedom at each of the four corner nodes; a sheathing-to-frame connector element based on power curves proposed by Dolan (1989); and a sheathing-bearing element formulated as a bilinear spring element with high modulus of elasticity in compression and low modulus of elasticity in tension, similar to a gap element. The results obtained from WALSEIZ compared favorably with the experiment results.

Dolan and Madsen (1992) described static and slowly cyclic racking tests of full-size shear walls sheathed with plywood and waferboard, respectively. They concluded that the response of shear walls under cyclic loading is dominated by the hystereric behavior of sheathing-to-frame connections. The hysteresis of the shear wall was shown to be contained in the envelope defined by the monotonic racking load-displacement curve. However, there are two problems with this type of detailed numerical analysis. One is the large requirement for computer storage and the other is the large requirement for computer time. Kasal and Leichi (1992) successfully demonstrated that these two issues could be resolved. They transformed detailed three-dimensional wall models into simple equivalent two-dimensional models by applying energy concepts. The application of the simple model in a full-structure nonlinear

analysis captures the global behavior of the structure such as deflections and reactions in reasonable computing time and with reasonable computer storage. But, their models require some kind of calibration process to validate the models. Experimental data had to be available for the calibration process.

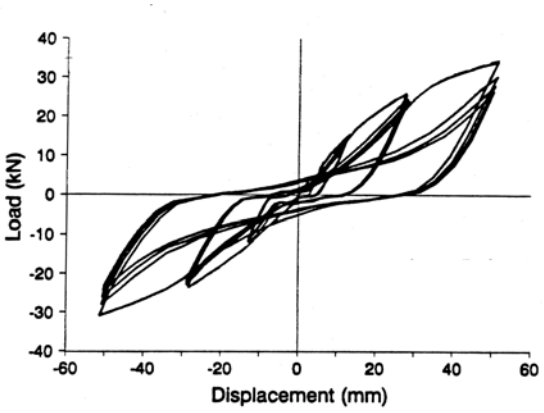

Figure 2-8 - Experimental Hysteresis Loop

(From Dolan, 1989).

Kasal and Leichi (1992) proposed an equivalent shear wall model based on the properties of a detailed model. For the detailed wall model, studs and sheathing were modeled as two-dimensional shell elements with linear orthotropic properties. The joints were modeled using one-dimensional springs clustered at common nodes for sheathing and studs. One spring was defined for withdrawal and one was defined for shear resistance. The spring behavior was nonconservative and unloading was set to follow the initial slope. Spring constants representing

the non-linear load-displacement relationship of nail connections were obtained from experiments conducted by Polensek (1975), Phillips (1990), and Groom (1992). The equivalent shear wall model was designed to respond in the same way as the detailed model, but with fewer degrees of freedom to minimize the number of equations to be assembled and solved. Shear stiffness was modeled by a nonlinear and non-conservative diagonal spring and a three-dimensional truss was created by beam elements pinned at corners. The stiffness of the non-linear spring represents the global shear stiffness of the wall, including openings. Beam elements make it possible to specify additional nodes at the boundary and these nodes are used to connect the wall to the rest of the structure. Out-of-plane stiffness is the bending stiffness resisting wind pressure perpendicular to walls. It was modeled by superimposing a two-dimensional plate element with the membrane stiffness removed. The plate is orthotropic to account for the different stiffness in the height and width directions of the wall. Compression stiffness was modeled using truss elements in the stud direction. In-plane shear tests were conducted on both the detailed and the equivalent model. A 7000 lb (31.3 kN) in-plane shear force was applied on top of the wall in 10 steps of 700 lb (3.1kN) each. The equivalent wall model agreed well with both the experiment and the detailed model. With the equivalent model, both computer storage and execution time were reduced dramatically.

Dinehart and Shenton (2000) developed a discrete three-degree-of-freedom shear wall model for simplified analysis of full structures. A single-story wood frame structure was modeled and a response spectrum analysis was performed to demonstrate the usage of the wall model. A linear-viscoelastic element was used to simulate the sheathing-to-frame connections. It accounted for the effects of wall geometry, framing and sheathing materials, fastener type, and

spacing. Based on the test data, properties of connections can be calibrated. This linear model captured the overall behavior but failed to predict the pinching in the loop.

2.3.4 The Impact of Static and Dynamic Analysis on Seismic Design

For most timber structures, dynamic analysis is not required for seismic design. An equivalent procedure, called the static lateral force procedure, allows designers to transform dynamic loads to a set of equivalent static loads resisted by lateral load resisting systems such as shear walls (UBC, 1994). From a table of allowable loads, mostly based on the results of static tests, a shear wall can be specified. Dinehart and Shenton (1998) and Shenton and Dinehart (1998) pointed out the significant differences between the static and dynamic response of shear walls in ductility (the displacement at ultimate load divided by the displacement at yielding load) and load factors (the ultimate load divided by the design allowable) based on static and dynamic tests. These results showed a 34% reduction in ductility for plywood walls and a 42% reduction for OSB walls for the dynamic response with respect to static results. The test results also showed a change in the load factors over constant amplitude cycles. The largest decrease in load factor is between the first and the second cycle. There was nearly a 30% decrease in the load factor for both plywood and OSB walls between the static value and the fourth cycle value in dynamic tests. The differences between the static and dynamic response directly impact seismic design procedures. A clear understanding of static and dynamic response is crucial for design in the new spirit of high performance levels in seismic design.

2.4 Seismic Behavior of Wood-Framed Building Systems

Foliente (1995) pointed out that the 1994 Northridge earthquake revealed the inadequacies of current engineering analysis, detailing, and construction practices through severe

structural and non-structural damage in recently constructed light-frame buildings. The lack of investigation into earthquake behavior for light-frame buildings is due to the difficulties in taking into account the sensitivity of material properties, inelastic behavior of components of the building systems, and the complexity of wood construction. Kasal (1992) modeled a wood framed house for which only static analysis was performed. Tarabia and Itani (1997) explored the static and dynamic response of light-frame buildings using numerical modeling. They were able to achieve good agreement with some of the available test data, such as plywood sheathed and waferboard sheathed wall displacement time history and peak displacements from Dolan (1989) and peak displacements and peak wall reaction and displacement time history from Kamiya (1988). He et al (2001) expanded a 2D diaphragm analysis program for timber buildings subjected to static monotonic loading written by Foschi (1997) to a 3D structural analysis program called LightFrame3D. This program has the ability to perform static and cyclic analysis either by load control or displacement control. The program was improved from a previous version by including nail cyclic behavior. Their success in modeling wood framed buildings demonstrated the effectiveness of the numerical method. The insights obtained from these numerical studies were seen as valuable.

Kasal and Leichti (1994) modeled the three-dimensional experimental structure described by Phillips (1990). In modeling the full structure, the following assumptions were made: shear walls behave nonlinearly in shear but linearly in bending and torsion; the roof behaves linearly when loaded in bending (i.e., its diaphragm behavior is linear); the floor behaves linearly in bending and acts as an orthotropic plate; intercomponent connections behave nonlinearly; and self-weight of the horizontal structures is applied as a dead load. The bending properties of the

walls were computed using orthotropic plate theory. The axial stiffness of the wall was modeled by truss elements. Floors and the roof were considered to behave linearly and only the degrees of freedom on boundaries entered the solution. Intercomponent connections were modeled by nonlinear springs connecting substructure, superelements (roof and floors), and quasisuperelements (walls) on their boundaries. Model verification was done by applying one cycle of load corresponding to the last experimental cycle in the analysis. Deformations of walls and reaction forces at boundaries were compared with experimental results. One limitation of the model is that it could not accommodate the stiffness degradation of the structure that results from loose connections, which appears to be a significant characteristic of wood frame structures. Lack of the ability to perform dynamic analysis made the verification incomplete, but the static analysis did yield promising results.

2.5 Supplemental Damping in Timber Shear Walls

In general, the life-safety performance of light-framed structures during earthquakes is considered satisfactory. However, as the design community shifts the design philosophy to one of performance level, different standards are used for life safety criteria than those for economic loss. Supplemental damping is one way that has been proposed to achieve both higher strength and reduced damage compared to unprotected structures. Because their potential value in increasing safety and decreasing damage in wood structures, the effectiveness of viscous fluid dampers was investigated using the new techniques for seismic modeling. The applications of supplemental damping to timber structures have drawn a great deal of interest in both the manufacture and research communities.

Symans et al (2002a) provided a detailed literature review on advanced seismic protection for wood framed structures. Table 2-1 shows research conducted on supplemental damping methods by various authors within the last decade.

Table 2-1 - Supplemental Damping Systems (Adapted from Symans et al, 2002a)

Authors	Year	Topic	Type of Study
Filiatrault	1990	Friction dampers applied to shear wall	Analysis
Dinehart and Shenton Dinehart et al. Dinehart and Lewicki	1998 1999 2001	Viscoelastic dampers applied to shear wall	Experimental
Higgins	2001	Hysteretic dampers applied to shear wall	- Analysis - Experimental
Symans et al.	2002	Fluid viscous dampers applied to shear wall and wood building	Analysis

Filiatrault (1990) investigated the seismic response of friction-damped timber shear walls. The hysteresis loop of lateral force vs. displacement for conventional light-framed shear walls is shown in Figure 2-9. Stiffness degradation and pinching of the hysteresis loops of a shear wall are apparent. The concept of supplemental energy dissipation via additional elements, namely friction dampers, was proposed by Filiatrault (1990) and carried out by installing them at the four corners of a timber framed shear wall (see Figure 2-10). A numerical model of a friction-damped-shear-wall (2.4 m x 2.4 m) and friction dampers was created and the shear wall model was verified with experimental data obtained from shaking table tests by Dolan (1989). The model takes both stiffness degradation and pinching of the hysteresis loops into account. A comparison of the hysteretic behavior of the shear wall with and without the supplemental

friction dampers was made. The El Centro record (component NS) of the 1940 Imperial Valley Earthquake was used as the input in the numerical analysis. The friction dampers were to shown to improve the seismic performance by reducing the peak force and displacement at the top of the wall and result in the elimination of the pinching in the hysteresis loops as shown in Figure 2-11. The analysis shows the effectiveness of friction dampers in reducing strain energy over time and dissipating more than half of the seismic input energy at the end of the analysis as shown in Figure 2-12.

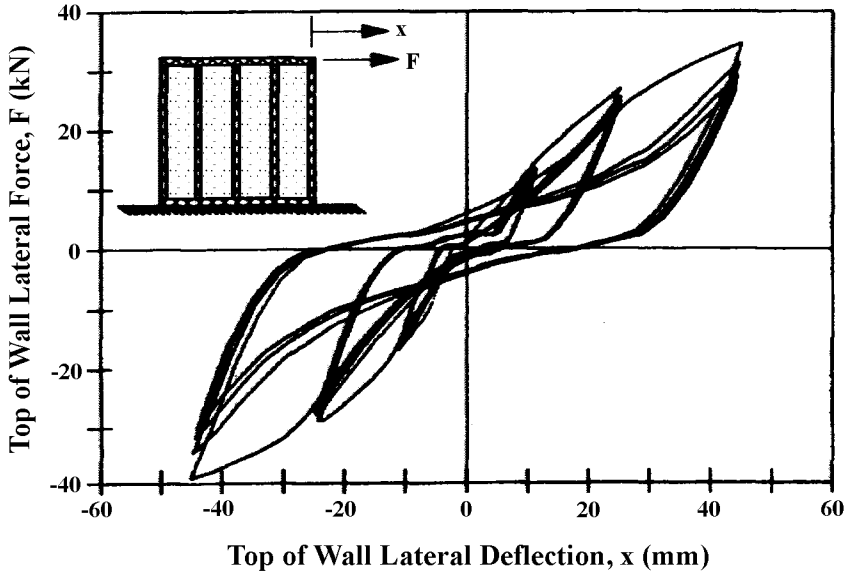

Figure 2-9 - Hysteretic behavior of conventional light-framed wood shear wall (From Filiatrault, 1990).

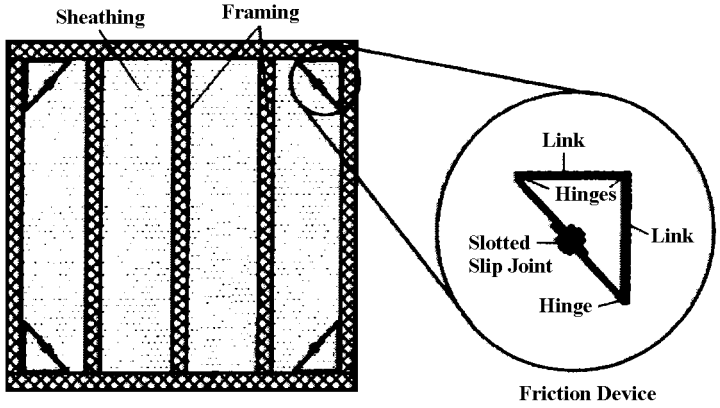

Figure 2-10 – Timber Shear Wall With Slotted Friction Dampers Installed at Four Corners (From Filiatrault 1990, © John Wiley & Sons Ltd. Reproduced with permission).

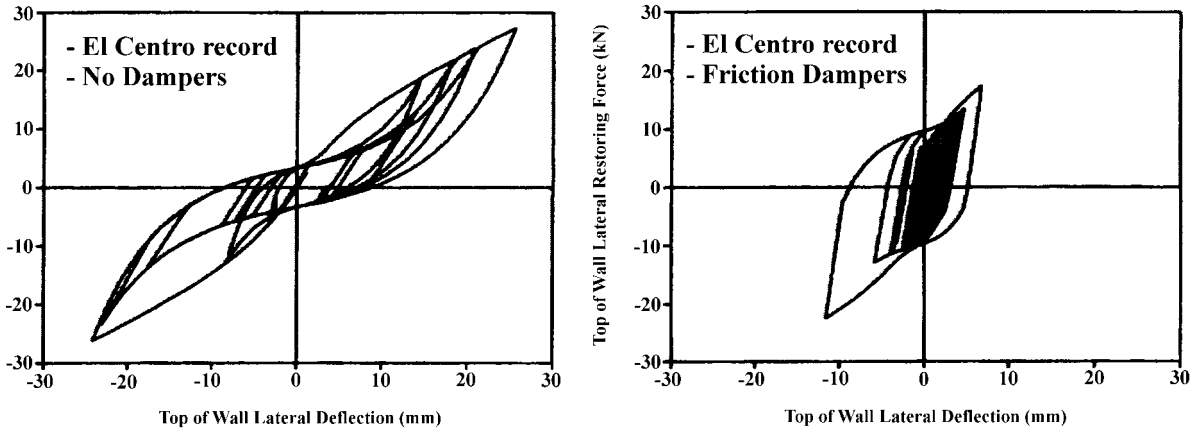

Figure 2-11 – Comparison of Hysteretic Loop of a Wood-Framed Shear Wall Without and With Friction Dampers When Subjected to El Centro Earthquake Record (From Filiatrault, 1990).

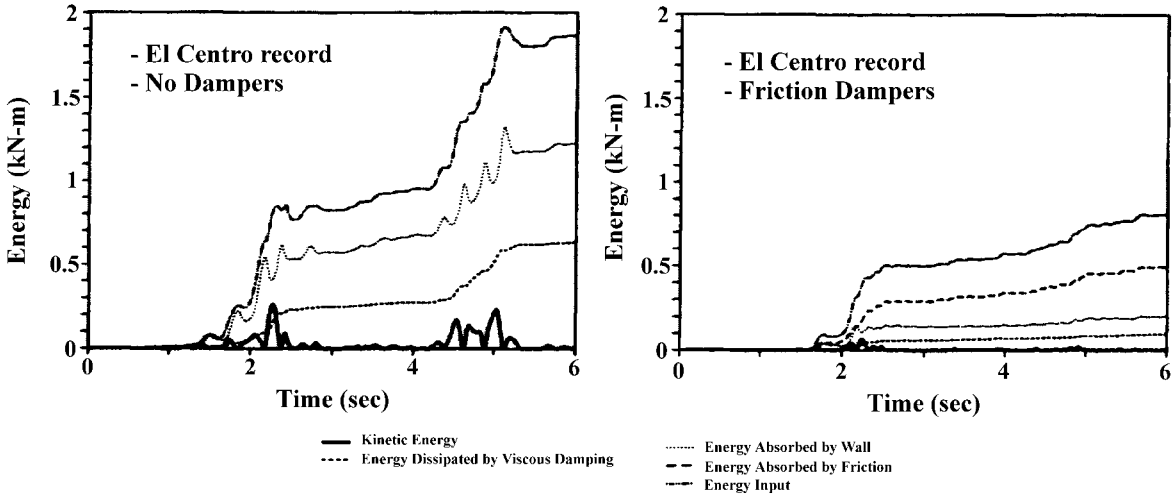

Figure 2-12- Comparison of Energy Distribution Over Time of a Wood-Framed Shear Wall Without and With Friction Dampers When Subjected to El Centro Record (From Filiatrault, 1990).

Viscoelastic dampers are another type of passive energy dissipation device. They have been applied to reinforced concrete structures and steel structures to reduce seismic demand. However, application of passive energy dissipation devices to light farmed structures has only recently been tried. Dinehart and Shenton (1998) and Dinehart et al (1999) experimentally investigated the dynamic behavior of conventional plywood shear walls with viscoelastic dampers. Figure 2-13 shows the conventional configuration of a shear wall. Comparisons were made between walls without and with dampers. Five damper configurations were selected as shown in Figure 2-14. Corner dampers installed at the top and bottom of the wall were tested, respectively. The result shows that dampers could dissipate up to 59% of the input energy.

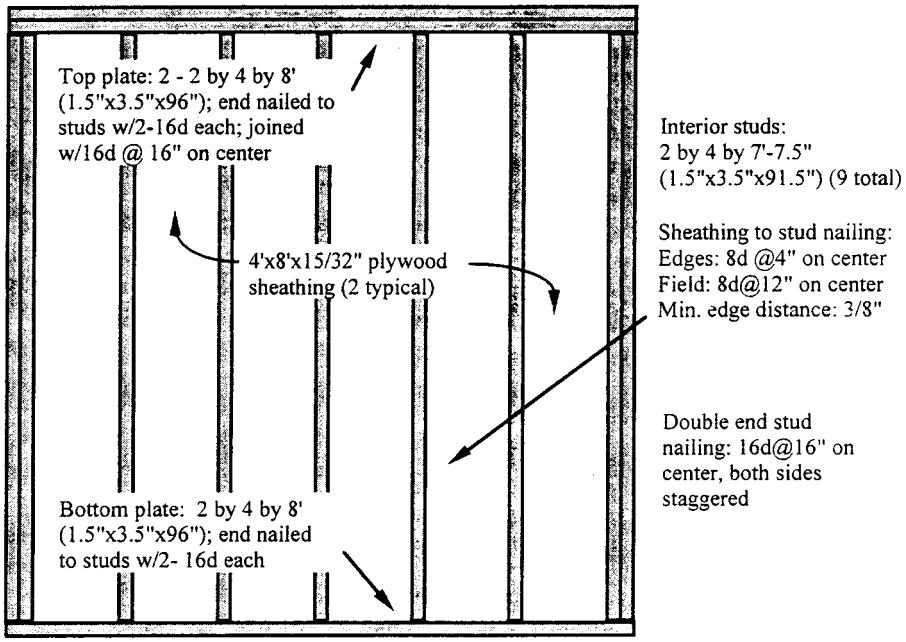

Figure 2-13– Plywood shear wall used for cyclic test with and without dampers.

(From Dinehart et al. 1999).

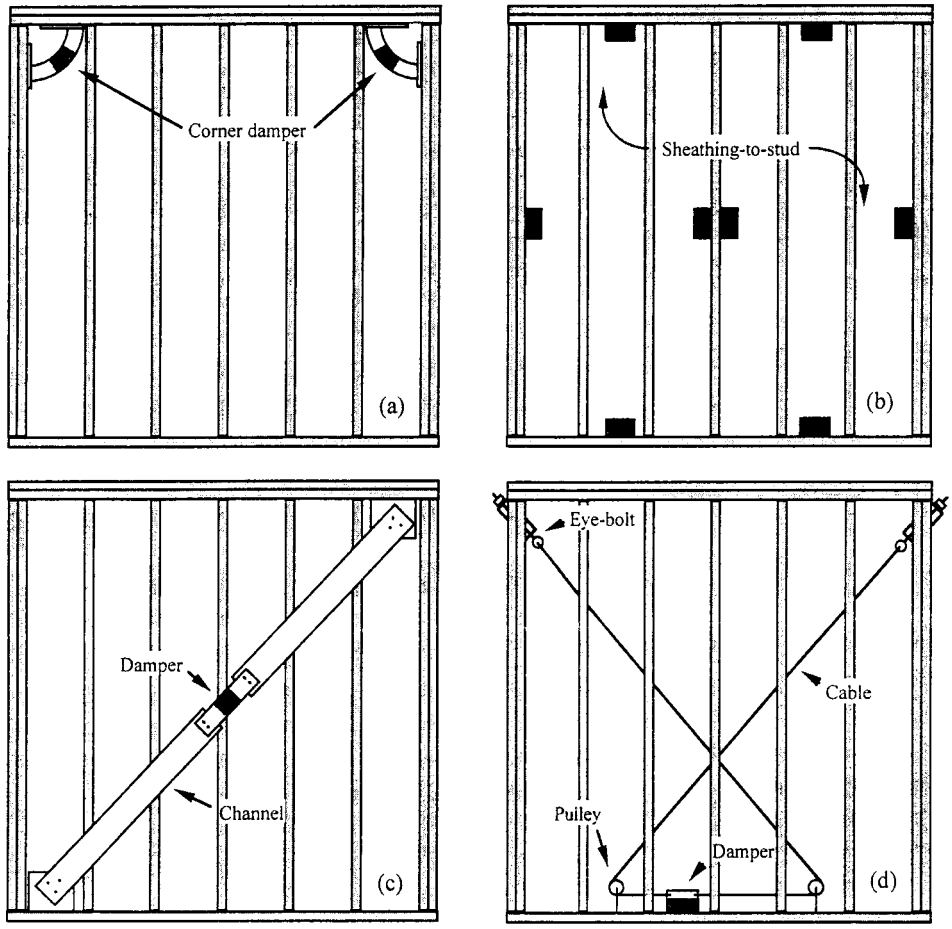

Figure 2-14 – Damper configurations used in cyclic tests: (a) corner dampers at top of the wall, (b) sheathing-to-stud dampers, (c) single diagonal brace with damper, (d) tendon damper (From Dinehart et al 1999).

2.6 Summary

The literature shows that techniques that can accurately model timber structures are vital to performance studies of components of buildings and entire structures. More research in

nonlinear modeling is necessary to develop methods that are accurate, yet economical. Literature also shows that supplemental damping, such as the use of visocous fluid dampers, can be applied to light-framed structures. It can provide additional protection to structures during earthquakes so that higher strength and less damage can be achieved compared to those that are unprotected.

3. Hysteretic Response of Wood Nailed Joints

3.1 Introduction

Shear walls are designed to resist horizontal loads, such as those from earthquakes or wind. It is commonly recognized that, for shear walls, the sheathing-to-frame connections dominate their hysteretic behavior in horizontal resistance. These connections also resist the relative displacement between sheathing and framing members. In this chapter, the derivation of two-dimensional wood nailed joint models based on the Finite Element Method and associated assumptions are presented. Two types of Connection Element Models within the commercial software ABAQUS were formulated and the calculations to produce the stiffness matrix, the response of the connection under monotonic and reversed horizontal cyclic loads, and various forms of energy were implemented. Comparisons were made with available experimental data. The accuracy of the evaluation of the connection is essential to the accuracy of the simulations of shear walls and three-dimensional buildings since the nail connections are the primary source of the nonlinearity in the systems without any external damping devices.

3.2 Introduction to ABAQUS (1998)

ABAQUS/STANDARD (1998) is a general purpose, finite element analysis system. STANDARD is the implicit version of ABAQUS, which has a special feature that allows users to define elements not included in the ABAQUS element library. The user-defined element is invoked in the same way as the native ABAQUS elements. A nonlinear user-defined element representing the two dimensional connection properties of a nail was implemented as a user subroutine called UEL. All material behavior was defined in subroutine UEL based on the material constants defined via UEL PROPERTY data and on solution-dependent state variables

associated with the element. The stiffness, the response, and the energy values corresponding to the loading directions and nail slip at any given time were calculated in the UEL subroutine. The nail element captures the load-path dependent behavior shown in the hysteretic loops in which a pinching zone is developed. ABAQUS was executed on a HP workstation with 10Gb of disk space available to this research. ABAQUS/POST (1998) and self-written FORTRAN programs were used to produce the output plots and extract data. ABAQUS input files were created and modified by hand and a FORTRAN program was developed for two-dimensional nail connector element UEL.

3.3 Sheathing-to-frame Connector Element

3.3.1 Assumptions and Test Protocol for Nailed Joint Simulation

A sheathing connection associated with each nail was modeled as two orthogonal uncoupled nonlinear springs; one is horizontal and the other is vertical. A schematic of the finite element model of the connection is shown in Figure 3-1 (d). This assumption applies to both Dolan's Power Curves Model and the Linear Model that was modified based on Dolan's Model. A schematic showing typical usage of nails in shear walls connecting sheathing to frame members is shown in Figure 3-1 (a). Illustrations of typical failure modes in nails from both monotonic loading and reversed cyclic loading are shown in Figure 3-1 (b) and (c).

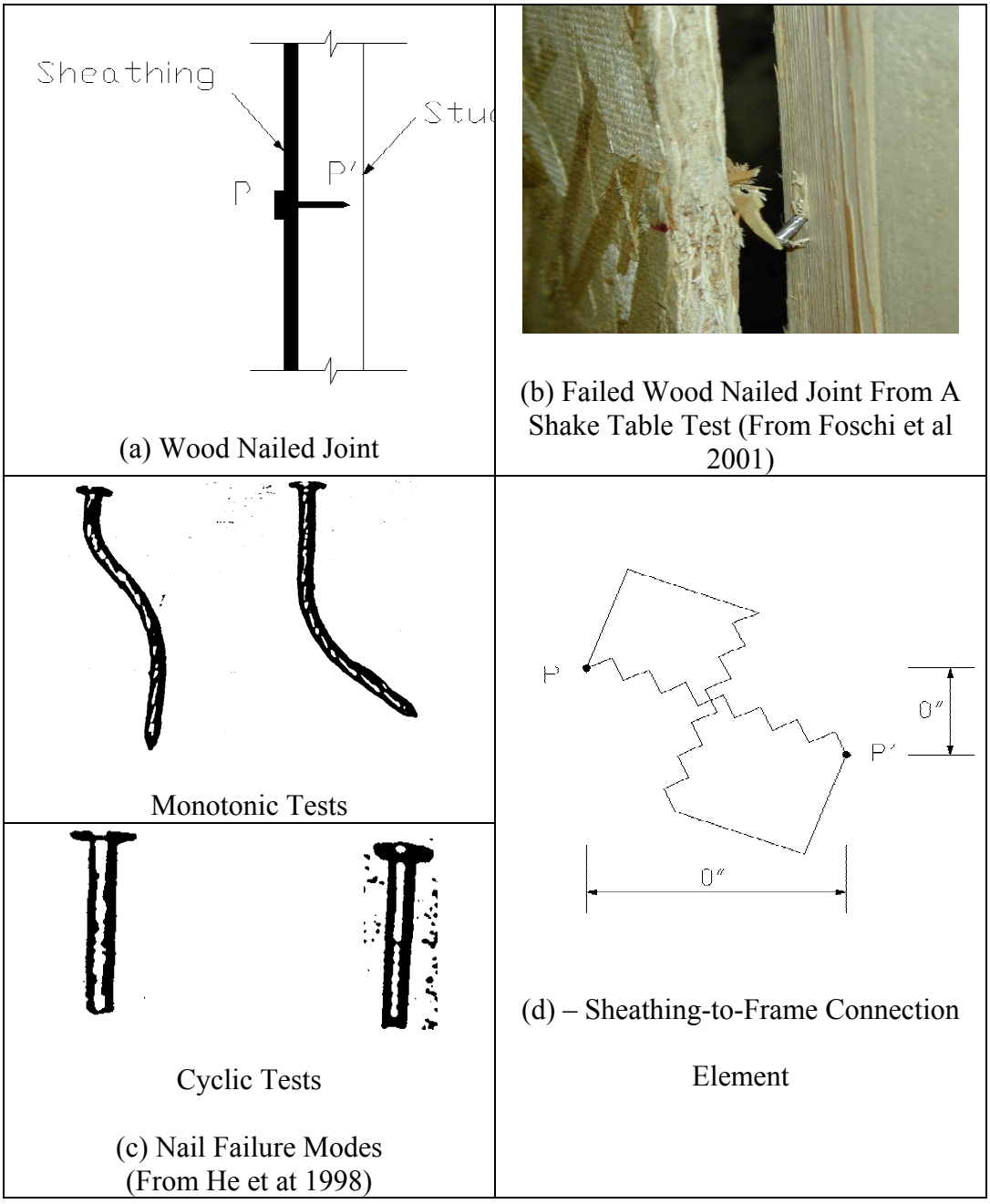

Figure 3-1– Wood Nailed Joint (a) Sheathing-to-Frame Connection; (b) Failed Wood Nailed Joint From A Shake Table Test (adapted from Foschi et al 2001); (c) Nail Failure Modes; (d) Finite Element Model of Connection.

The static cyclic test protocol used in wood joint nail simulations is as shown in Figure 3-2.

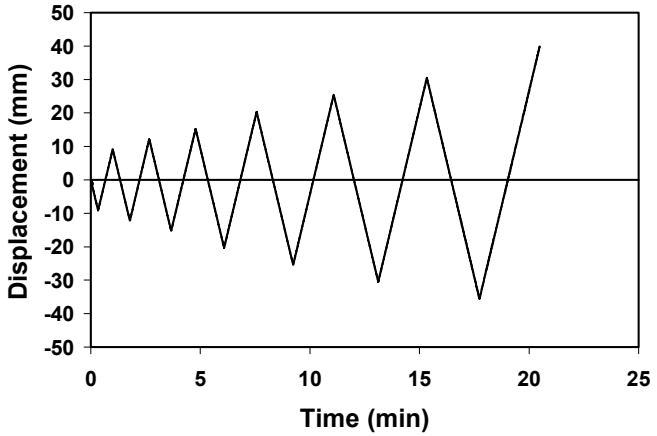

Figure 3-2- Static Cyclic Loading Protocol (Adapted from Dolan (1989))

3.3.2 Dolan (1989) Exponential Segments Model

A connection model (see Figure 3-3), which is defined using power curves, was developed. One of the characteristics of the connection model is the use of an exponential backbone curve, defined by equation (3-1), which represents the monotonic resistance to lateral displacement and serves as an envelope for the force developed during horizontal cyclic motion. The model also includes loading and unloading segments defined using power curves. Figure 3-4 shows all of the parameters used in defining the model. Monotonic and Static cyclic tests were performed and comparisons were made to the experimental data from Dolan (1989).

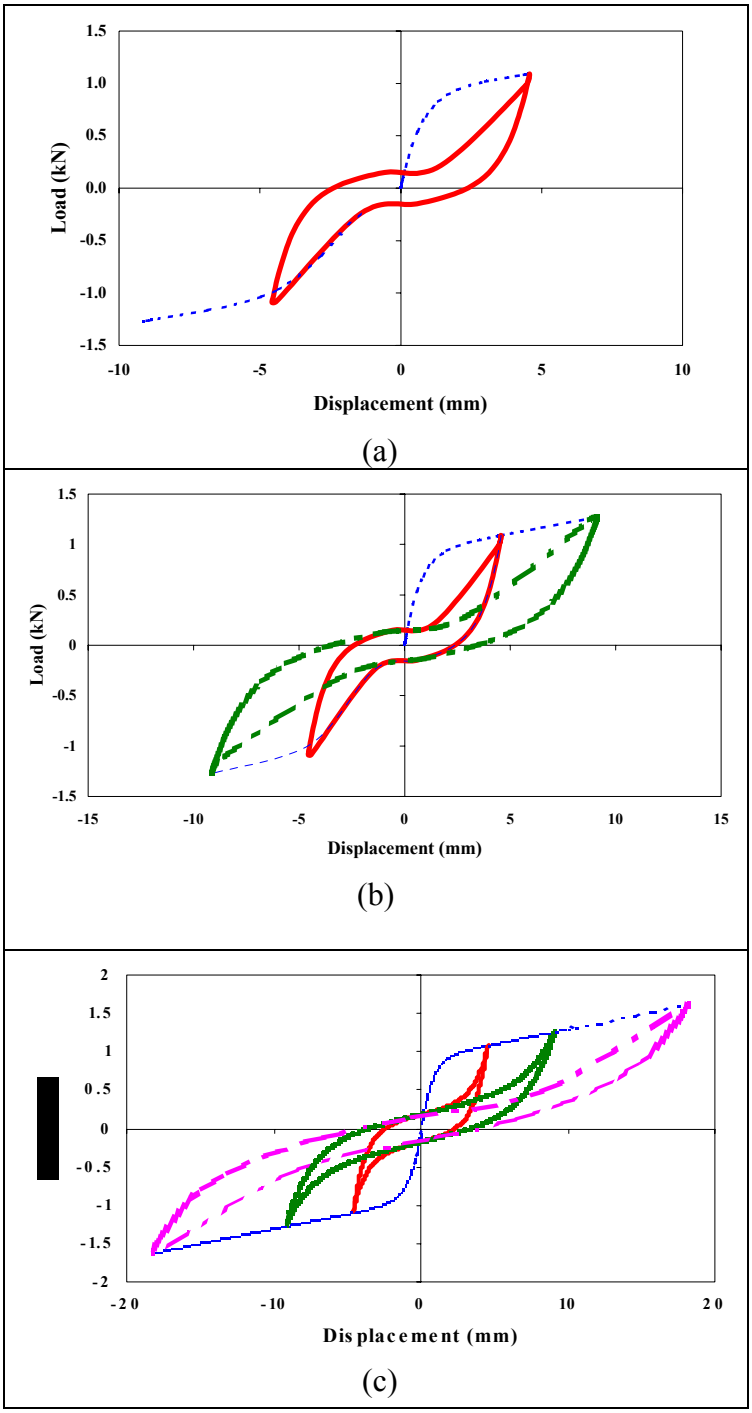

Figure 3-3 – Wood Nailed Model Defined by Power Curves (a) One Complete loop (b) Two Complete Loops (c) Three Complete Loops.

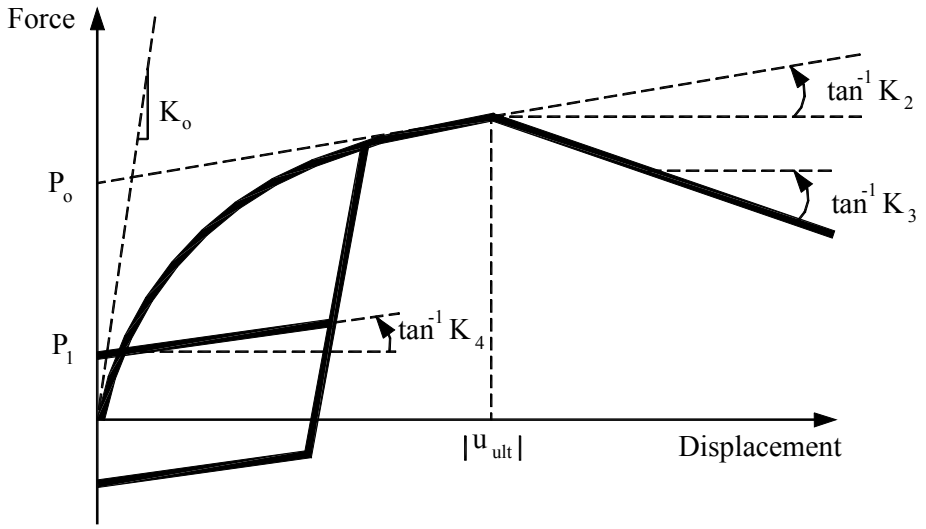

Figure 3-4 - Illustration of sheathing connection parameters defining the monotonic and cyclic load-displacement behavior.

3.3.3 Hybrid Stewart - Dolan Model Defined By Linear Segments

For efficient analysis, some modifications were made to the Dolan (1989) connection model. The sheathing connections associated with each nail were modeled as two orthogonal (one vertical and one horizontal) uncoupled nonlinear springs whose characteristics were defined by a modified hybrid Stewart-Dolan connector model consisting of a series of straight-line segments (Stewart 1987) and an exponential backbone curve (Dolan 1989) including a linear pinching zone. Figure 3-4 illustrates the parameters used in defining the entire model. Monotonic and static cyclic tests were performed and comparisons were made to the experimental data from Dolan (1989).

The hysteresis loop for the connection model is shown in Figure 3-5 (b) For qualitative comparison, a hysteresis loop obtained from experimental testing of a similar sheathing

connection is shown in Figure 3-5 (c). The idealized hysteretic loop shown in Figure 3-5 (b) is generated using a rule-based model for loading/unloading behavior. The connector model includes an exponential backbone curve, which represents the monotonic resistance to lateral displacement and serves as an envelope for the force developed during cyclic motion. In addition, the model includes linear loading/unloading segments and a linear pinching region. The backbone curve is given by the following expression relating the connection shear force, P, and the connection displacement, u:

$$P = \left(P_o + K_2 u\right)\left[1 - \exp\left(\frac{-K_o u}{P_o}\right)\right] \tag{3-1}$$

where the parameters defining the hysteretic behavior are given by (see Figure 3-4):

P_o = force intercept corresponding to slope of backbone curve at ultimate displacement

P_1 = force intercept within pinching region

u_{ult} = ultimate displacement corresponding to ultimate force (i.e., displacement at which stiffness degradation initiates)

K_o = initial elastic stiffness of the connection (i.e., initial slope of the backbone curve)

K_2 = stiffness of the connection at ultimate displacement (i.e., slope of backbone curve at ultimate displacement)

K_3 = stiffness of connection beyond ultimate displacement (i.e., degrading stiffness)

K_4 = stiffness of connection within pinching region

Four of the seven parameters of the sheathing connection model (P_o, P_1, K_o, and K_2) were obtained from experimental test data (see Dolan, 1989). The other three parameters (K_3, K_4, and u_{ult}) were determined via a calibration procedure in which experimental monotonic and cyclic test data was compared with the results of numerical analyses (see Section 3.3 below). The parameters defining the sheathing connection model are summarized in Table 3-1.

Table 3-1: Values of parameters defining sheathing connection model.

P_o	P_1	K_0	K_2	K_3	K_4	u_{ult}
915 N (206 lb)	180 N (40 lb)	1320 N/mm (7536 lb/in)	39 N/mm (220lb/in)	-3.0N/mm (-17.1lb/in)	29.5N/mm (168.4lb/in)	15.24mm (0.6 in.)

Note: Values of P_o, P_1, K_o, and K_2 were taken from experimental data (Dolan, 1989) which represents average results from static-monotonic, static-cyclic, and dynamic cyclic tests of plywood sheathing connections with framing grain parallel and sheathing grain perpendicular to load.

The pinched shape of the hysteresis loops of Figure 3-5 (a) and (b) for small displacements is due to the crushing of the wood sheathing and framing along with nail yielding as the connections are cycled. Note that the commonly observed strength degradation and stiffness degradation for repeated cycles at the same displacement were neglected. Beyond the displacement u_{ult} (corresponding to the ultimate load P_{ult}) the nail begins to withdraw from the framing and sheathing, resulting in a rapid reduction in load-carrying capacity. Softening was considered by allowing stiffness and strength degradation to develop at a small rate comparing to

the initial stiffness of the connection. This helps avoid difficulties in convergence caused by sudden change in quantity and sign of connection stiffness.

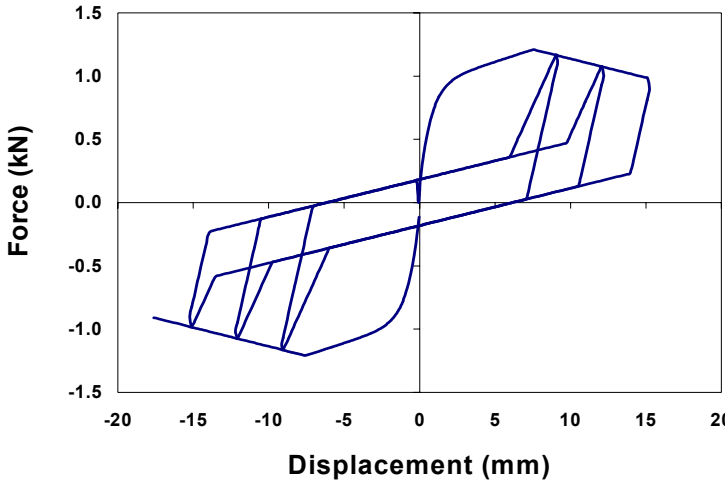

(a)

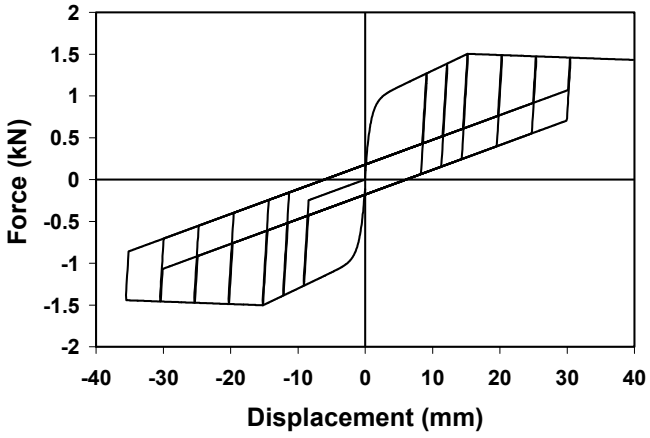

(b)

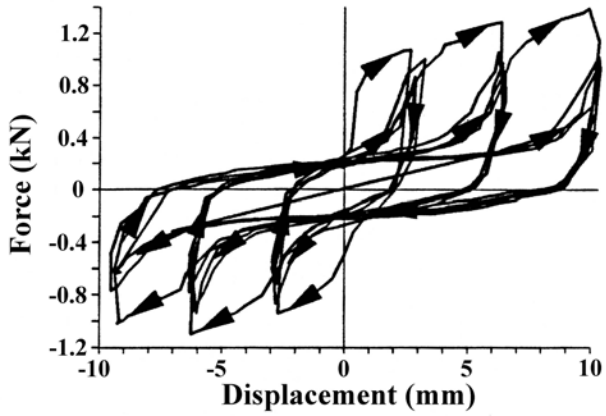

(c)

Figure 3-5 - Hybrid Stewart – Dolan Nail Models: (a) Stiffness degradation in reloading path; (b) Same stiffness in reloading and unloading path; (c) Experimental Test Data (Adapted From Dolan 1989).

4. Finite Element Model of Wood Frame Shear Wall

4.1 Introduction

A typical 2.4 m (8 ft) x 2.4 (8 ft) shear wall was modeled in detail. It was calibrated against the experimental results from a series of tests by Dolan (1989). Dolan performed both static and quasi-dynamic tests on a series of walls. Parameters used in defining Dolan's static monotonic response of shear walls were obtained based on component test data. The wall modeled herein is similar to the series of walls that were experimentally tested by Dolan. The wood nailed connector element (Hybrid Stewart-Dolan Model) described in section 3.3.3 was used in simulating sheathing-to-frame connections. The detailed wall model was formulated and then loaded with monotonic and cyclic static loads. The results obtained closely matched those from the tests. In addition, a simplified equivalent wall model with many fewer degrees of freedom was calibrated against the detailed wall model with the intention of modeling a full-scale house without exceeding available computer storage.

4.2 Assumptions of the Detailed Wall Model

It was assumed that the response of a shear wall to lateral loads consists of racking behavior of the framing system and hysteretic behavior induced by sheathing-to-frame connections. Hinges were assumed to exist at the connections between framing members to simulate the racking behavior of the framing system. Out-of-plane stiffness was ignored here for pure in-plane loading. The bottom sill plate was assumed to be fixed to the foundation with the uplifting effect being neglected. Although, according to Fischer et al (2001) and Gatto and Uang (2002), finishing materials on the walls can appreciably increase the shear resistance of the wall to horizontal loads, finishing materials were not considered for the wall model shown in Figure

4-1. Note that, for practical purposes a tributary mass was added to the top of the sill plate to simulate the load from the above story. It is only intended to affect motion in the horizontal direction when horizontal dynamic loads are applied from prescribed ground accelerations. Therefore, in both static monotonic and static cyclic tests, the P-Delta effect was removed as done by Dolan (1989) in his static tests. Vertical loads representing the weight above were assumed to be distributed along the top sill plate and passed on to each stud. To imitate this load path, a lumped mass was associated with the node at the top of each stud.

4.3 Description of The Detailed Wall

4.3.1 Dimensions and Material Properties

The dimensions of the shear wall were 2.44 m x 2.44 m (8 ft x 8 ft) (see Figure 4-1). The framing members of the wall consisted of 38.1 mm x 88.9 mm (nominal 2 in. x 4 in.) lumber with the vertical studs spaced at 60.96 cm (24 in.) on center. Single end studs and sill/sole plates were used. The wall was sheathed with 1.22 m x 2.44 m (4 ft x 8 ft) plywood sheathing panels. The thickness of the sheathing was 9.53 mm (3/8 in.). The sheathing-to-framing-connections consisted of 6.35 cm (2.5 in.) 8d galvanized common nails with field and perimeter nail spacing of 15.24 cm (6 in.). A tributary weight of 44.5 kN (10 kips) was used to represent the load from the above story.

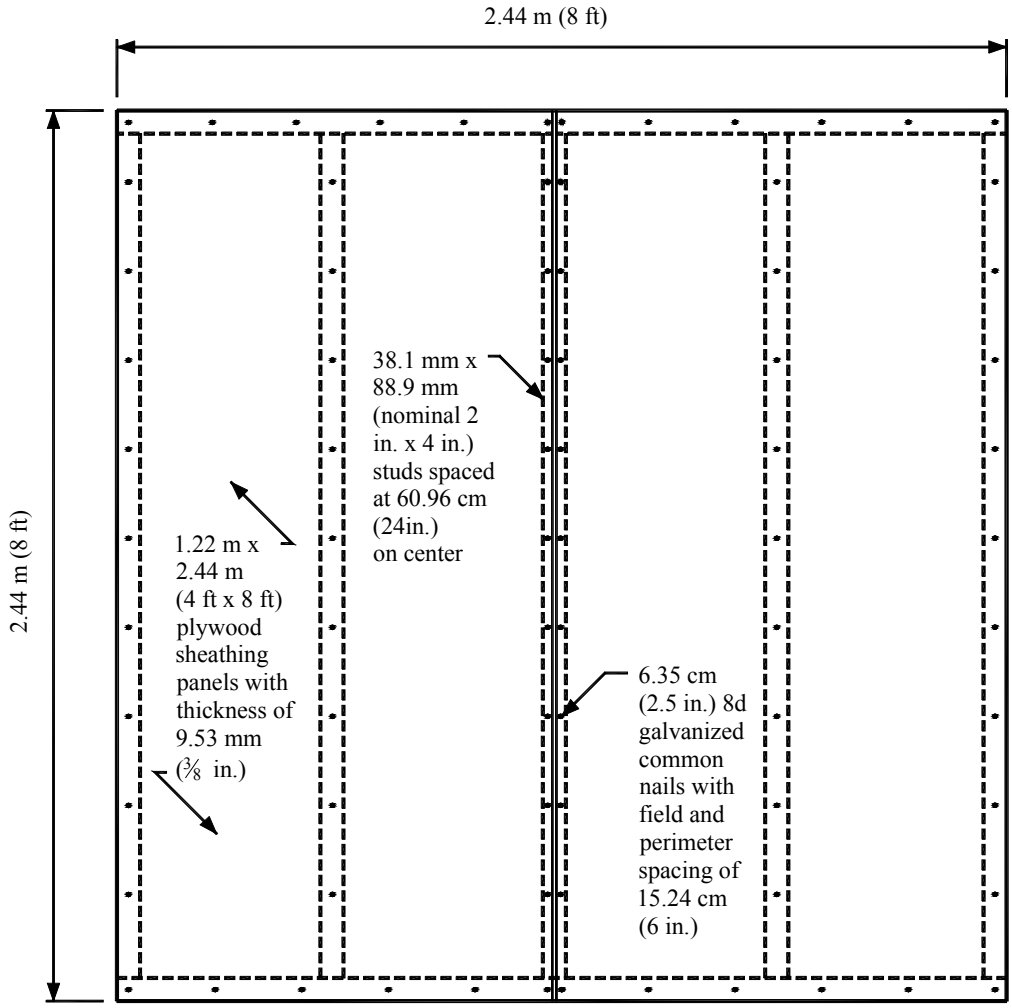

Figure 4-1 - Schematic of wood shear wall used for numerical analysis (nail location shown is not representative of actual nail position).

4.3.2. Finite Element Model of The Detailed Wall

A nonlinear finite element model of the detailed wall described above was modeled (see Figure 4-2) using commercial software, ABAQUS (ABAQUS 1998). An introduction to ABAQUS is given in section 3.2. The framing members were modeled as two-dimensional

isoparametric, isotropic, elastic, cubic beam elements. The sheathing was modeled as two-dimensional isoparametric, orthotropic, elastic linear plane stress elements. The reason that elastic framing members were assumed is that it is commonly acknowledged that the hysteretic behavior of shear walls is induced by the sheathing-to-frame connections. A total of 415 nodes were used in the detailed wall model. Each panel was modeled individually. The initial clearance between the two panels was assigned a value of 7.94 mm (5/16 in.). The interaction between the two sheathing panels was accounted for via a softened contact pressure-clearance relationship with an exponential law. (ABAQUS, 1998)

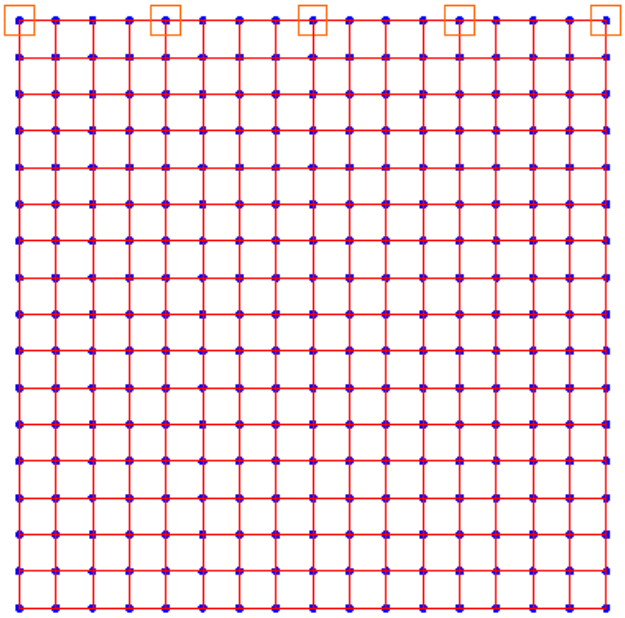

Figure 4-2 - Finite Element Model of Detailed Wood-Framed Shear Wall.

4.4 Calibration of the Detailed Shear Wall Model

4.4.1 Introduction

The detailed shear wall model was calibrated via static monotonic and static cyclic analyses in comparison with the available experimental data. Throughout the analyses, adjustments to three parameters, K_3, K_4, and u_{ult} (Shown in Figure 3-4 in Chapter three, with values given in Table 3-1), of the total of seven parameters used in defining wood nailed connections were made and a comparable wall model was achieved. Stiffness, K_3, which defines the strength degradation, needed to be assigned an arbitrary small value to avoid the numerical problems associated with the rapid change in stiffness at ultimate displacement. Thus, K3 was assigned the value of one-tenth of the stiffness K_4 at the pinching zone.

Note that, for practical purposes a tributary mass was added to the top of the sill plate to simulate the load from the above story. It is only intended to affect motion in the horizontal direction when horizontal dynamic loads are applied from prescribed ground accelerations. Therefore, in both static monotonic and static cyclic tests, the P-Delta effect was removed as done by Dolan (1989) in his static tests.

Also, note that the loading rate is known to have an effect on the behavior of the wall. However, for static and pseudo-static assumptions, all inertial and viscous effects were neglected.

4.4.2 Static Monotonic and Static Cyclic Response

The static monotonic test was performed by applying linearly increasing prescribed displacement in the plane of the wall along the top sill plate opposite an assumed rigid support at

the bottom sill plate. This method is similar to standard practice for a static load test for shear resistance of a framed wall, as described in the ASTM E564 Standard. The purpose is to evaluate the stiffness and the strength of any light-framed wall to be used as a shear-wall on a rigid support. Figure 4-3 (a) presents the static test protocol and Figure 4-3 (b) is the plot of the load vs. Drift Ratio from a static monotonic test. Figure 4-4 shows similar results from a static cyclic test. A reasonably close comparison was obtained when compared to the experimental data.

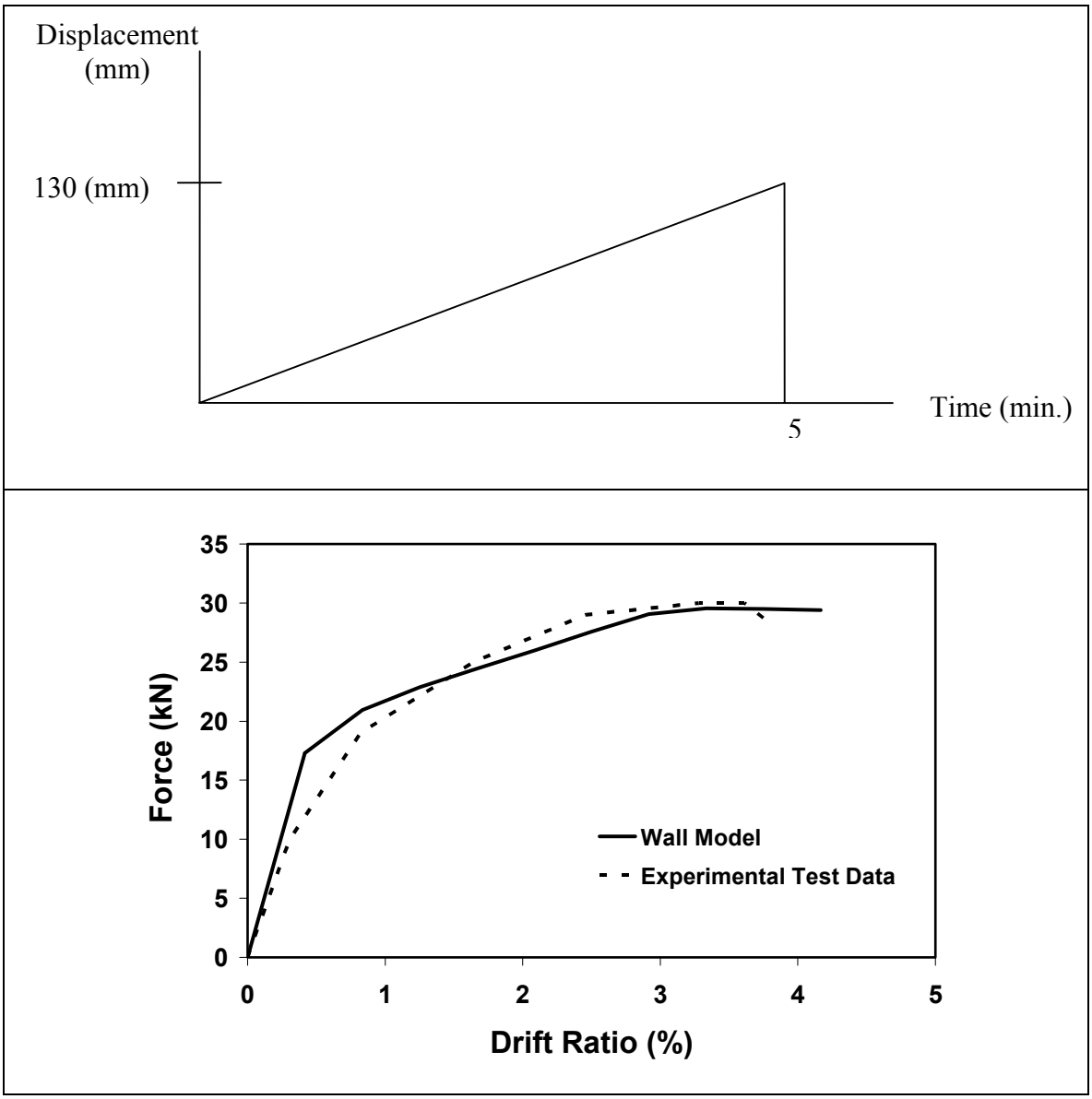

Figure 4-3 - Static Monotonic Response of Detailed Shear Wall without P-Delta Effect: (a) Test Protocol (Dolan 1989); and (b) Force vs. Drift Ratio (Experimental test data taken from Dolan 1989).

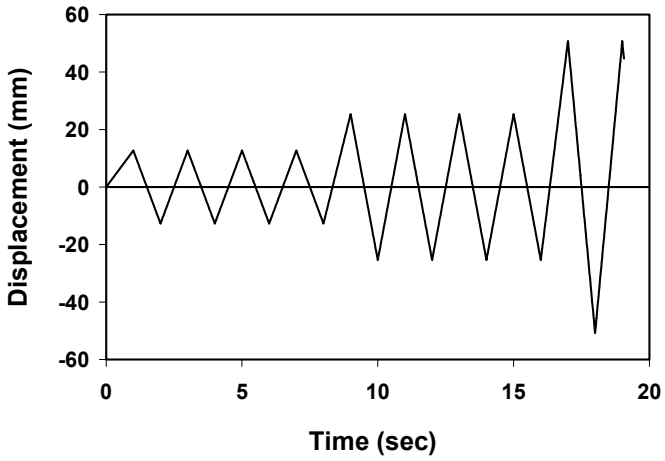

(a)

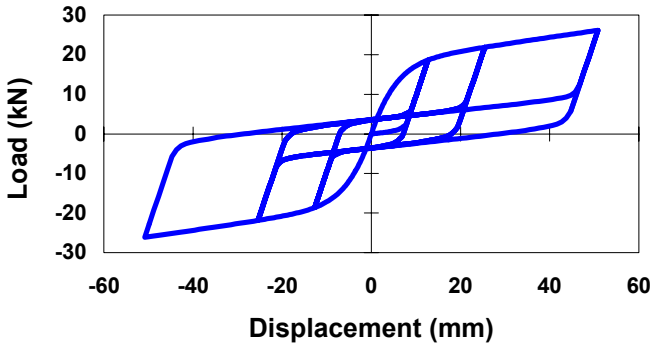

(b)

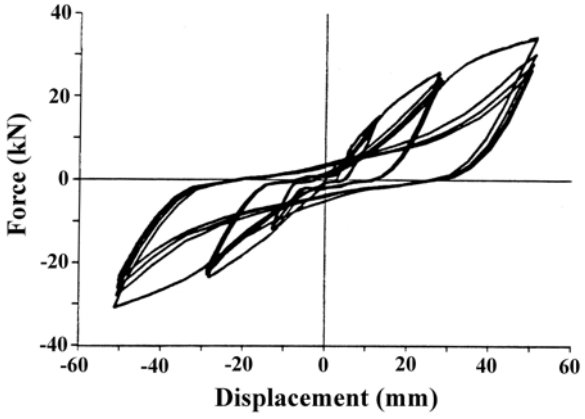

(c)

Figure 4-4 - Static Cyclic Response of Detailed Shear Wall: (a) Static Cyclic Loading Protocol; (b) Hysteresis Loop; and (c) Experimental Hysteresis Loop (adapted from Dolan 1989).

4.5 Effect of Fluid Damper on Wood framed Shear Wall

4.5.1 Dynamic Equations

The Dynamic response of a structural system is governed by equations that require the work of external forces to be balanced by the work of internal, inertial, and viscous forces. Cook (1989) has detailed the derivation of dynamic equations including mass and damping matrices. For a single element, the work balance can be written as:

$$\int_{Ve} \{\partial u\}^T \{F\} dV + \int_{Se} \{\partial u\}^T \{\Phi\} dS + \sum_{i=1}^{n} \{\partial u\}_i^T \{p\}_i = \int_{Ve} (\{\partial \varepsilon\}^T \{\sigma\} + \{\partial u\}^T \rho \{\ddot{u}\} + \{\partial u\}^T \kappa_d \{\dot{u}\}) dV \tag{4-1}$$

where displacement and its first two time derivatives can be expressed as

$$\{u\} = [N]\{d\} \qquad \{\dot{u}\} = [N]\{\dot{d}\} \qquad \{\ddot{u}\} = [N]\{\ddot{d}\} \tag{4-2}$$

Combining equations (1) and (2) yields:

$$\begin{aligned} &\{\partial d\}^T [\int_{Ve} ([B]^T \{\sigma\} dV + \int_{Ve} \rho [N]^T [N] dV \{\ddot{d}\} + \int_{Ve} \kappa_d [N]^T [N] dV \{\ddot{d}\} \\ &- \int_{Ve} [N]^T \{F\} dV - \int_{Se} [N]^T \{\Phi\} dS - \sum_{i=1}^{n} \{p\}_i] = 0 \end{aligned} \tag{4-3}$$

Equation (3) can be rewritten as:

$$[m]\{\ddot{d}\} + [c]\{\dot{d}\} + \{r^{\text{int}}\} = \{r^{ext}\} \tag{4-4}$$

Where

$$[m] = \int_{Ve} \rho [N]^T [N] dV \tag{4-5}$$

$$[c] = \int_{Ve} \kappa_d [N]^T [N] dV \tag{4-6}$$

$$\{r^{\text{int}}\} = \int_{Ve} [B]^T \{\sigma\} dV \tag{4-7}$$

$$\{r^{ext}\} = \int_{Ve} [N]^T \{F\} dV + \int_{Se} [N]^T \{\Phi\} dS + \sum_{i=1}^{n} \{p\}_i \tag{4-8}$$

For elastic material behavior,

$$\{\sigma\} = [E][B]\{d\} \tag{4-9}$$

Equation (7) becomes

$$\{r^{\text{int}}\} = [k]\{d\} \tag{4-10}$$

The stiffness matrix is

$$[k] = \int_{Ve} [B]^T [E][B] dV \tag{4-11}$$

Equation (4) becomes

$$[m]\{\ddot{d}\} + [c]\{\dot{d}\} + [k]\{d\} = \{r^{ext}\} \tag{4-12}$$

For an assembled structures,

$$[M]\{\ddot{D}\} + [C]\{\dot{D}\} + [K]\{D\} = \{R^{ext}\} \tag{4-13}$$

For nonlinear material behavior,

$$[M]\{\ddot{D}\} + [C]\{\dot{D}\} + \left\{R^{\text{int}}\right\} = \{R^{ext}\} \tag{4-14}$$

Note: $\{\delta u\}$, $\{\delta \varepsilon\}$ = small displacements and their corresponding strains

$\{F\}$ = Body Forces

$\{\Phi\}$= Prescribed surface tractions

$\{p\}_i$= Concentrated loads acting at a total of n points on the element

$\{\delta u\}_i^T$= The displacement of the point at which load $\{p\}_i$ is applied

ρ = The mass density of the material

κ_d = Material damping parameter analogous to viscosity

Ve = Element volume

Se = Element surface

$\{u\}$ = Displacement field

$\{\varepsilon\}$= Strain field

[N] = Shape functions

$\{d\}$ = Nodal d.o.f. of the element

[m] = Element mass matrix

[c] = Element damping matrix

$\{r^{int}\}$= Element internal force

$\{r^{ext}\}$=Element external load vectors

[M] = Assembled structure mass matrix

[C] = Assembled structure damping matrix

$\{R^{int}\}$= Assembled structure internal load vectors

$\{R^{ext}\}$= Assembled structure external load vectors

$\{\sigma\}$= Element stress vector

[E] = Material property matrix

[B] = Strain displacement matrix

[k] = Element stiffness matrix

[K] = Assembled structure stiffness matrix

4.5.2. Rayleigh Damping

Damping in timber structures is due to mechanisms such as hysteresis in the material and slip in the connections. To quantify these mechanisms requires a thorough understanding of them, which is not easily achieved. A popular approximate damping scheme, called Rayleigh or Proportional Damping, was therefore applied. Rayleigh damping includes both mass and stiffness proportional contributions, defined as:

$$[C] = \alpha[K] + \beta[M] \tag{4-15}$$

where α and β are the stiffness and mass proportional damping constants. The damping matrix, [C], is orthogonal. Thus, for a system of multiple degrees of freedom, it allows modes to be uncoupled by eigenvectors associated with the undamped problem. The stiffness and mass proportional damping constants α and β can be expressed as

$$\alpha = \frac{2(\xi_2\omega_2 - \xi_1\omega_1)}{\omega_2^2 - \omega_1^2} \tag{4-16}$$

$$\beta = \frac{2\omega_1\omega_2(\xi_1\omega_2 - \xi_2\omega_1)}{\omega_2^2 - \omega_1^2} \tag{4-17}$$

where ξ_1 and ξ_2 are fractions of critical damping (i.e., when the damping ratio, ξ=1) at frequencies ω_1 and ω_2, which normally are chosen to bound the design spectrum for the structural system. In this case, the fundamental frequency and the frequency of the third mode were considered as the lower and upper bound. Contributions from modes higher than the third were not considered significant. According to Cook et al. (1989), 30 Hz is often used as the upper frequency in seismic analysis. The spectral content of the seismic design spectra are insignificant above 30 Hz. The detailed wall natural frequencies, ω_1 and ω_2 in the fundamental mode and the third mode, were determined by solving the eigenvalue problem associated with the undamped wall using the initial elastic stiffness as described in section 4.6.3. The inherent damping ratio for the first mode and the third mode was assumed to be 2% and 10%, respectively. The stiffness and mass proportional damping coefficients are listed in Table 4-1.

Table 4-1– Natural Frequencies and Rayleigh Damping Coefficients

	Frequency (Hz)		Damping Ratio (%)		Stiffness Proportional Damping α (sec.)	Mass Proportional Damping β (rad./sec.)
	Mode 1	Mode 3	Mode 1	Mode 3		
Model Prediction	4.18	22.8	2	10	0.001392	0.090591
Rule of Thumb (Cook et al. 1989)	3.21	30.0	2	10	0.00105	0.379489

4.5.3 The Eigenvalue Problem

Standard Eigenvalue analysis was conducted on the detailed wall model. According to Cook et al (1989), an undamped structure with no external loads applied to unrestrained d.o.f

undergoes harmonic motion excited by initial conditions. Each d.o.f moves in phase with all other d.o.f. and can be decided by solving

$$\{D\} = \{\overline{D}\}\sin\omega t \quad \text{and} \quad \{\ddot{D}\} = -\omega^2\{\overline{D}\}\sin\omega t \tag{4-18}$$

where $\{\overline{D}\}$ = Amplitude of nodal d.o.f vibration

ω = Circular frequency (radians per second)

The relationship between circular frequency, cyclic frequency, and period is

$$f = \frac{\omega}{2\pi} \quad \text{and} \quad T = \frac{1}{f} \tag{4-19}$$

where f = cyclic frequency (Hertz)

T = Period (seconds)

With no damping or no external loads, the equation of motion (14) becomes

$$([K] - \lambda[M])\{\overline{D}\} = \{0\}\text{, where } \lambda = \omega^2 \tag{4-20}$$

Nontrivial solutions to equation (19) are obtained from

$$\det([K] - \lambda[M]) = 0 \tag{4-21}$$

Each eigenvalue λ_i is associated with an eigenvector $\{\overline{D}\}_i$ or normal mode.

The eigenvalue analysis of the detailed wall yielded natural frequencies and vibration modes. The fundamental frequency obtained from the experiments by Dolan (1989), Foschi et al (2001), and the detailed wall model were compared to evaluate the wall model. Results are summarized in Table 4-2. The first ten modes of vibration are plotted as seen in Figure 4-5,

Figure 4-6, and Figure 4-7. The Eigenvalue analysis predicted 4.18 Hz and 22.8 Hz for the fundamental frequency (the lowest nonzero frequency) and the frequency of third mode, respectively. These two frequencies were close to the ones predicted by Cook et al (1989) as lower and upper boundaries in seismic analysis of timber structures, which are 3.0 Hz and 30 Hz respectively.

Table 4-2 – Shear Wall Fundamental Frequency

	Experimental Results		Finite Element Model Prediction
	Dolan (1989)	Foschi et al (2001)	
Shear Wall Fundamental Frequency (Hz)	3.1	4.5	4.18

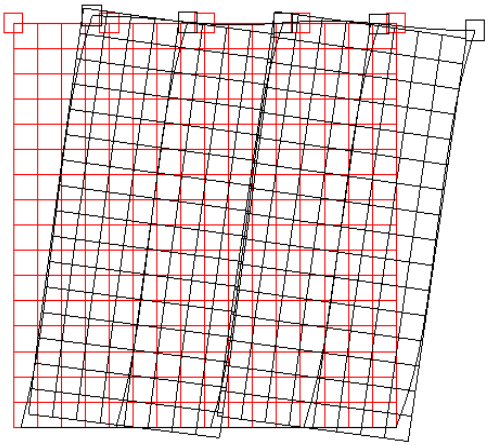

(a) Mode 1

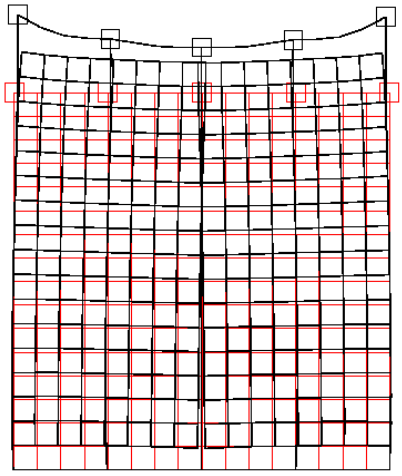

(b) Mode 2

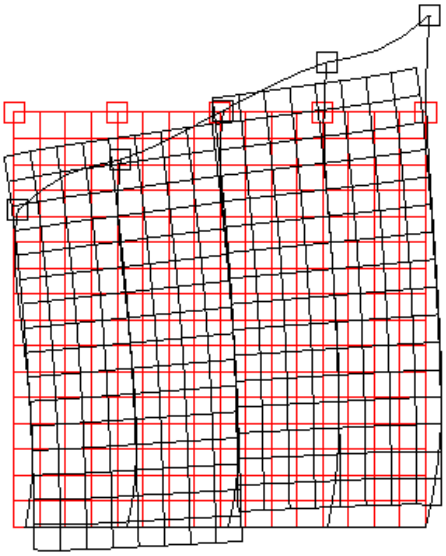

(c) Mode 3

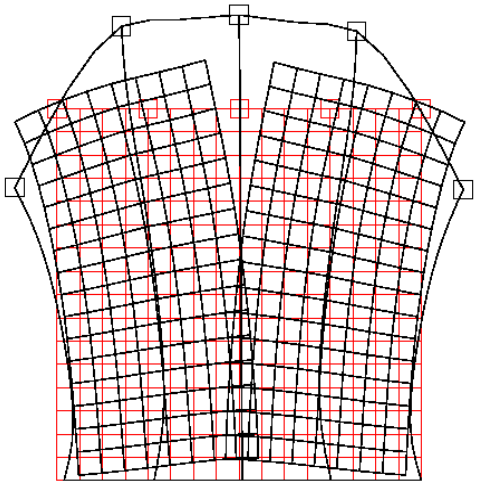

(d) Mode 4

Figure 4-5 – Eigen Modes 1-4 of the Shear Wall Model.

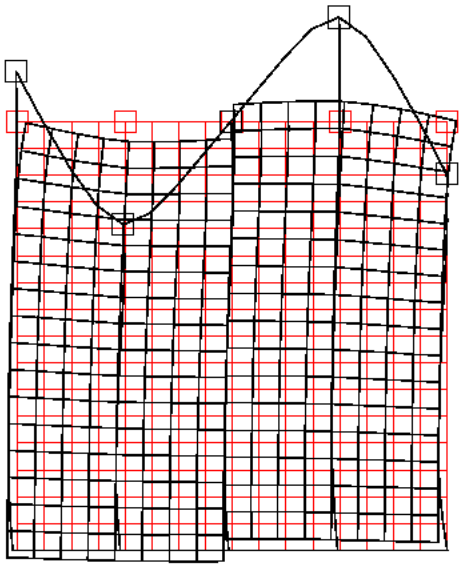

(e) Mode 5

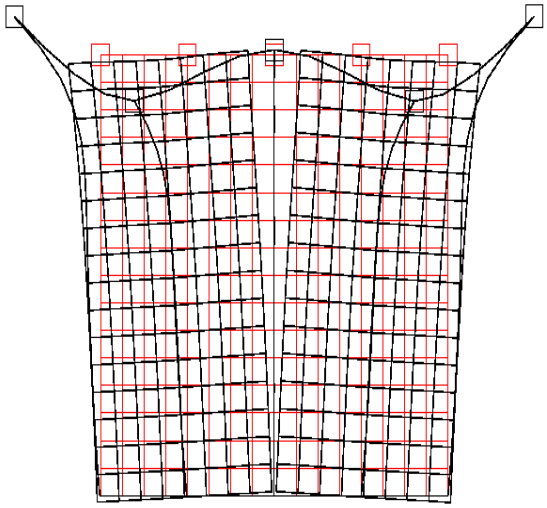

(f) Mode 6

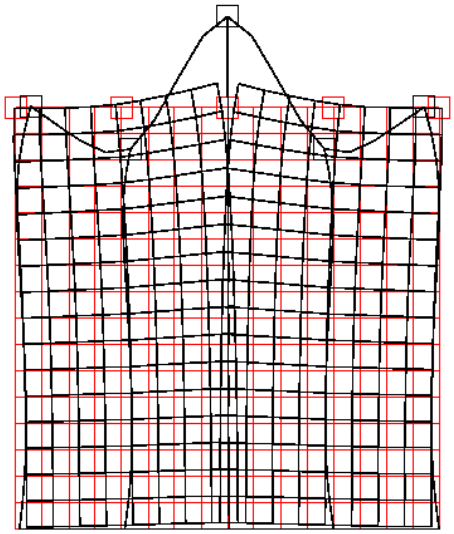

(g) Mode 7

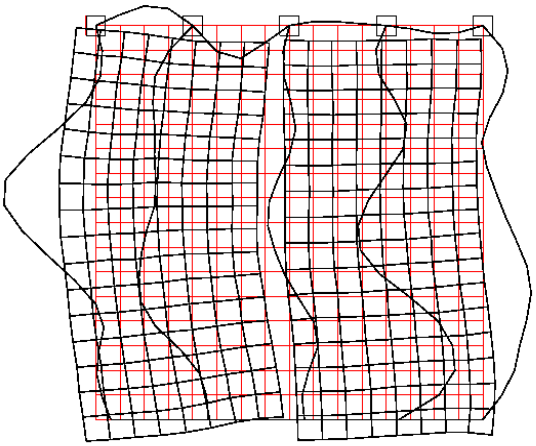

(h) Mode 8

Figure 4-6 - Eigen Modes 5-8 of the Shear Wall Model.

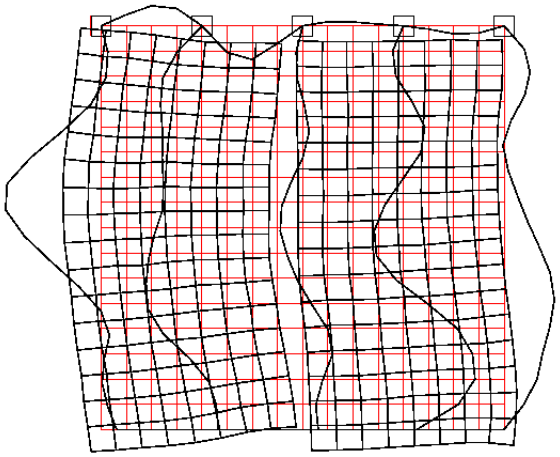

(i) Mode 9

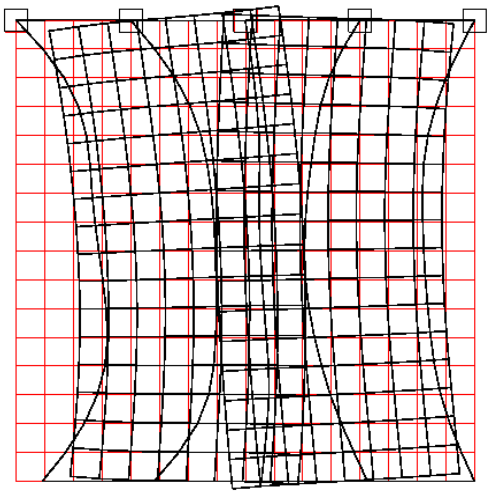

(j) Mode 10

Figure 4-7 – Eigen Modes 9-10 of the Shear Wall Model.

4.5.4 Introduction to Fluid Dampers

Fluid dampers are designed to have high-energy dissipation capacity. Figure 4-8 shows the cross section view of a typical fluid damper.

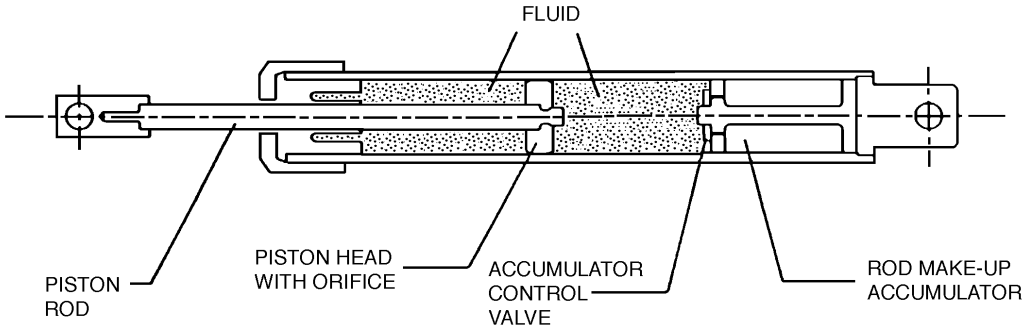

Figure 4-8 – Cross Section View of Typical Fluid Damper (From Symans 2002b)

A study was conducted on an 8.9 kN (2-kip) capacity fluid damper subjected to sinusoidal input motions for room temperature of 23^{o} and frequencies of 1, 2, and 4 Hz by Symans and Constantinou in 1998 (see Figure 4-9). Their study indicates that the damper under

such conditions acts as a linear viscous damper since the hysteretic loops are basically elliptical shape with slight slope, which is negligible. The Eigenvalue analysis described in the previous section predicted the fundamental frequency of the detailed wall is 4.18Hz, which is typical for light framed timber houses and within the range of the linearity assumption. According to Symans et al (Symans et al 2002b), the mathematical model for the damper can be simulated by a simple linear viscous dashpot:

$$P(t) = C\dot{u}(t) \tag{4-22}$$

where P (t) is the damping force, C is the damping coefficient, and $\dot{u}(t)$ is the velocity of piston head with respect to the cylinder.

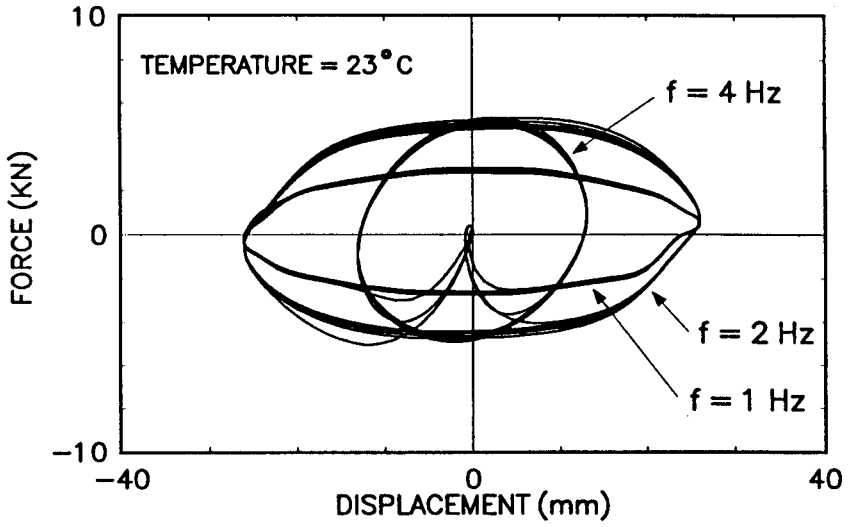

Figure 4-9 - Hysteretic loops of 8.9-kN (2-kip) capacity fluid damper subjected to harmonic motion (From Symans et al 2002b).

A possible configuration for the installation of a fluid damper within a timber shear wall was proposed by Symans et al (Symans et al 2002b) as shown in Figure 4-10. The damper orientation is important, as it can impact the load path. The damper in this configuration can be located at upper right or lower left corner (Symans et al 2002b).

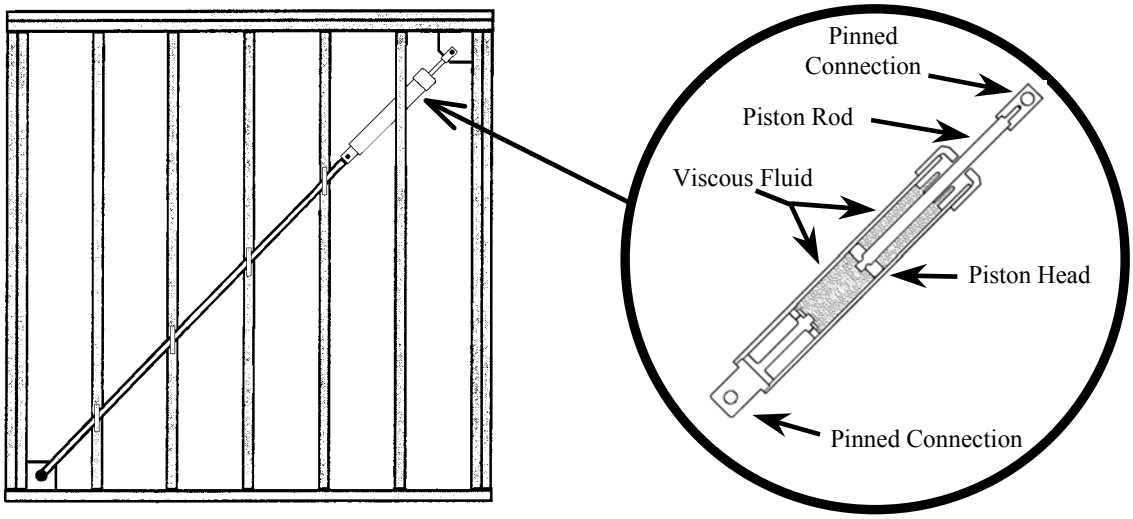

Figure 4-10 – Configuration of The Installation of Fluid Damper (From Symans et al 2002b).

The viscous damper was modeled using linear Dashpot element in ABAQUS. A Dashpot is a finite element used to model relative velocity-dependent force. In addition, it provides an energy dissipation mechanism, which is exactly what a damper is designed to do. For geometrically nonlinear analysis,

$$\Delta v = \frac{(\underline{v}_2 - \underline{v}_1)(\underline{x}_2 - \underline{x}_1)}{l} \tag{4-23}$$

where: Δv = Relative velocity of the dashpot.

$\underline{v}_1$ = Velocity at dashpot's first node.

$\underline{v}_2$ = Velocity at dashpot's second node.

$\underline{x}_1$ = Current position of dashpot's first node.

$\underline{x}_2$ = Current position of dashpot's second node.

l = Current length of the dashpot.

4.5.5 Dynamic Response With and Without Fluid Dampers

A single damper was installed along the diagonal of the wall as shown in Figure 4-10. Two different dampers were used in evaluating the effectiveness of the fluid damper. The damping coefficients were 17.5 kN-s/m (100 lb-s/in) and 87.6 kN-s/m (500 lb-s/in), respectively. Only the results from the analysis using damping coefficient of 87.6 kN-s/m (500 lb-s/in) are presented here. A far-field earthquake ground motion and a near-field earthquake ground motion were chosen for seismic response analysis. One of the earthquake records chosen was the South–East 69 degree component of Taft record from the Kern County earthquake, which occurred in 1952. The other earthquake record chosen was the 90-degree component of the Newhall record from the Northridge earthquake, which occurred in 1994 (see Figure 4-11). These two earthquake records are representative of two different types of earthquakes. That is, the Taft record represents a weak ground motion being considered as a relatively frequent earthquake in California, and the Newhall record represents a strong ground motion being considered as a design level event. Figure 4-11 (Symans et al 2002b) shows both records.

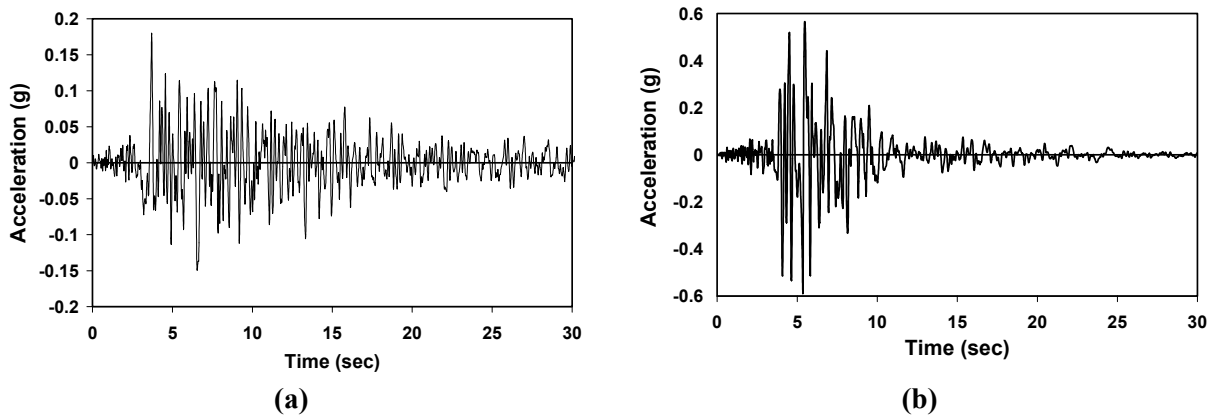

Figure 4-11 - Ground Acceleration: (a) the Taft Record – Lincoln School Tunnel (S69E Comp.) of 1952 Kern County Earthquake and (b) the Newhall Record (90^{o} Comp.) of 1994 Northridge Earthquake.

4.5.5.1 Shear Wall Subjected to the Far-Field Ground Motion (Taft Record) – Kern County Earthquake

The analysis consisted of only the first 15 seconds of the earthquake record due to the limitation of the computer storage. This was considered sufficient since the major earthquake motion occurred within that 15 seconds, as shown in Figure 4-11 (a). The hysteresis loops for the wall with and without the damper are different in shape due to the role that the damper played in shear resistance, as shown in Figure 4-12. For the case without the damper, the wall experienced inelastic deformation, and the peak Drift Ratio was about 0.36%. For the case with the damper, the peak Drift Ratio reduced to 0.17%, which led to an approximate 53% reduction. The Drift Ratio is an important parameter in shear wall analysis, chosen for use in measuring their damage state and performance level in the *NEHRP Guidelines* (FEMA 1997). Table 4-3 lists the

definition of damage states at the corresponding Drift Ratio. The damage state of the wall without the damper was designated as Moderate Damage corresponding to the Immediate Occupancy performance level. With the damper, the damage state reduced to a level of Slight damage while the performance level, Immediate Occupancy remains the same. A similar contrast between the wall with and without a damper was also observed in the peak Base Shear Coefficient. Without the damper, the peak Base Shear Coefficient was 0.36. With the damper, however, the peak Base Shear Coefficient reduced to 0.24, which led to a reduction of approximately 33%. The above results indicate that, with the installation of a damper, inelastic energy demand on the wall reduces dramatically. Therefore, the damage in the wall is less severe resulting in better performance.

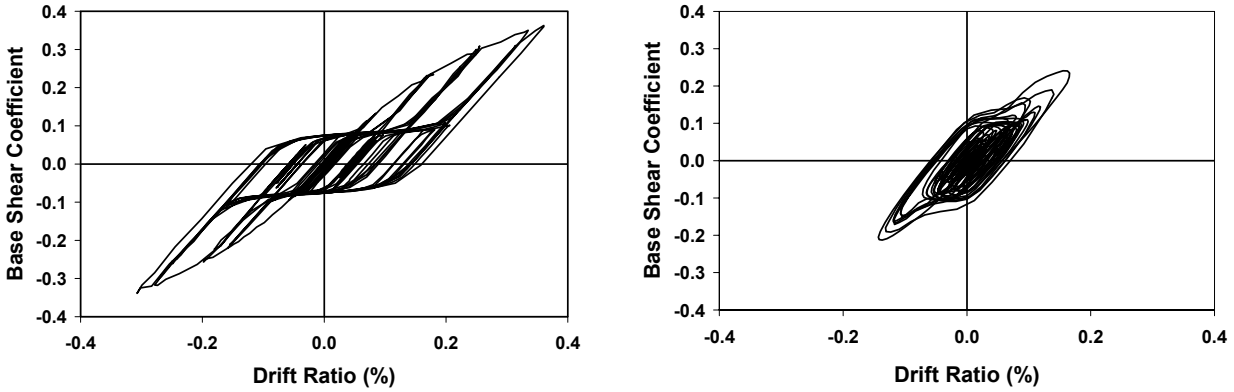

No Damper **C = 87.6 kN-s/m**

Figure 4-12 - Hysteresis Loops of the Shear Wall Without and With Fluid Dampers Subjected to the Taft Record (*plotted to same scale*).

The contribution to the dissipation of the seismic input energy from the wall itself and the damper were plotted separately to demonstrate the performance of the damper (see Figure 4-13).

The effectiveness of the damper is perceptible from the ellipsoidal shape of the hysteresis loop of the damper. The energy dissipated is within the area of the loop. It is clear that the area within the wall loop is smaller than the area within the damper loop. The area within the wall loop is smaller than the area within the damper loop.

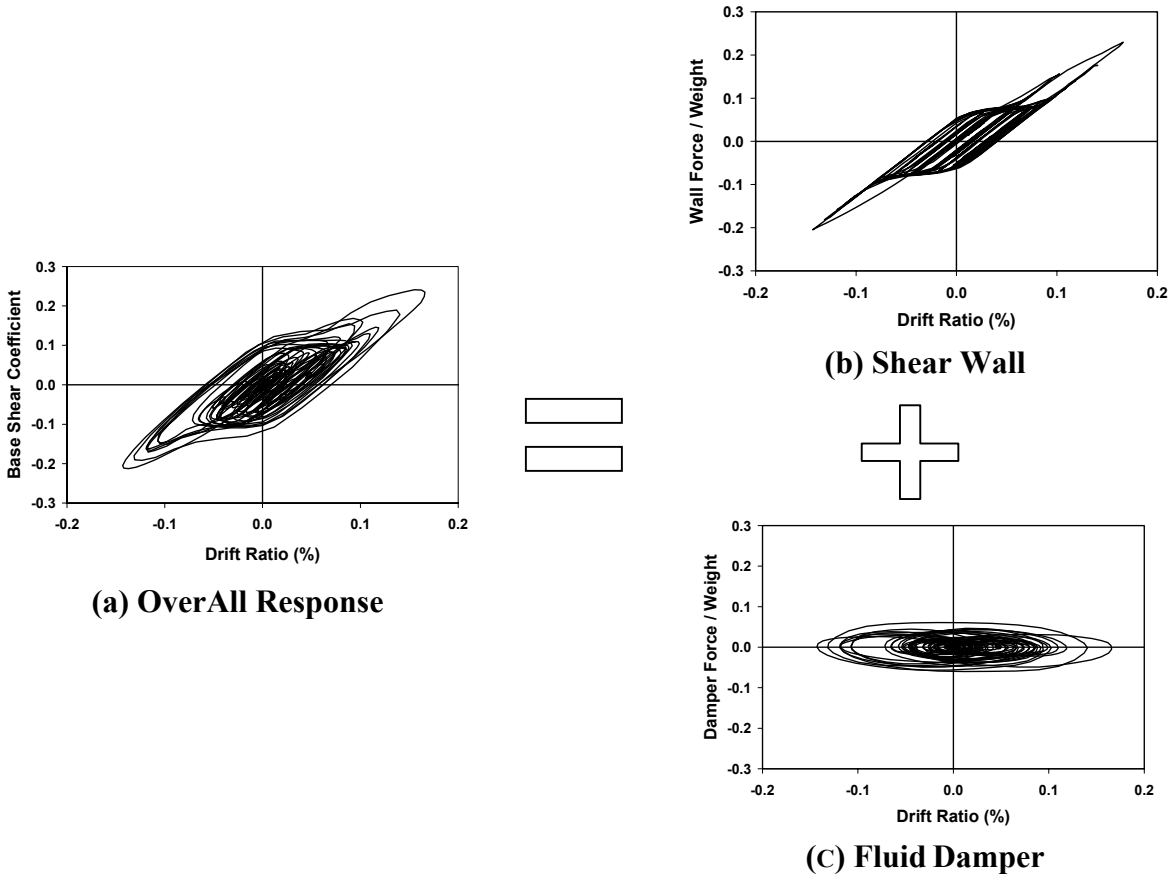

Figure 4-13 - Decomposition of the Hysteresis Loop into the Wall and Fluid Damper Contributions When the Shear Wall is Subjected to the Taft Record: (a) Overall Response of the Wall; (b) Shear Wall Contribution; and (c) Fluid Damper Contribution.

Table 4-3 Performance Levels for Light-Framed Wood Buildings.

Damage State	Wall Condition	Performance Level	Drift Ratio Limits
No damage	---	O – Operational	---
Slight damage	Minor cracking.	IO – Immediate Occupancy	1% transient 0.25% permanent
Moderate damage	Large cracks at corners of door/window openings.	---	---
Extensive damage	Large cracks across shear walls.	LS – Life Safety	2% transient 1% permanent
Complete damage	Large permanent displacements.	CP – Collapse Prevention	3% transient or permanent
Collapse	---	---	---

The Time-history of the Drift Ratio (see Figure 4-14) and the Base Shear Coefficient (see Figure 4-16) depict the reduction over time in these two quantities when the fluid damper was installed. Figure 4-15 and Figure 4-17 summarized the Peak values of the Peak Drift Ratio and the Peak Base Shear Coefficient.

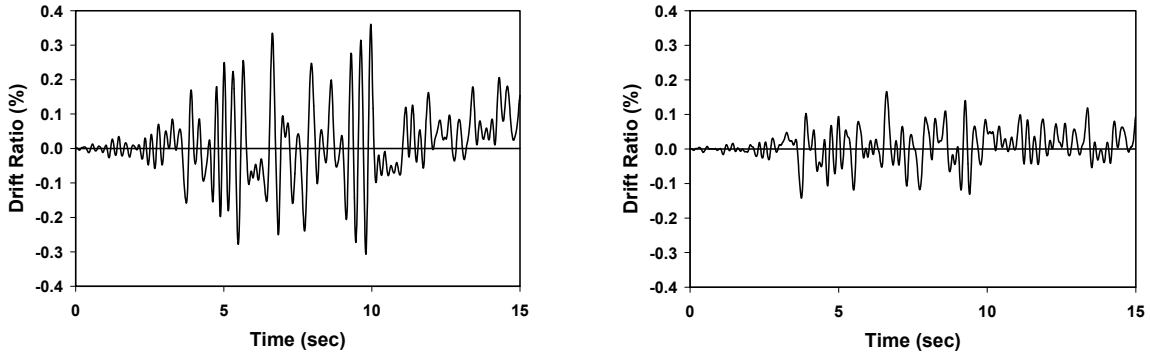

No Dampers **C = 87.6 kN-s/m (500 lb-s/in)**

Figure 4-14 – Time History of the Drift Ratio for the Wall With and Without Fluid Dampers When Subjected to the Taft Record.

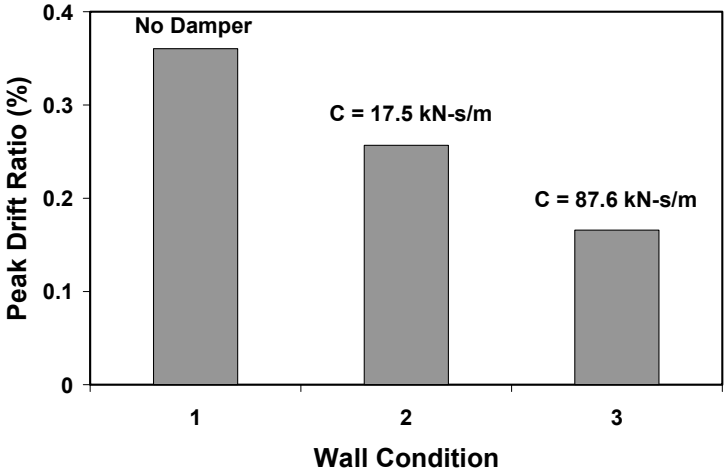

Figure 4-15 – Comparison of the Peak Drift Ratio for the Wall With and Without Fluid Dampers When Subjected to the Taft Record

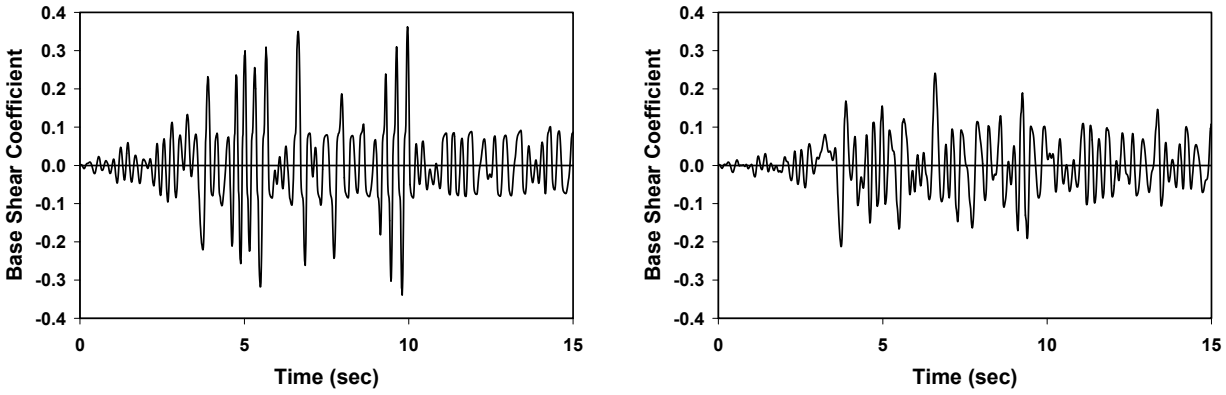

Figure 4-16 - Time History of the Base Shear Coefficient for the Wall With and Without the Fluid Damper when Subjected to the Taft Record

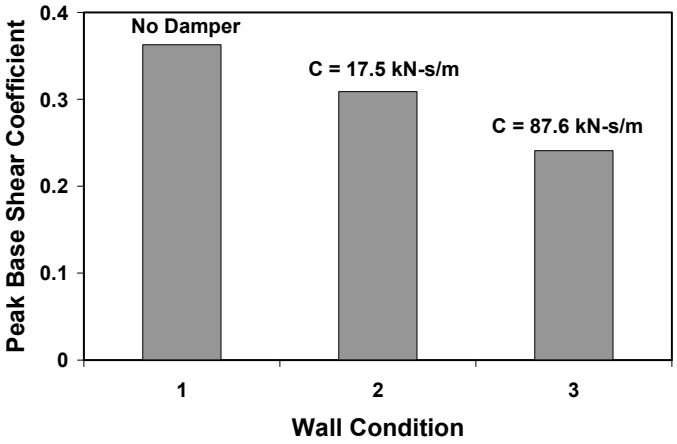

Figure 4-17 – Comparison of the Peak Base Shear Coefficient for the Wall With and Without a Damper when Subjected to the Taft Record

Figure 4-15 and Figure 4-17 show the comparison of Peak Drift Ratio and Peak Base Shear Coefficient, respectively. It is noticeable that the reduction rate in Peak Drift Ratio when the damper is installed is different from the one in Peak Base Shear Coefficient. This is due to the fact that the stiffness in shear wall is nonlinear. Therefore, Base Shear is not proportional to displacement. As a result, Base Shear Coefficient is not proportional to Drift Ratio. Thus, for a certain percentage reduction in Peak Drift Ratio, it does not necessary yield the same percentage of reduction in Peak Base Shear Coefficient if the stiffness of the wall is not linear.

The energy distribution over time also reveals the effectiveness of the fluid damper. The Time History of various energy measures was plotted to the same scale for cases with and without a damper to show the significant shift in energy distribution. For the case without the damper, almost all of the seismic input energy was dissipated via the wall itself as inelastic energy. The amount of viscous energy is insignificant since the only source of viscous damping in the system was Rayleigh damping (see Figure 4-18). With the damper installed, the inelastic

energy absorbed by the wall reduced from about 53% of the seismic input energy to approximately 12% of the seismic input energy. As for viscous energy, it went up from approximately 3% of the seismic input energy to 64% of the seismic input energy. The reduction in energy demand on the wall is about 78%.

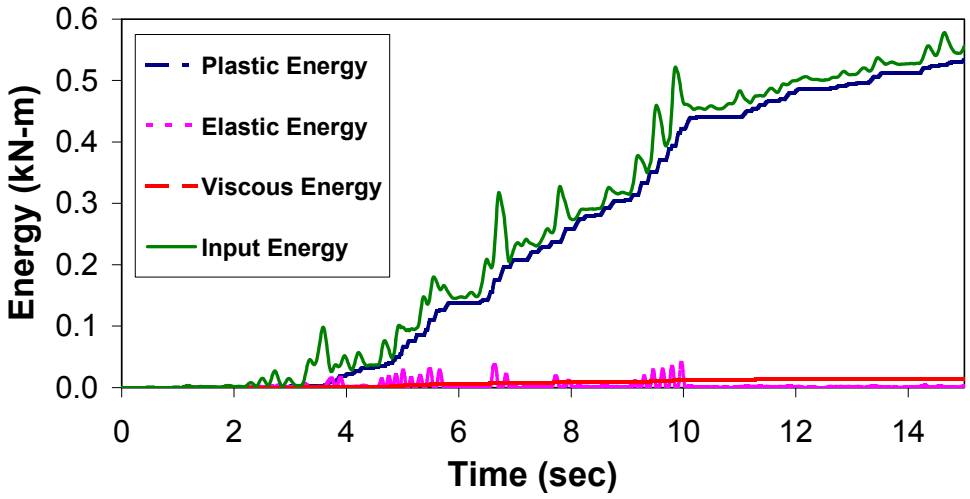

(a) No Damper

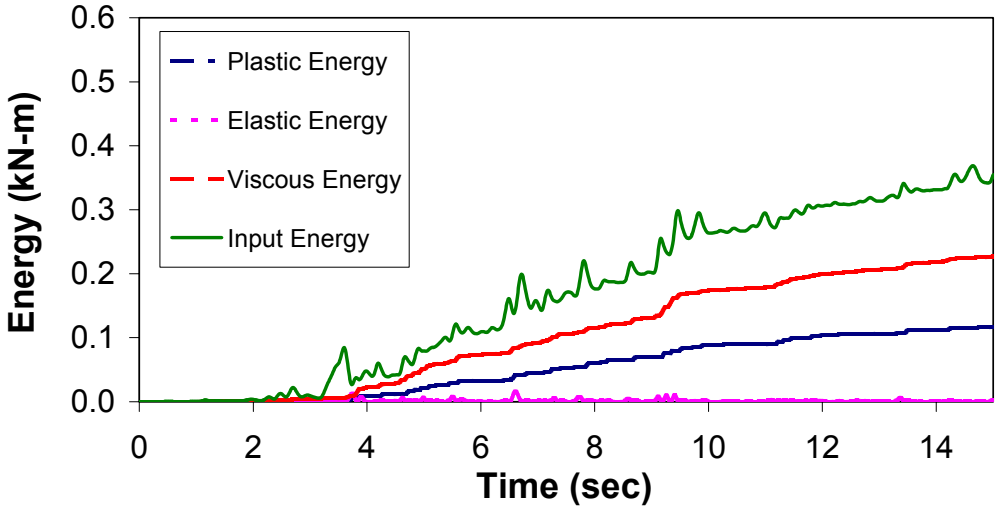

(b) C = 87.6 kN-s/m (500 lb-s/in)

Figure 4-18 - Energy Distribution Over Time Within the Wall for the Taft Record

Table 4-4 - Summary For the Taft Record

		Without Fluid Damper	With a Fluid Damper C = 87.6 kN-s/m	Reduction (%)	Increase (%)
Peak Drift Ratio (%)		0.36	0.17	53	
Peak Base Shear Coefficient		0.36	0.24	33	
Energy	Input (kN-m)	0.556	0.355	36	
Viscous	Viscous(kN-m)	0.0144	0.2270		15
	Percentage of Input Energy (%)	2.6	64		
Inelastic	Inelastic (kN-m)	0.534	0.117	78	
	Percentage of Input Energy (%)	96	33		

4.5.5.2 Shear Wall Subjected to the Near-Field Ground Motion (Newhall Record)-Northridge Earthquake

The Northridge earthquake was chosen for analysis because it is one of the most destructive earthquakes. Only the first 15 seconds of the earthquake record was used in the analysis. However, Figure 4-11 (b) shows that the major motion occurred within that time period. The hysteresis loops in Figure 4-19 and Figure 4-20 demonstrate that the wall without a damper reached a level of drift that would indicate collapse. The damage state is designated as Collapse and the performance level was beyond that of Collapse Prevention, which was life threatening. With the damper installed, however, the peak Drift Ratio was reduced to about 0.38%, which not only enhances the wall performance level to Life Safety (LS) but also reduces the damage state to Moderate damage. Recall, in the previous analysis with the Taft record, with the fluid damper, the damage state was less severe but the wall performance level remains the same since the Taft record represents relatively weak ground motion. However, the analysis with

the Newhall record clearly demonstrates that when a wall is subjected to strong earthquake motion, a fluid damper can improve the performance level and lower the damage state.

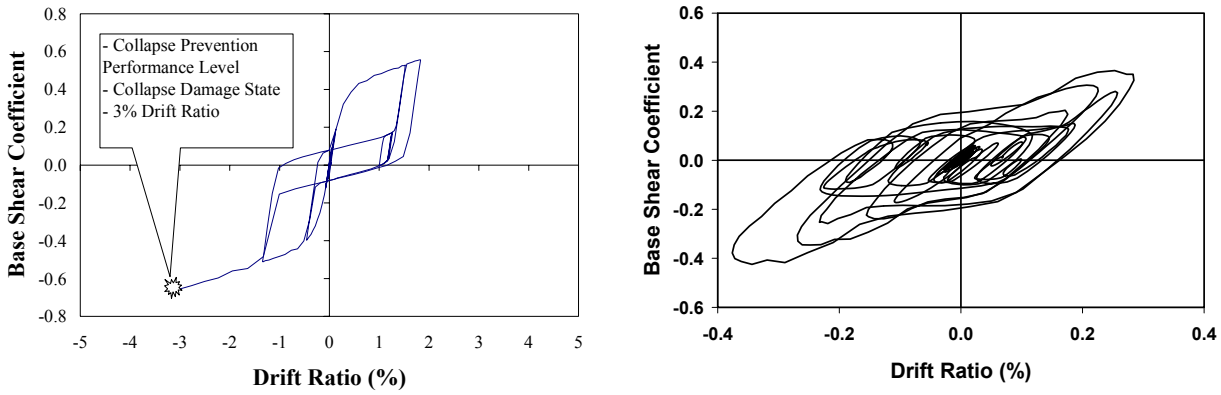

No Damper **C = 87.6 kN-s/m (500 lb-s/in)**

Figure 4-19 - Hysteresis Loops of Shear Wall Without and With Fluid Dampers Subjected to the Newhall Record (*not plotted to same scale*).

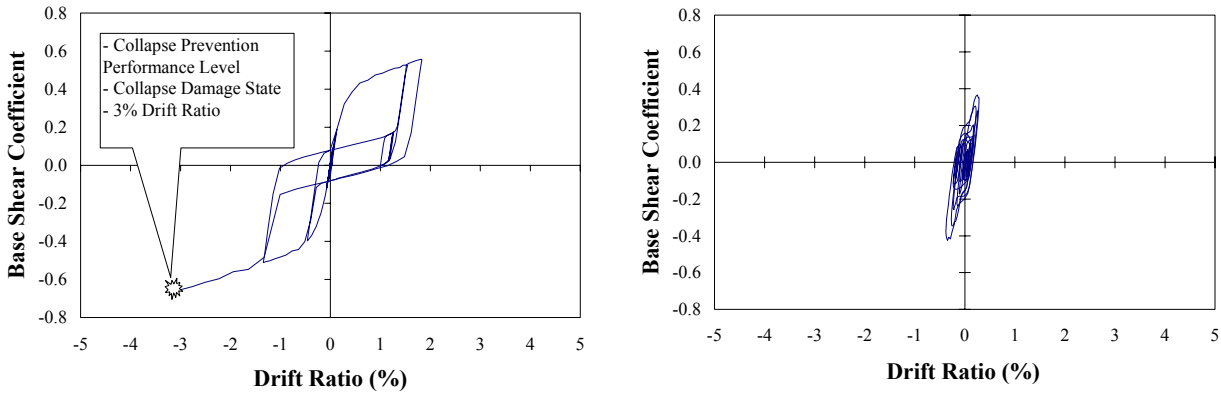

No Damper **C = 87.6 kN-s/m (500 lb – s/in)**

Figure 4-20 - Hysteresis Loops of Shear Wall Without and With Fluid Dampers Subjected to the Newhall Record (*plotted to same scale*).

Figure 4-21 indicates how the wall itself and the fluid damper performed in contributing to energy dissipation. Again, the damper dissipated considerable amount of the seismic input energy while the wall itself dissipated only a small amount of the seismic input energy through its inelastic hysteretic behavior. The hysteretic response is mainly induced by the behavior of the sheathing-to-frame connections.

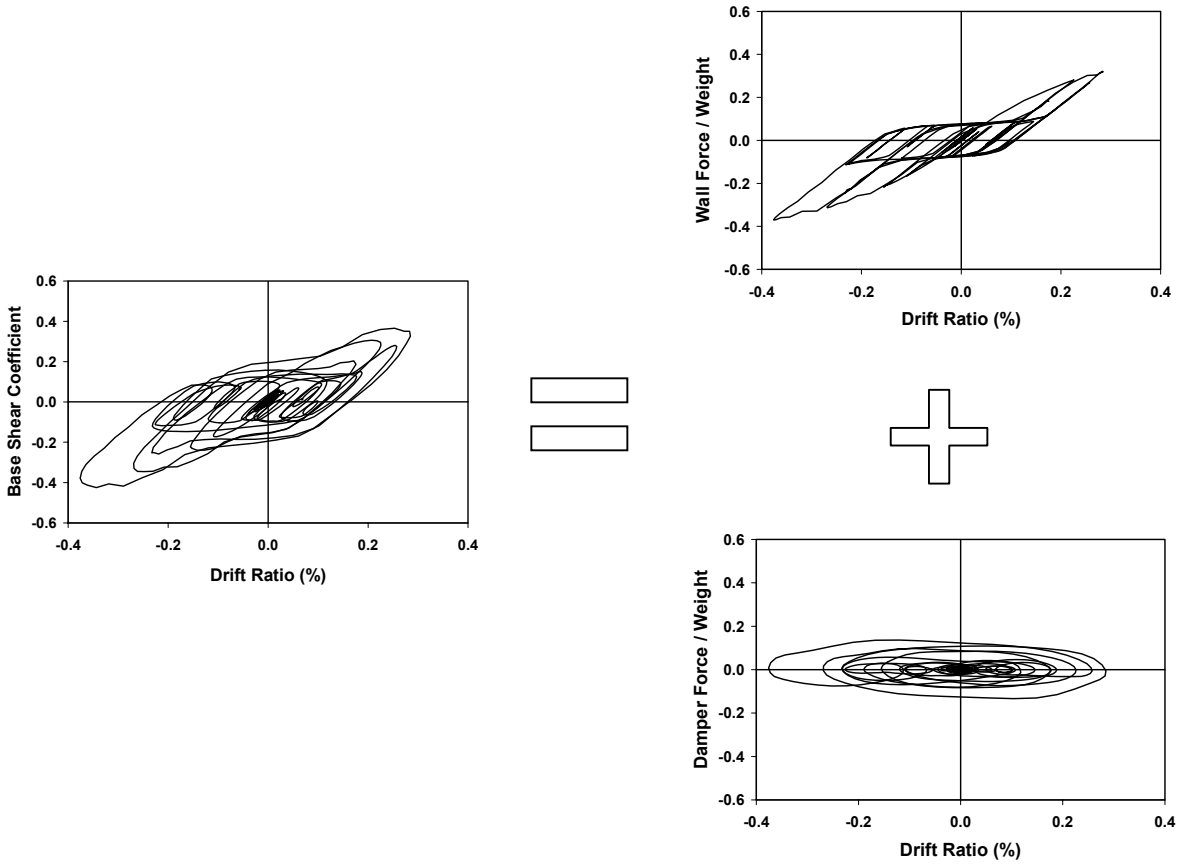

Figure 4-21 - Decomposition of Hysteresis Loop into the Wall and the Damper Contributions When Shearwall Subjected to the Newhall Record.

Figure 4-22 and Figure 4-23 exhibit the time history of the Drift Ratio and the Base Shear Coefficient, respectively. The wall without a damper collapsed about 6 seconds into the earthquake. With a damper installed, however, the wall was able to withstand the entire 15 seconds of the earthquake, which included the major ground motion. Therefore, it can be predicted that the wall with a damper can survive the entire earthquake.

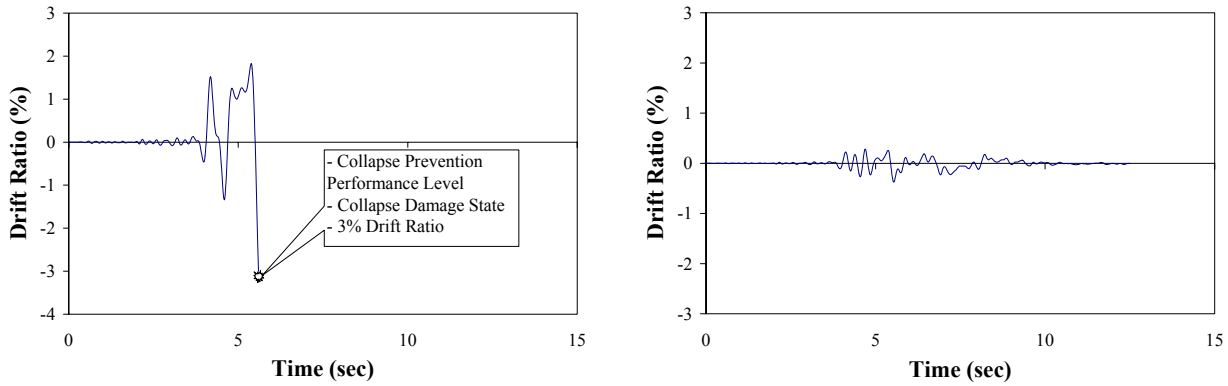

No Damper **C = 87.6 kN-s/m (500 lb-s/in)**

Figure 4-22 - Time-History of the Drift Ratio for the Wall With and Without Dampers Subjected to the Newhall Record

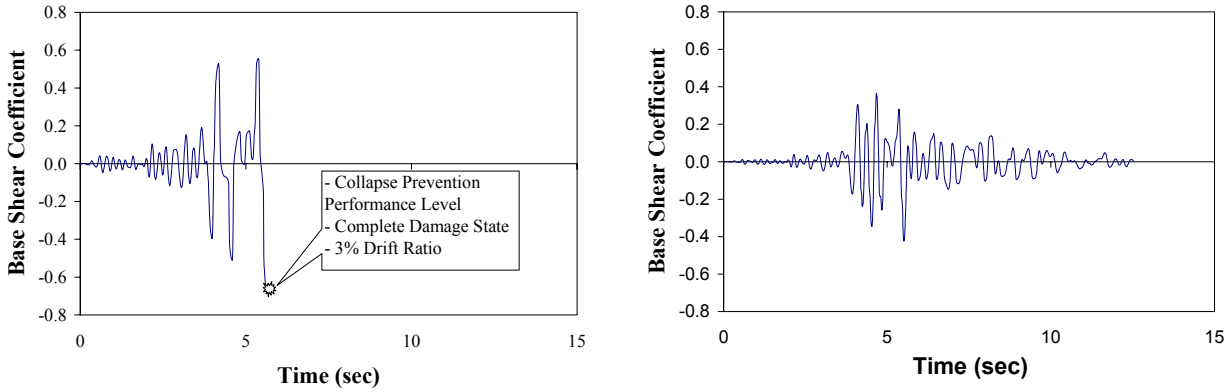

No Damper **C = 87.6 kN-s/m (500 lb-s/in)**

Figure 4-23 - Time-History of the Base Shear Coefficient for the Wall With and Without Fluid Dampers Subjected to the Newhall Record.

The seismic input energy level for the wall without a damper was much higher in magnitude compared to that with a damper, as seen in Figure 4-24. The increase in viscous energy and the reduction in inelastic energy demand on the wall results from the application of the fluid damper.

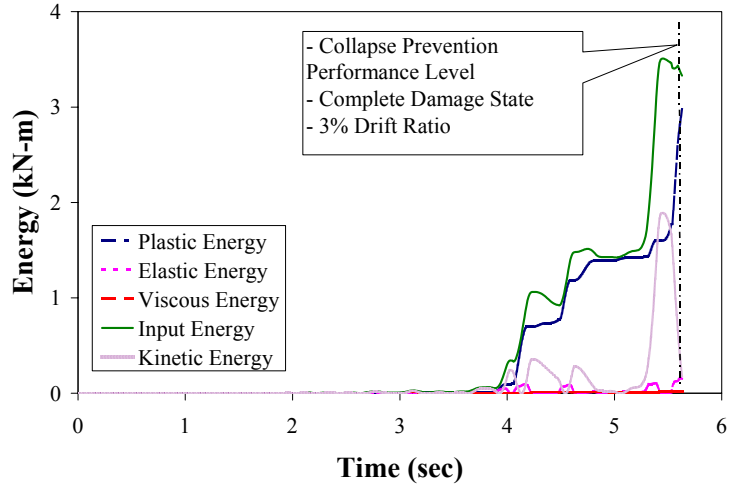

(a) No Damper

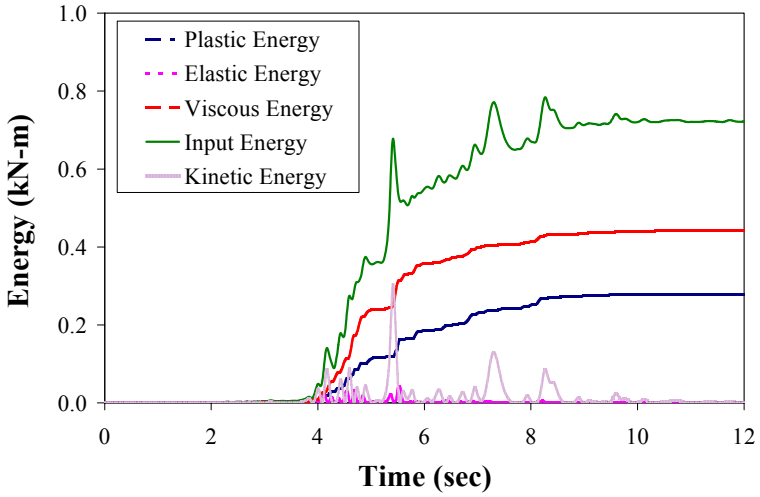

(b) C = 87.6 kN-s/m (500 lb-s/in)

Figure 4-24- Energy Distribution Over Time Within the Wall for the Newhall Record

5. Two-Story Three–Dimensional Wood Frame Building Model

5.1 Introduction

The details of the correlation between a typical 2.4 m (8 ft) x 2.4 (8 ft) shear wall model and experimental data were presented in Chapter 4. With that, the intention of modeling a two-story three-dimensional house with multiple shear walls and various configurations was carried out by using a calibrated Simplified Equivalent Shear Wall Model (SESWM). The SESWM was calibrated by comparing the results of static and dynamic analyses to those of the experimental tests of Dolan (1989) and the predictions from the detailed shear wall model described in Chapter 4. The results obtained from the analyses closely matched those from both the experimental and the analytical predictions, but the SESWM has significantly fewer degrees of freedom than the detailed shear wall model described earlier. Thus, it was considered to be appropriate for performing nonlinear seismic analysis of a two story, three – dimensional structure. The analyses of this Chapter were used to further evaluate the performance of viscous fluid dampers for use in timber structures.

5.2 Two-Story Three–Dimensional Wood Frame Building Model

5.2.1 Geometry of the Building

The dimensions of the building modeled herein were 5.79 m x 7.32 m x 2.4 m (19 ft x 24 ft x 8 ft), which was similar to the full-scale, two-story, light-framed wood residential building recently tested on a shake table at the University of California at San Diego (UCSD) as part of the CUREE-Caltech Wood Framed Project by Fischer et al. (2001*)*. The plan dimensions of the UCSD building are 4.88 m x 6.10 m (16 ft x 20 ft) with nominal story heights of 2.44 m (9 ft).

Modifications in dimension were made so that the 2.44 m x 2.44 m (8 ft x 8 ft) SESWM described in Section 5.5.2 could be directly used in the building model.

The elevation and the plan views of the building model are presented in Figure 5-1 (a) and Figure 5-1 (b), respectively. In Figure 5-1 (b), the solid rectangles indicate the location of shear walls and the blanks indicate empty spaces in walls, where windows or doors are likely to be placed. Two different versions of the building were analyzed, one with symmetric placement of wall panels and the other with asymmetric placement, which is most common in practice. The finishing materials and the interior partition walls were not included in the model. The building model was meant to capture the global behavior of buildings similar to the UCSD building, but not to exactly represent any specific building. The goal was to a numerically investigate the effectiveness of supplemental fluid dampers on reducing damage in three-dimensional timber structures via this building model.

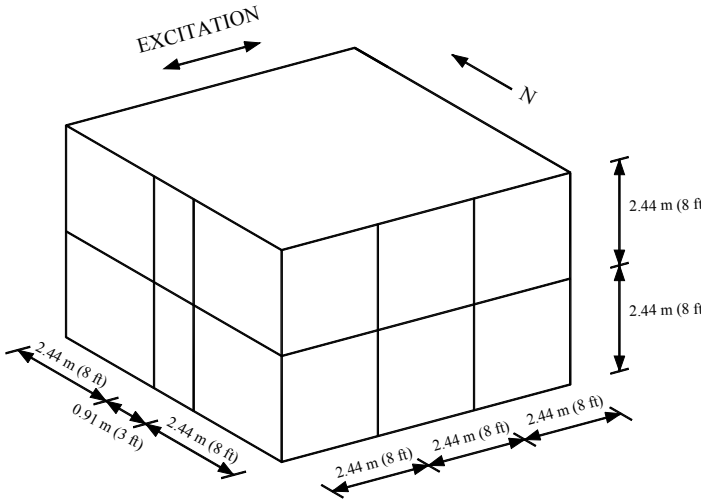

(a)

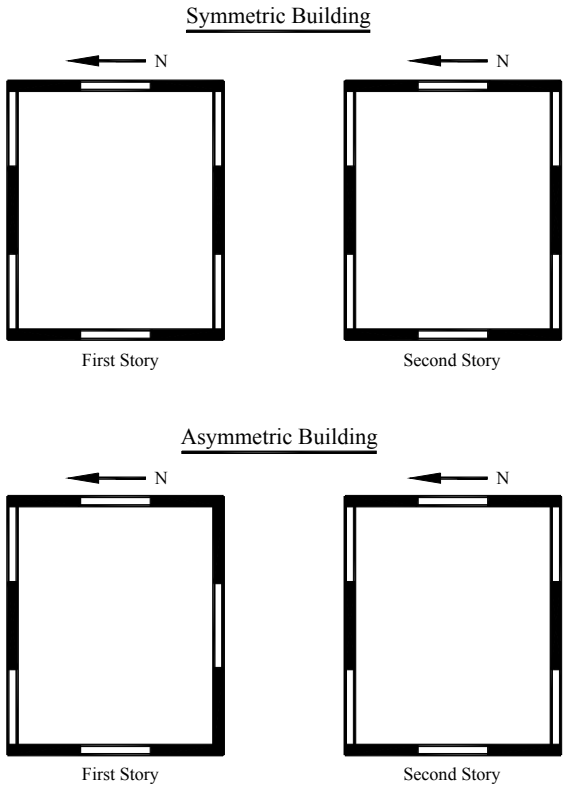

(b)

Figure 5-1 – Two-Story Three-Dimensional Building Model: (a) Isometric View of both Symmetric and Asymmetric Building and, (b) Plan Views of Symmetric and Asymmetric Building (solid rectangles indicate location of shear walls).

5.2.2. Calibration of the Simplified Equivalent Shear Wall Model (SESWM)

A Simplified Equivalent Shear Wall Model (SESWM) was calibrated against the detailed shear wall model via static and dynamic simulations. The resistance to shear force in wall is provided by sheathing panels and sheathing-to-frame connections. Without these sheathing panels, the studs, sill plate, and sole plate would form a racking mechanism. To simulate these phenomena, truss elements were used to form the framing system of the simplified equivalent shear wall. The two vertical elements of the framing members were designed to have significant higher axial stiffness relative to shear stiffness. The two vertical framing members were to carry vertical loads from the roof and upper stories.

Two diagonal springs were used as shear resisting elements, as illustrated in Figure 5-2. Their hysteretic behavior was defined according to the connection elements described in Chapter 3, i.e., the same mathematical form of backbone and hysteresis loops defining connection elements were used herein to define the spring elements. The reason for this is the fact that the entire shear resistance is dominated by the connections between sheathing and framing members. The values of the parameters that define the hysteretic behavior of the simplified shear wall are presented in Table 5-1. These parameters were calibrated via both static and seismic simulations through which the responses were compared to make sure that equivalent performance was achieved. Comparisons of the response to static pushover analysis and to dynamic seismic analysis are shown in Figure 5-3 and Figure 5-4. The first 9-second portion of the Taft earthquake record was used in the seismic analysis due to the limitation in computer storage (see Figure 4-11 (a)). Figure 5-3 shows that there is close agreement between the simplified and the

detailed wall models with static pushover analysis. Figure 5-4 indicates differences in peak response and displacement in seismic evaluation while the shape of the loops from both models remains similar. It appears that the detailed wall was slightly stronger than the SESWM and allowed slightly larger displacement. This is expected because only two single brace elements were used to define the simplified model, rather than a large number of nail elements used in defining the detailed model. The SESWM experienced a lack of convergence prior to the final hysteresis loop. The reason for that is due to the fact that the brace loses strength abruptly compared to the multiple nail connectors in the detailed model. There are total of 126 connector elements in the detailed model. Each brace in SESWM is equivalent to 61 connector elements in the detailed model. Once a brace yields, it is as if 61 connector elements in the detailed model yield at the same time. But, in fact, each connector yielded one at a time. Therefore, the detailed model did not show the abrupt failure that was observed in the SESWM.

Although the simplified model is not an exact representation of the detailed shear wall model, it is deemed adequate for the purpose of modeling the two-story building by which the effect of viscous fluid dampers on the seismic response of the building could be evaluated.

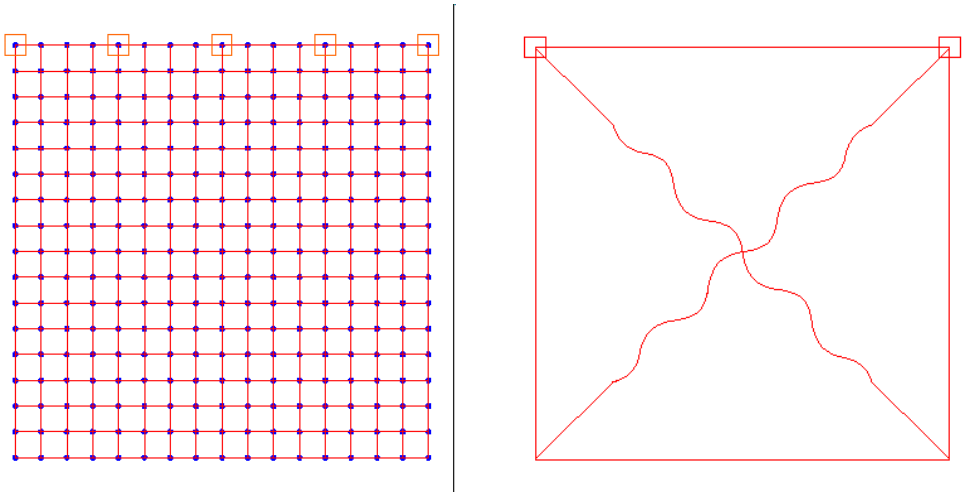

(a) **(b)**

Figure 5-2 – Shear Wall Finite Element Models: (a) Detailed Shear Wall and (b) Simplified Shear Wall.

Table 5-1: Values of Parameters Defining SESWM.

P_o	P_1	K_0	K_2	K_3	K_4	u_{ult}
915 N (2600 lb)	180 N (387 lb)	1320 N/mm (25000 lb/in)	39 N/mm (600 lb/in)	-3.0 N/mm (-1464 lb/in)	29.5 N/mm (2311 lb/in)	15.24mm (1.0 in.)

The definition of each parameter is explained in Section 3.3.3.

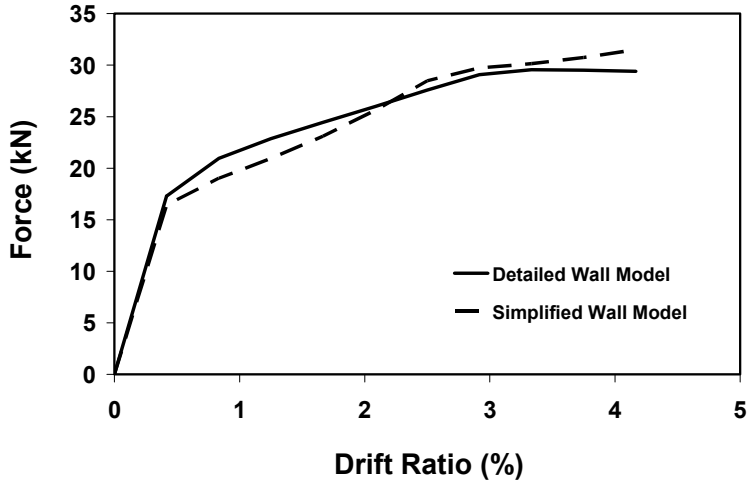

Figure 5-3 –Static Pushover Response for Detailed Wall Model and Simplified Wall Model.

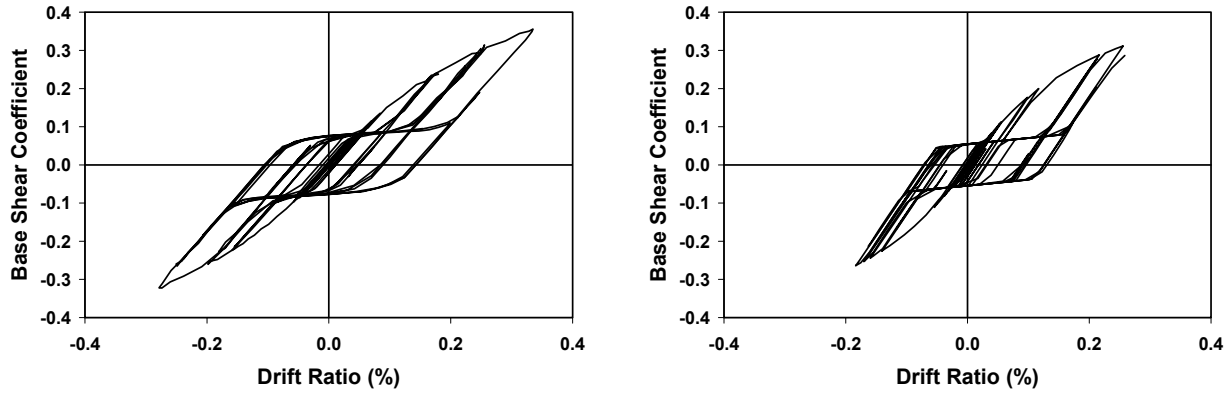

(a) Detailed Wall Model (b) Simplified Wall Model

Figure 5-4 –Seismic Response When Subjected to Taft Record: (a) Detailed Wall Model and, (b) Simplified Wall Model.

5.2.3. Finite Element Model of a Three Dimensional Wood Framed Building

A two-story three-dimensional nonlinear finite element model of a wood-framed building was developed for numerical analyses using the commercial program, ABAQUS (ABAQUS,

1998) (see Figure 5-5). As stated in Section 5.2.1, the dimensions of the building were adjusted in order to directly apply the 8 ft x 8 ft (2.44 m x 2.44 m) wall model in the building model. As a result, the size of all panels in the building model was 8 ft x 8 ft (2.44 m x 2.44 m) and represented by the SESWM. Truss elements were used for studs, which were designed to carry self weight and lumped masses to match the specimen and assigned much higher axial stiffness than shear stiffness to act as rigid diaphragms, the roof and floor were considered to have much higher in-plane stiffness relative to the in- plane shear stiffness of shear walls. The diaphragms were modeled using 4-node, isoparametric shell elements.

The total mass of the building included the contribution from roof, floor, and walls. The weight densities for roof, floor, and shear walls were assigned according to *Design of Lateral Forces* by Ambrose and Vergun (1987). The distribution of the weight was on the basis of tributary area. For the roof and floor, the mass was distributed to the nodes on top of the studs at the perimeter of the diaphragms. Half of the weight from the walls on the second story was lumped to the roof level and the other half assigned to the first floor level. Half of the weight of the first story was lumped to the first floor level and the other half lumped to the ground level. The resulting total mass was 8,344 kg (47.6 lb-s^2/in). The distribution of the total mass is listed in Table 5-3. The description of the building elements and their average weights that were used to calculate the total building weight and mass density are presented in Table 5-2. The thickness of both the floor and the roof was assumed to be 7.62 cm (3 in.). Two versions of the building model were used in this study, one symmetric and one asymmetric. For the asymmetric case, an additional wall panel was added to create a large opening in the first story on the south side of

the building (see Figure 5-1(b)). The weight of the additional panel was not accounted for since it was only 3.5% of the total weight of the symmetric building.

Table 5-2 – Dead Weight of Building Element

Elements	Description	Weight (N/m^2) / (lb/ft^2)	Mass Density (Kg/m^3) (lbm/in^3)
Roofs	Light wood frame, 3-fly felt plus gravel, gypsum drywall ceiling	575 (12)	1.993 (7.2×10^{-5})
Floors	Wood joist, plywood deck, carpet, drywall ceiling	479 (10)	1.661 (6.0×10^{-5})
Walls	Exterior, wood studs, wood siding, drywall	479 (10)	1.661 (6.0×10^{-5})

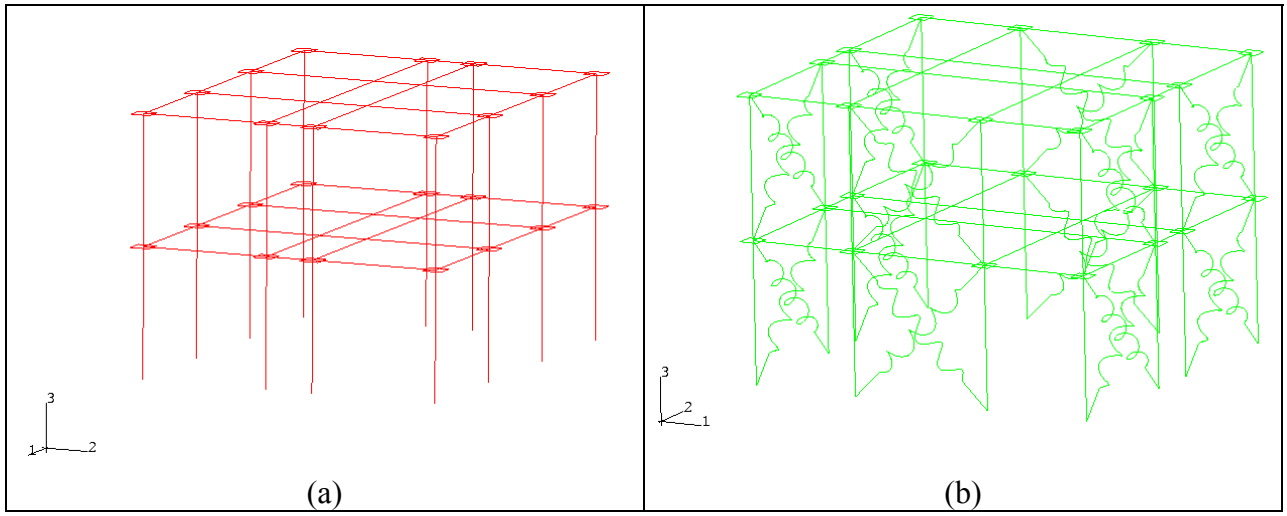

Figure 5-5 - Finite Element Model of Wood-Framed Building: (a) Shear wall panels are not shown, and (b) Shear wall panels are where braces are shown.

Table 5-3 – Mass Distribution of Wood Building Model

Vertical Location of Lumped Mass	Mass kg (lb-s^2/in)
Roof Level	3,353 (19.13)
Floor Level	3,811 (21.74)
Ground Level	1,180 (6.73)
Total Mass	8,344 (47.6)

5.3 Effect of Fluid Dampers on the Seismic Response of the Three Dimensional Wood Frame Building

5.3.1 Dynamic Properties of the Building (Eigenvalue Analysis)

Standard Eigenvalue analysis was conducted on both the symmetric and asymmetric building models. The analysis yielded natural frequencies corresponding to each eigen modes. Using these results, the inherent damping of the buildings was accounted for via Rayleigh damping by assuming damping ratios of 2% and 10% associated with lower and upper bound frequency values. Rayleigh damping coefficients pertaining to East - West and North - South directions were obtained by using the lower and upper bound natural frequencies associated with East-West and North-South directions, respectively. The Eigenvalue analysis predicted 4.38 Hz, 6.21 Hz, and 8.29 Hz for natural frequencies in the East-West translation mode, North-South translation mode, and torsion mode, respectively, for the symmetric case. For the asymmetric case, the corresponding frequencies for the three modes were 5.03 Hz, 6.21 Hz, and 8.71 Hz, respectively, which were very close to those for the symmetric case (listed in Table 5-4). The first ten mode shapes for the two versions of the building model are basically the same. Figure 5-

6, Figure 5-7, and Figure 5-8 show the first ten eigen modes of the symmetric building model. Eigen modes for the asymmetric building model are not shown.

Table 5-4 – Natural Frequencies of The Three – Dimensional Building Model

	Natural Frequencies (Hz)		
	First Mode (E - W translation)	Second Mode (N - W translation)	Fifth Mode (Torsion)
Symmetric Building	4.38	6.21	8.29
Asymmetric Building	5.03	6.21	8.71

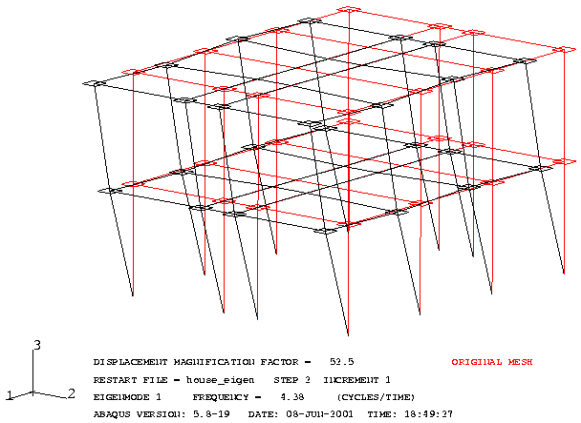

(a) Mode 1

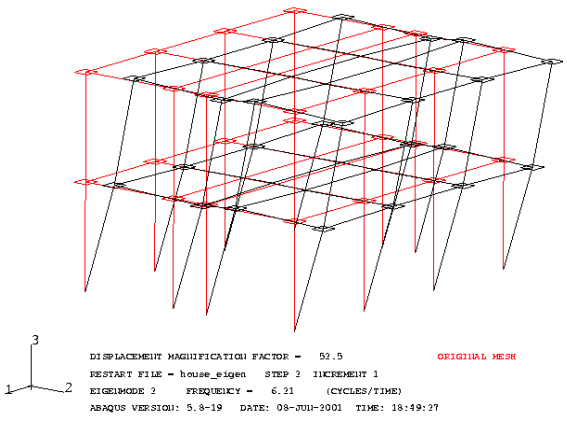

(b) Mode 2

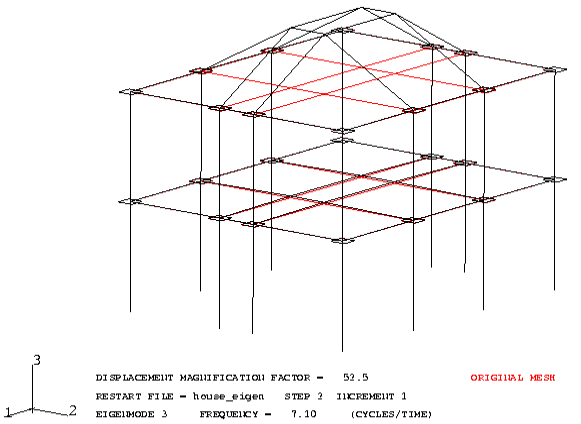

(c) Mode 3

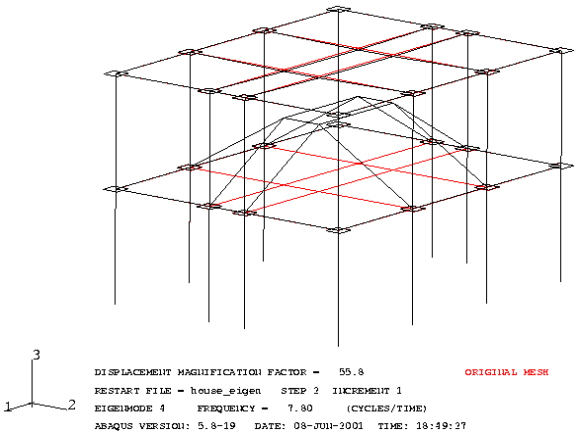

(d) Mode 4

Figure 5-6 – Eigen Modes 1-4 of the Symmetric Building Model.

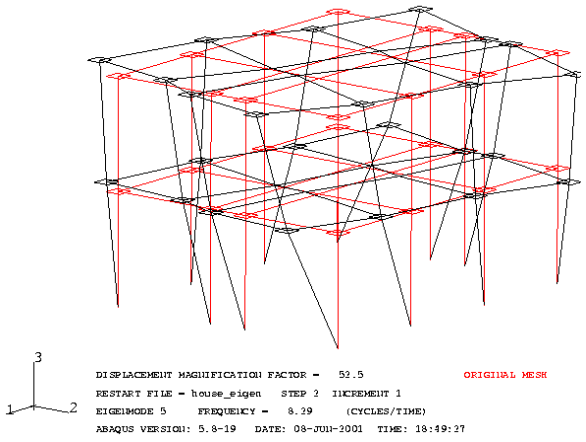

(e) Mode 5

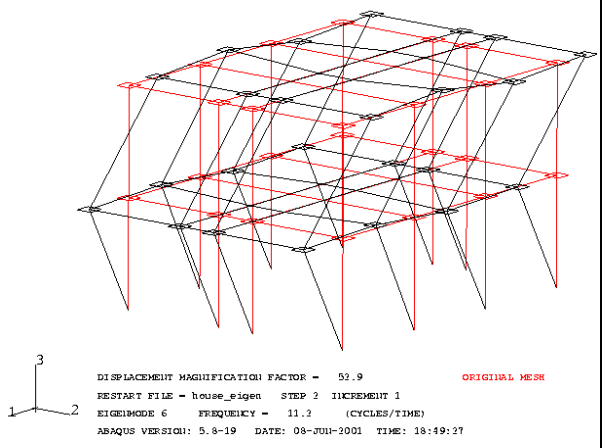

(f) Mode 6

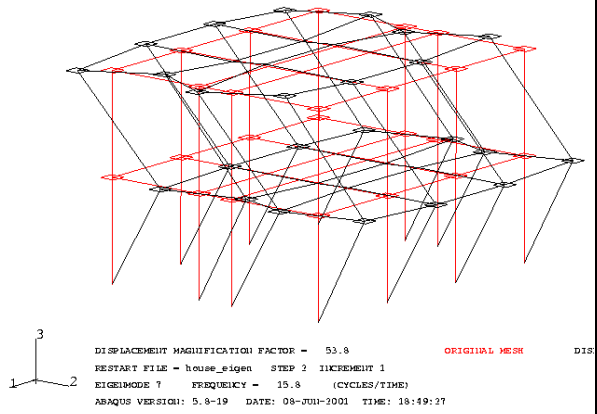

(g) Mode 7

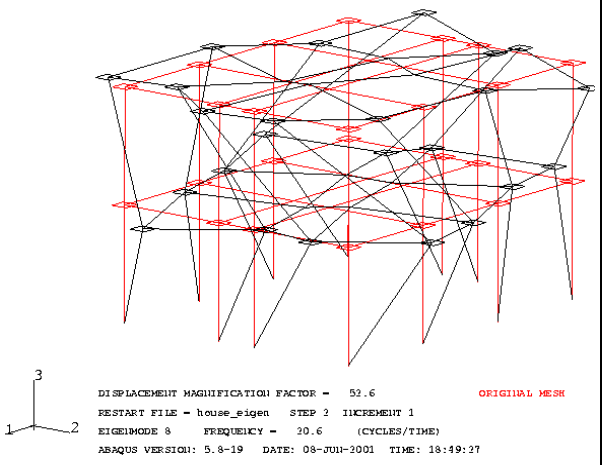

(h) Mode 8

Figure 5-7 –Eigen Modes 5-8 of the Symmetric Building Model.

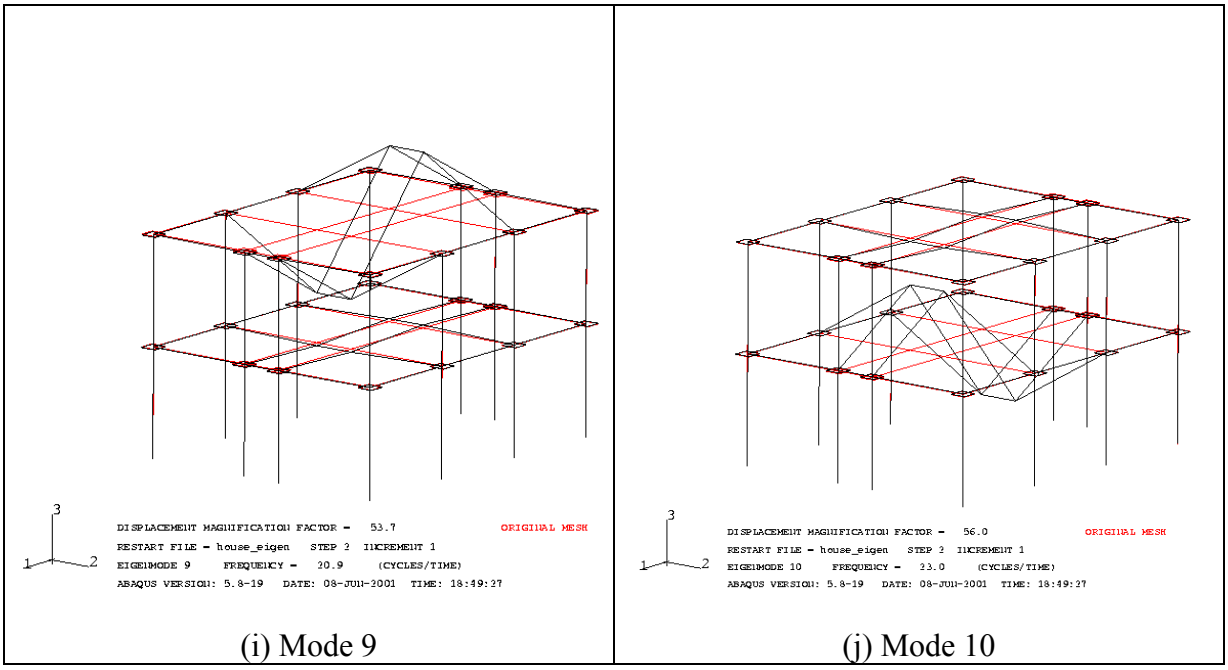

(i) Mode 9 (j) Mode 10

Figure 5-8 –Eigen Modes 9-10 of the Symmetric Building Model.

The stiffness and mass proportional damping coefficients pertaining to the East-West direction for symmetric and asymmetric cases are listed in Table 5-5.

Table 5-5 – Rayleigh Damping Coefficients Associated With East-West Direction – Seismic Excitation Direction

	Frequency (Hz)		Damping Ratio (%)		Stiffness Proportional Damping α (sec.)	Mass Proportional Damping β (rad./sec.)
	Lower bound	Upper bound	Lower bound	Upper bound		
Symmetric Building	4.38	22.0	2	10	0.00145	0.00521
Asymmetric Building	5.03	23	2	10	0.0009	0.38473

5.3.2 Seismic Response of the Symmetric Building

The damping coefficient of the dampers used herein was 87.6 kN-s/m (500 lb-s/in). They were installed along the diagonal of each shear wall on the first story (see Figure 5-9 (a)). As shown in Figure 5-9 (a), only a single damper was installed within each shear wall. The earthquake records of Taft and Newhall are shown in Figure 4-11 (b). The seismic excitation was applied to the weak direction of the building, which is along the East-West axis, parallel to the plane of the large opening on the first floor for the asymmetric case (see Figure 5-1 (a) and Figure 5-9 (b)).

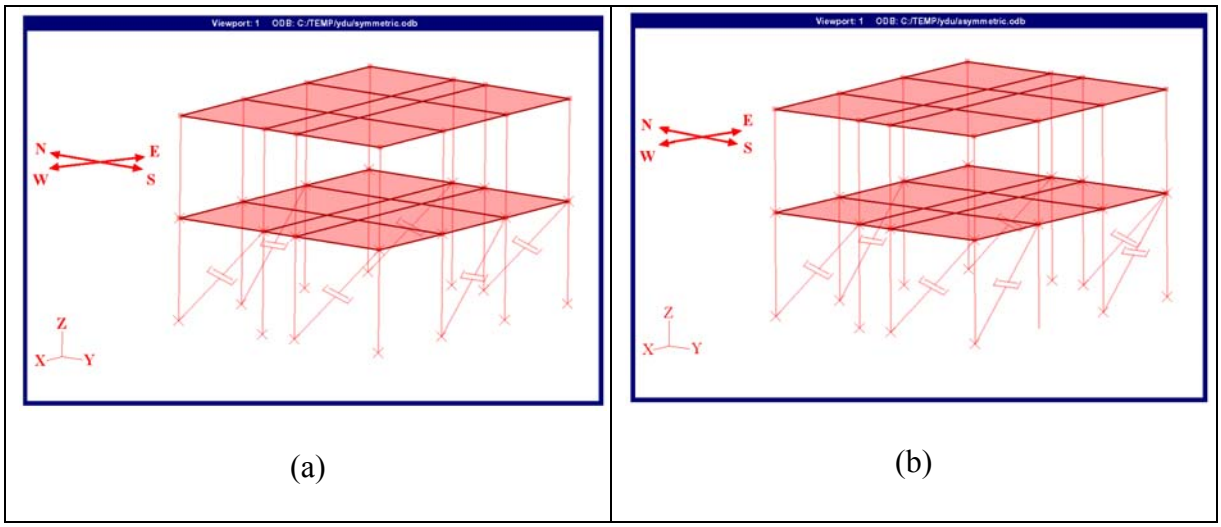

Figure 5-9 – Buildings with Dampers: (a) Symmetric Building, and (b) Asymmetric Building.

The intention was to see the effect of the fluid dampers on both symmetric and asymmetric buildings. The analysis consisted of the first 15 seconds of the earthquake record due to limitations of computer storage. This is considered acceptable since the major earthquake motion occurred within that 15 seconds as shown in Figure 4-11.

5.3.2.1 Symmetric Building Subjected to the Far-Field Earthquake (Taft Record) – Kern County Earthquake

The hysteresis loops for the first story and the second story of the building with and without dampers are shown in Figure 5-10 and Figure 5-11, respectively. As expected, the first story had a larger value of drift ratio than the second for both cases. A qualitative comparison between the two cases indicates that the hysteresis loop for the first story with dampers has round corners rather than sharp corners as observed in the hysteresis loop without dampers. In addition, the area within the pinching zone of the loop with dampers is much larger than the one without dampers. These differences are all within expectation due to the supplemental damping from the dampers. As for the performance level and damage state of the first story without dampers, a Peak Drift Ratio of 0.238% implied that the first story experienced slight damage with minor cracking at the Immediate Occupancy Performance level according to *NEHRP Guidelines* (FEMA 1997) (see Table 4-3). For the case with dampers, the Peak Drift Ratio of the first story reduced to 0.135%, which indicated that the building was at Operational Performance level with no damage. The dampers led to approximately a 53% reduction in the Peak Drift Ratio in the first story. Such distinction between the two cases can also be seen in term of the peak Base Shear Coefficient. Without dampers, the peak Base Shear Coefficient was about 0.324; with dampers, the peak Base Shear Coefficient reduced to 0.256. The reduction was about 21%. Second story shear was normalized with respect to the weight of the building. A similar reduction for the second story was also observed. The second story of the building exhibited a much smaller drift ratio and it was within the Operational Performance level in both cases (see Table 5-6).

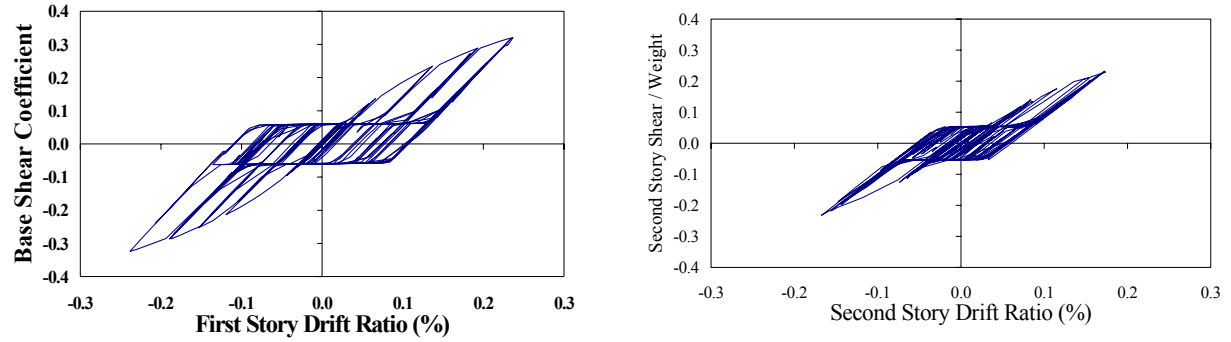

Figure 5-10 – Hysteresis Loops of the Symmetric Building Without Fluid Dampers Subjected to the Taft Record (*plotted to same scale*).

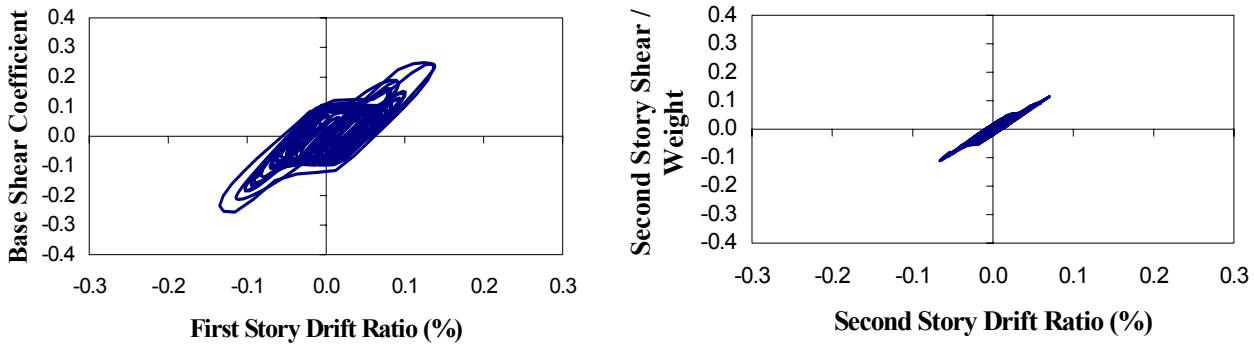

Figure 5-11 – Hysteresis Loops of the Symmetric Building With Fluid Dampers Subjected to the Taft Record (*plotted to same scale*).

The energy time history plots for both cases are presented in Figure 5-12. An obvious sign of role switching between inelastic energy and viscous energy is shown. Without dampers installed, 97% of the total seismic input energy was dissipated within the building system in the form of inelastic energy as seen in Figure 5-12 (a). However, with dampers installed, only 40% of the total seismic input energy was dissipated within the structure. The reduction of the inelastic energy as a percentage of the total seismic energy was around 73%, which is rather

significant. This reduced portion of the inelastic energy would have been demanded of the building structure had no dampers were installed. As to viscous energy, for cases without and with dampers, the viscous energy was 0.00211 kN-m (18.68 lb-in) and 0.39 kN-m (3452 lb-in), respectively. Viscous energy was negligible for the former case. The dampers were able to provide a dramatic increase in energy dissipated in the form of viscous energy. The total seismic input energy without and with dampers was 1.0 kN-m (8851 lb-in) and 0.683 kN -m (6045 lb-in), respectively. The reduction in total seismic input energy was roughly 31.7%.

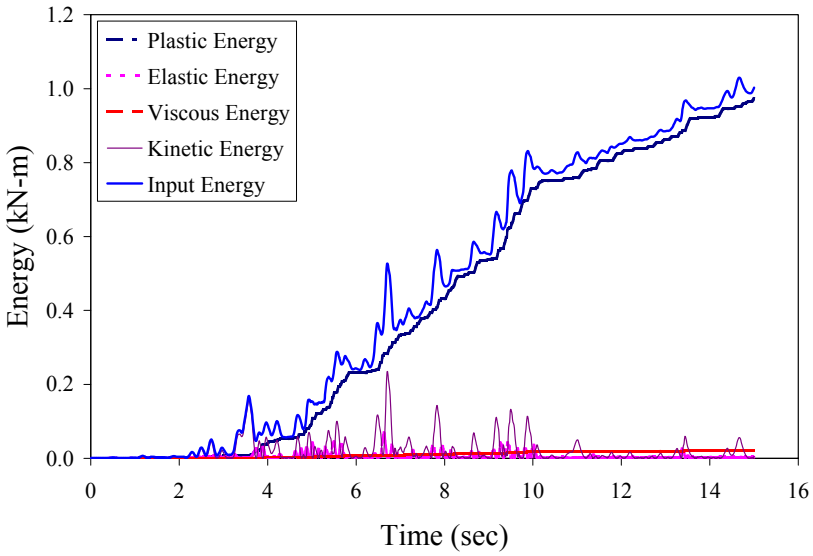

(a) Without Dampers

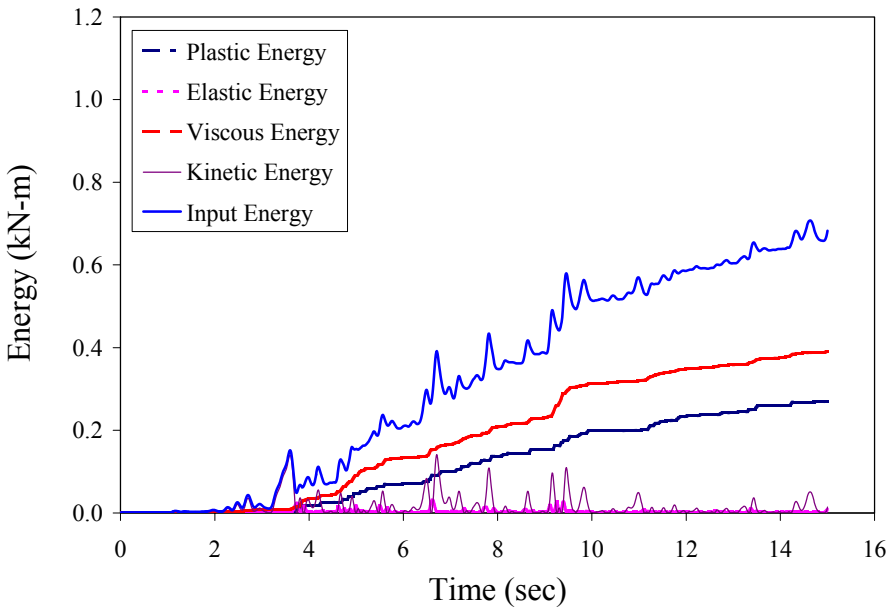

(b) With Dampers

C = 87.6 kN-s/m (500 lb-s/in)

Figure 5-12 - Energy Distribution Over Time for the Symmetric Building Without and With Fluid Dampers Subjected to the Taft Record (*plotted to same scale*).

The time-history of the Drift Ratio (see Figure 5-13 and Figure 5-14) for the symmetric building without and with fluid dampers depicts the reduction in drift ratio over time.

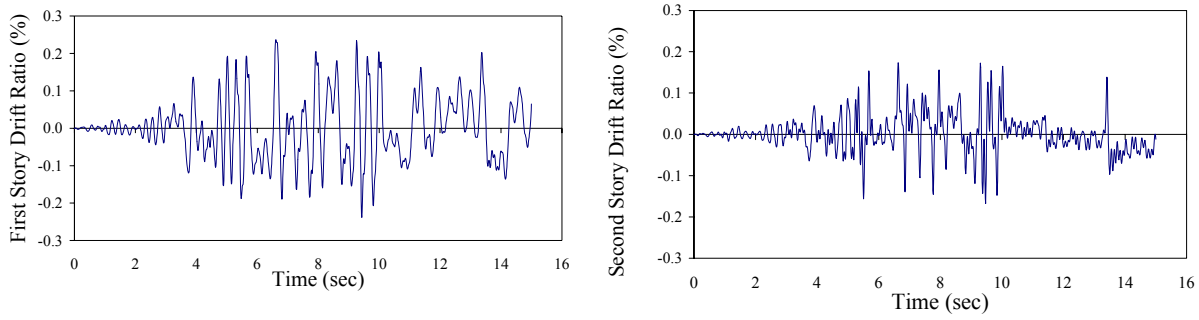

Figure 5-13 – Drift Ratio Time History of the Symmetric Building Without Fluid Dampers Subjected to the Taft Record.

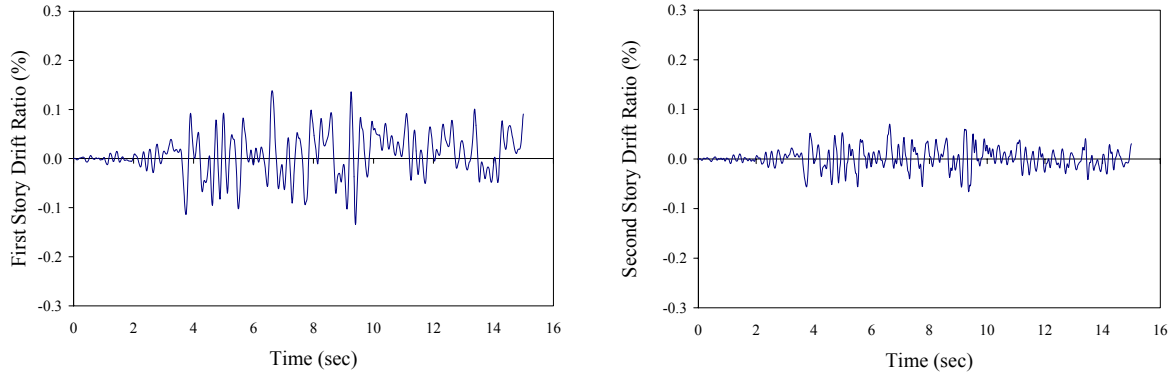

Figure 5-14 - Drift Ratio Time History of the Symmetric Building With Fluid Dampers Subjected to the Taft Record (plotted to same scale as Figure 5-13).

Table 5-6 - Summaries of the Seismic Response When the Symmetric Building Was Subjected to the Taft Record

		Without Fluid Dampers	With a Fluid Dampers C = 87.6 kN-s/m (500 lb-s/in)	Reduction (%)	Increase (%)
Peak Drift Ratio (%)	First Story	0.238	0.135	43	
	Second Story	0.173	0.00636	96	
Peak Base Shear Coefficient		0.324	0.256	21	
Second Story Shear/ Weight		0.232	0.115	50	
Input Energy	Total (kN-m) (lb-in)	1.0 8851	0.683 6045	31.7	
Viscous Energy	Total (kN-m) (lb-in)	0.00211 18.68	0.39 3452		18383
	Percentage of Input Energy (%)	0.211	57		
Inelastic Energy	Total (kN-m) (lb-in)	0.974 8620	0.27 2390	72	
	Percentage of Input Energy (%)	97.4	40		

5.3.2.2 Symmetric Building Subjected to The Near-Field Earthquake Motion (Newhall Record) - Northridge Earthquake

The Newhall record of the Northridge earthquake caused much more sever damage to the building systems when no dampers were installed compared to the case with dampers. The building collapsed after 5.71 seconds into the earthquake, as indicated by extremely large deflections and non-convergence. The hysteresis loops for the first story and the second story of the building with and without dampers are shown in Figure 5-15 and Figure 5-16, respectively. For the case without dampers, only activities of the first 5.71 seconds are shown for all related

plots. The effectiveness of the viscous dampers can be seen by comparing the hysteresis plots as well as the drift time history plots in terms of performance level and damage state. The first story without dampers reached a drift ratio larger than 3%, which led to complete damage of the building. With dampers, the first story had a Peak Drift Ratio of 1.24%, which implied that the first story experienced extensive damage with large cracks across shear walls at the Life Safety performance level according to *NEHRP Guidelines* (FEMA 1997) (refer to Table 4-3), but without collapse.

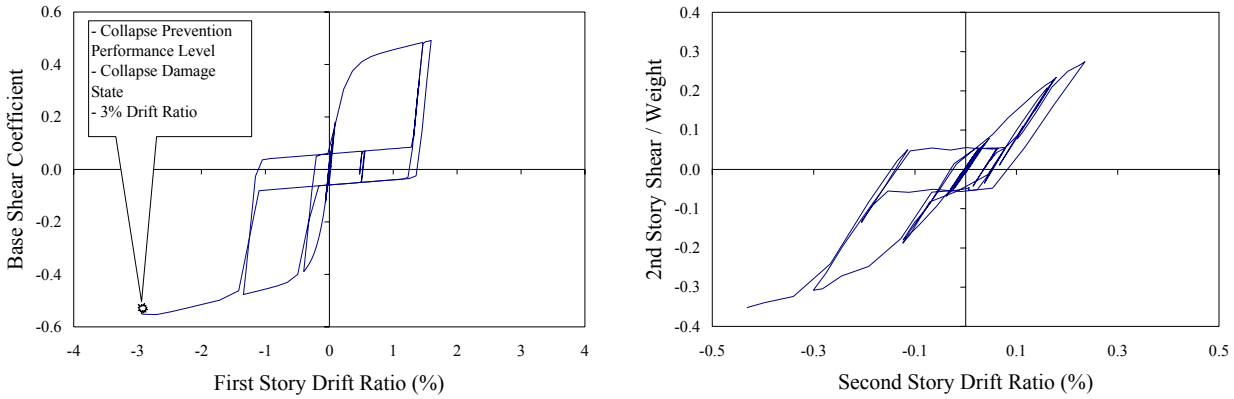

Figure 5-15 – Hysteresis Loops of the Symmetric Building Without Fluid Dampers Subjected to the Newhall Record (*not plotted to same scale*).

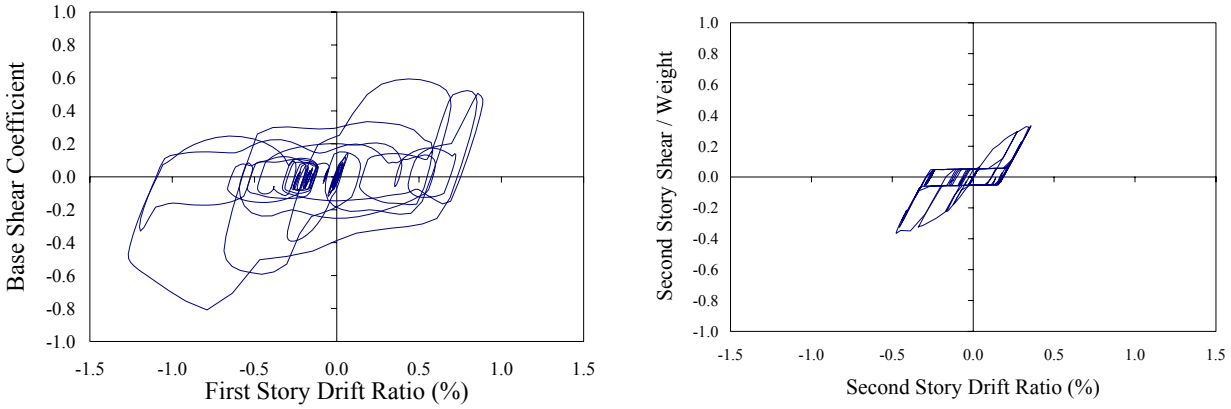

Figure 5-16 – Hysteresis Loops of the Symmetric Building With Fluid Dampers Subjected to the Newhall Record (*plotted to same scale*).

The energy time history plots for both cases are presented in Figure 5-17. 5.71 seconds into the earthquake, the viscous energy level for the case without dampers was much lower than that for the case with dampers. In addition, the plastic energy level was much higher for the case without dampers than that for the one with dampers. The high demand in inelastic energy on the building structure led to its collapse. The viscous dampers were able to bring inelastic energy demanded down to 44.4 % and dissipate 55.4 % of the total seismic input energy (See Table 5-7 for summary). The above shows that the viscous dampers were very effective when the symmetric building was subjected to the near-field earthquake.

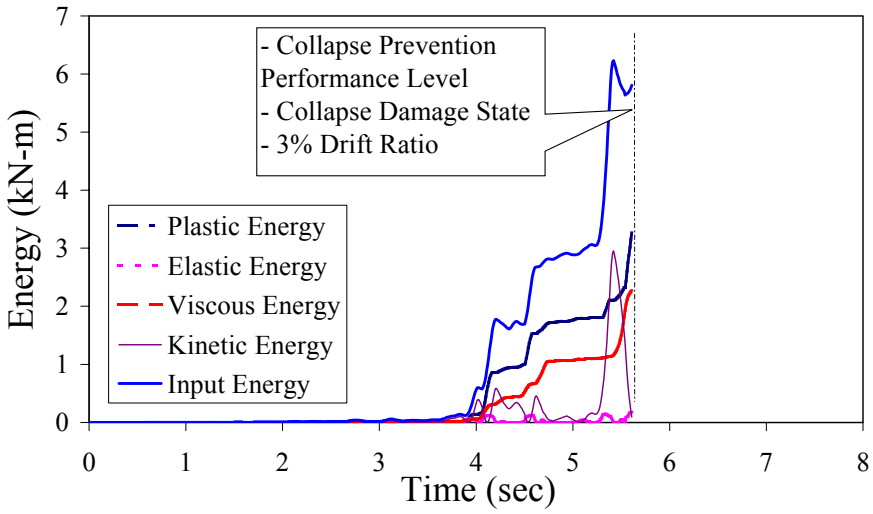

(a) Without Dampers

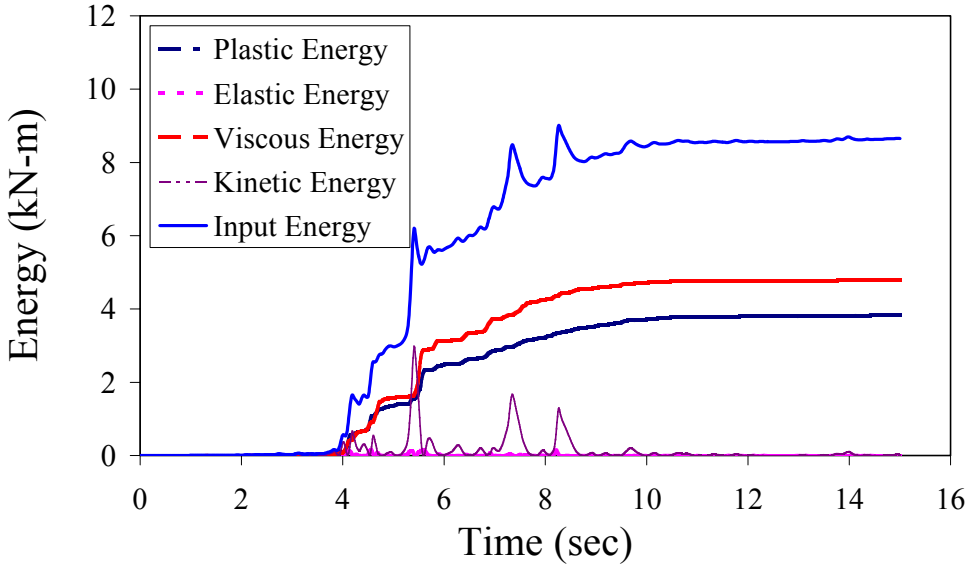

(b) With Dampers

C = 87.6 kN-s/m (500 lb-s/in)

Figure 5-17 - Energy Distribution Over Time for the Symmetric Building Without and With Fluid Dampers Subjected to the Taft Record.

The time-history of the Drift Ratio (see Figure 5-18 and Figure 5-19) for the symmetric building without and with the fluid dampers depicts the reduction in the drift over time. With dampers, the drift ratio was at Life Safety performance level with large cracks across shear walls, but again without collapse.

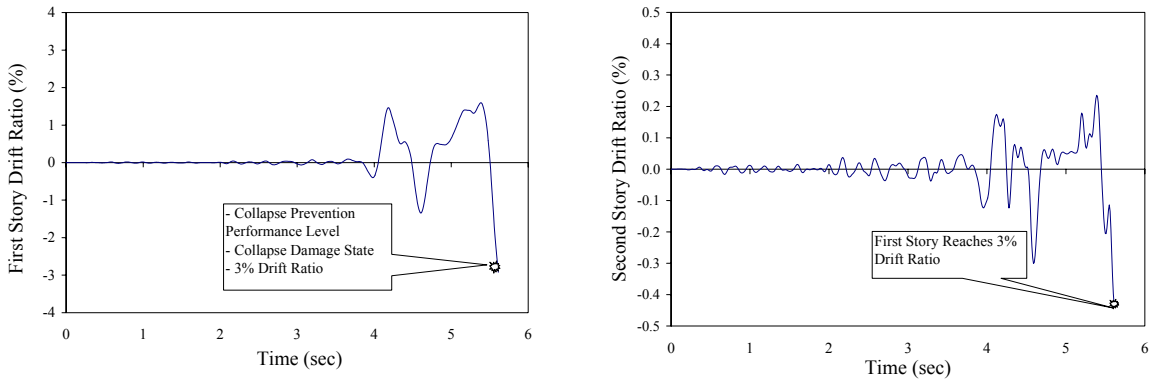

Figure 5-18 – Drift Ratio Time History of the Symmetric Building Without Fluid Dampers Subjected to the Newhall Record.

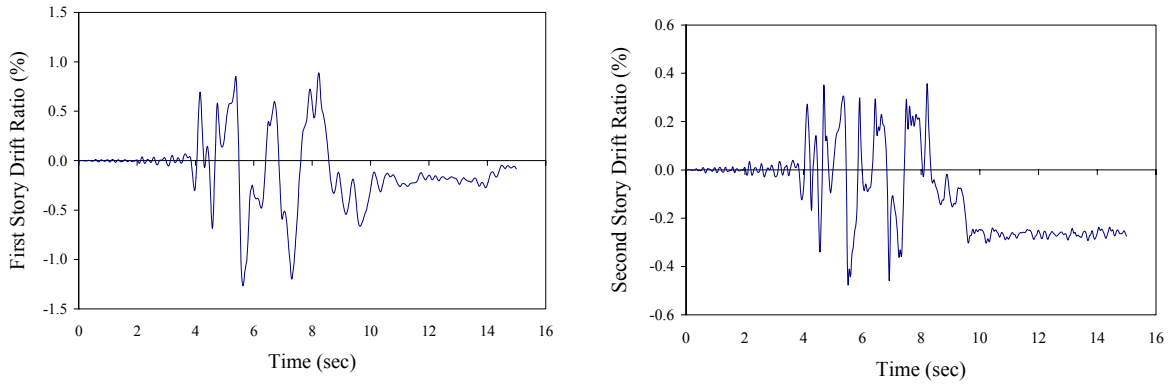

Figure 5-19 - Drift Ratio Time History of the Symmetric Building With Fluid Dampers Subjected to the Newhall Record (C = 87.6 kN-s/m (500 lb-s/in)).

Table 5-7 - Summaries of Seismic Response When Symmetric Building Subjected to the Newhall Record

		Without Fluid Dampers	With a Fluid Dampers C = 87.6 kN-s/m (500 lb-s/in)
Peak Drift Ratio (%)	First Story	*Symmetric Building Collapsed*	1.24
	Second Story		0.475
Peak Base Shear Coefficient			0.809
Second Story Shear/ Weight			0.354
Input Energy	Total (kN-m) (lb-in)		8.66 76647
Viscous Energy	Total (kN-m) (lb-in)		4.80 42484
	Percentage of Input Energy (%)		55.4
Inelastic Energy	Total (kN-m) (lb-in)		3.83 33898
	Percentage of Input Energy (%)		44.4

5.3.3 Seismic Response of the Asymmetric Building

The asymmetric building underwent rotational displacement in addition to the translational displacement when subjected to seismic excitations. The placement of the fluid dampers was not designed to minimize the displacement and the rotation of the building, although their placement could be chosen for that purpose. The results of the analyses confirm the effectiveness of the fluid dampers through aspects such as the hysteresis loops of the base

shear coefficient versus the drift ratio, energy level, and the drift ratio time history. Comparisons were made between the two cases, that is, with and without the fluid dampers installed.

5.3.3.1 Asymmetric Building Subjected to The Far-Field Earthquake Motion (Taft Record) – Kern County Earthquake

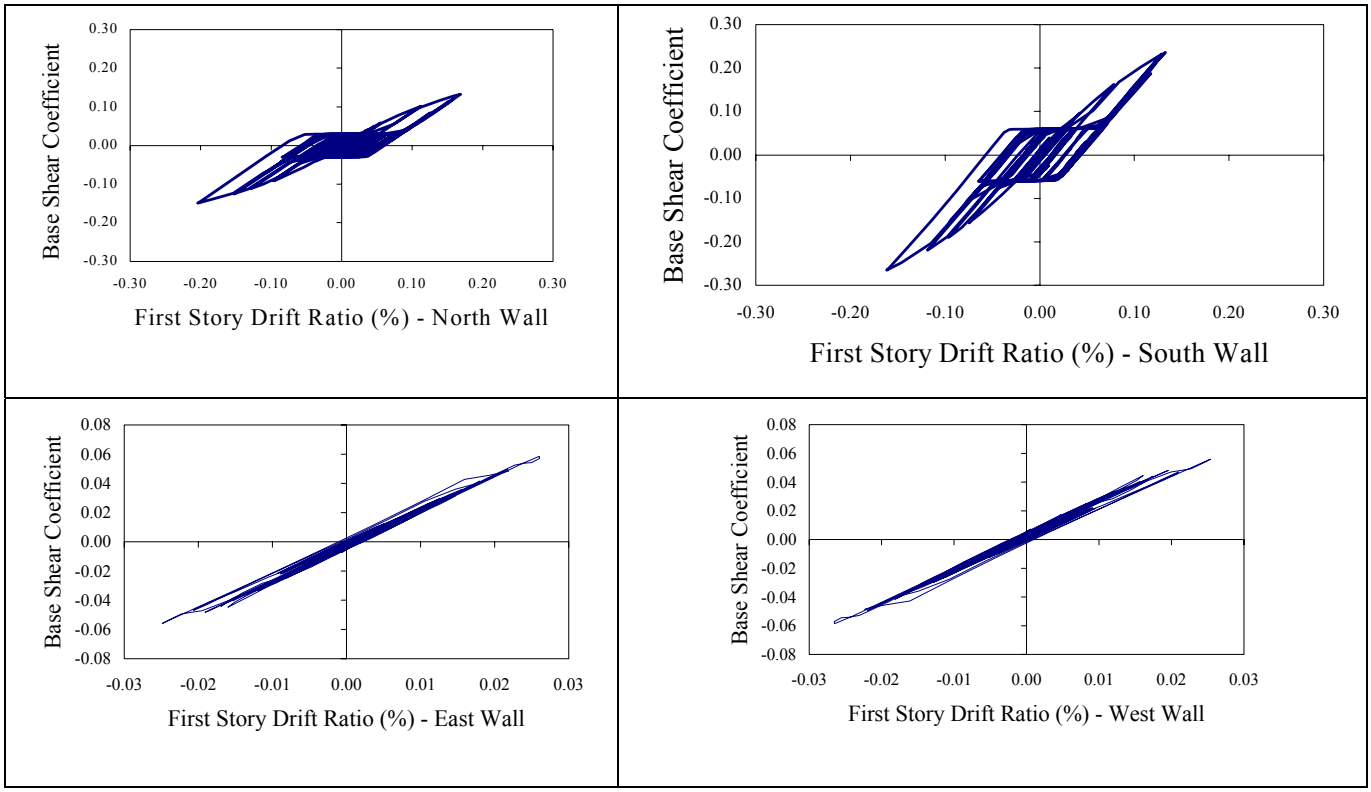

Figure 5-20 – Hysteresis Loops of the Asymmetric Building Without Fluid Dampers Subjected to the Taft Record.

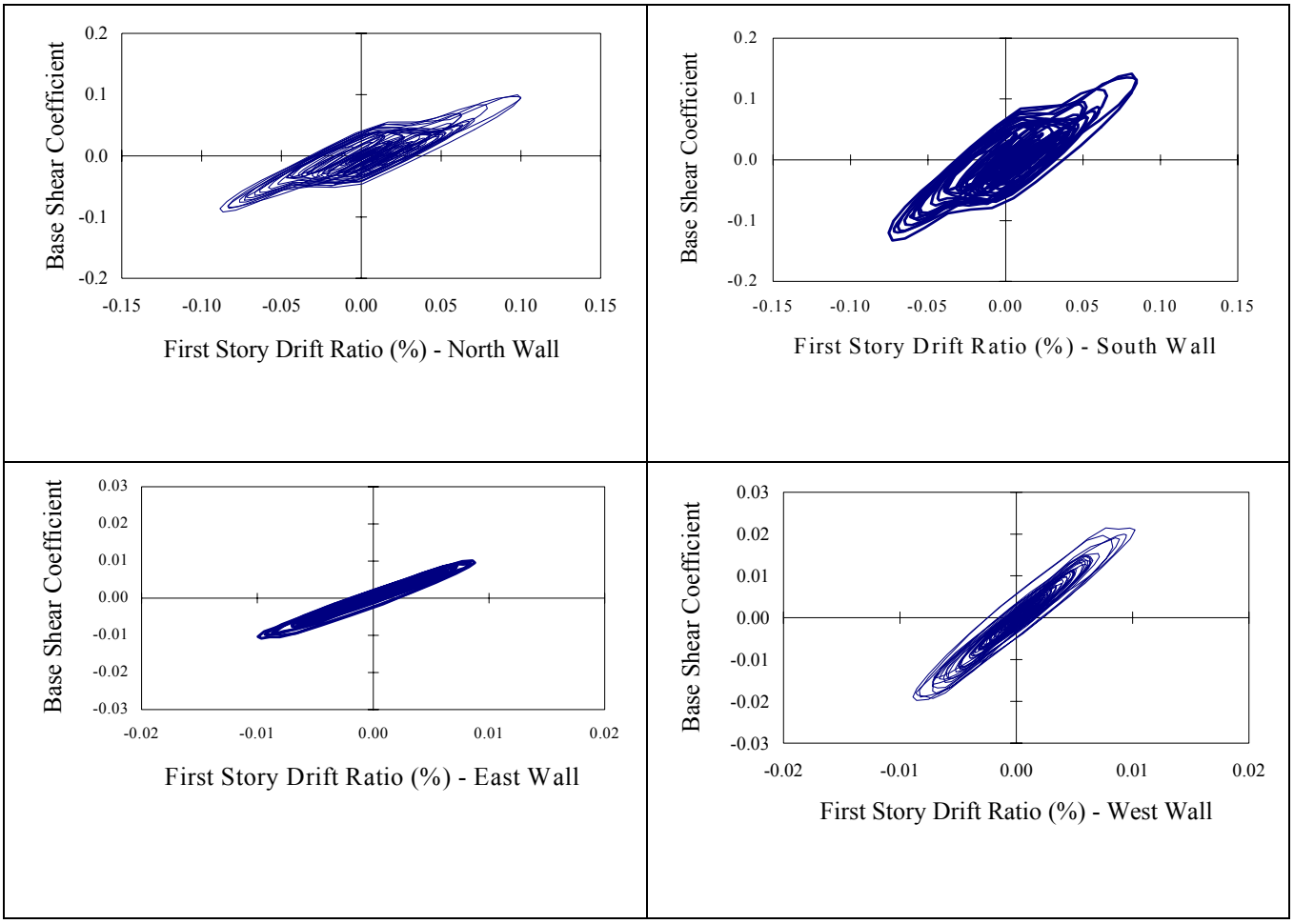

Figure 5-21 - Hysteresis Loops of the Asymmetric Building With Fluid Dampers Subjected to the Taft Record.

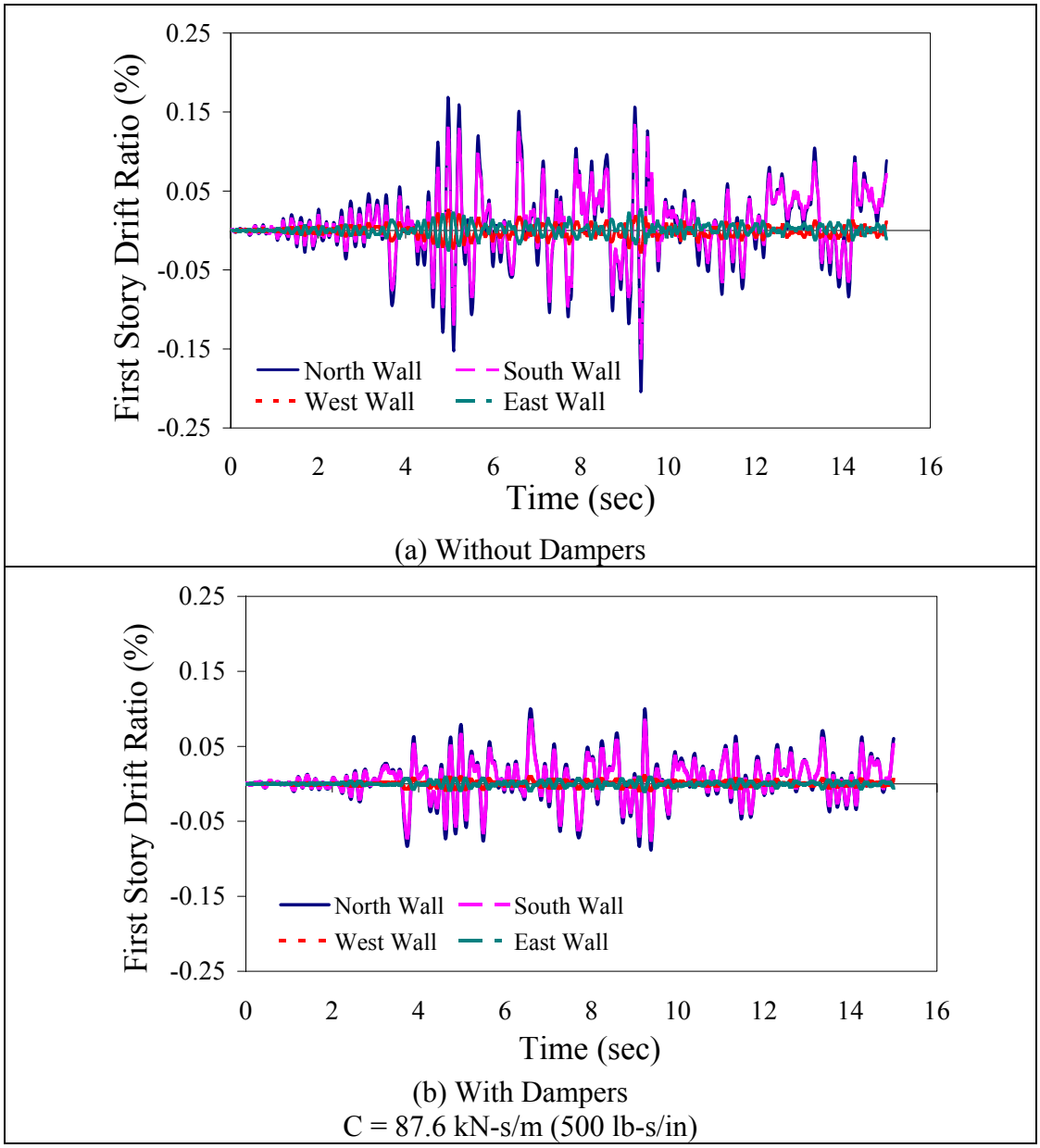

Figure 5-22 – First Story Drift Ratio Time History of the Asymmetric Building Without and With Dampers Subjected To the Taft Record.

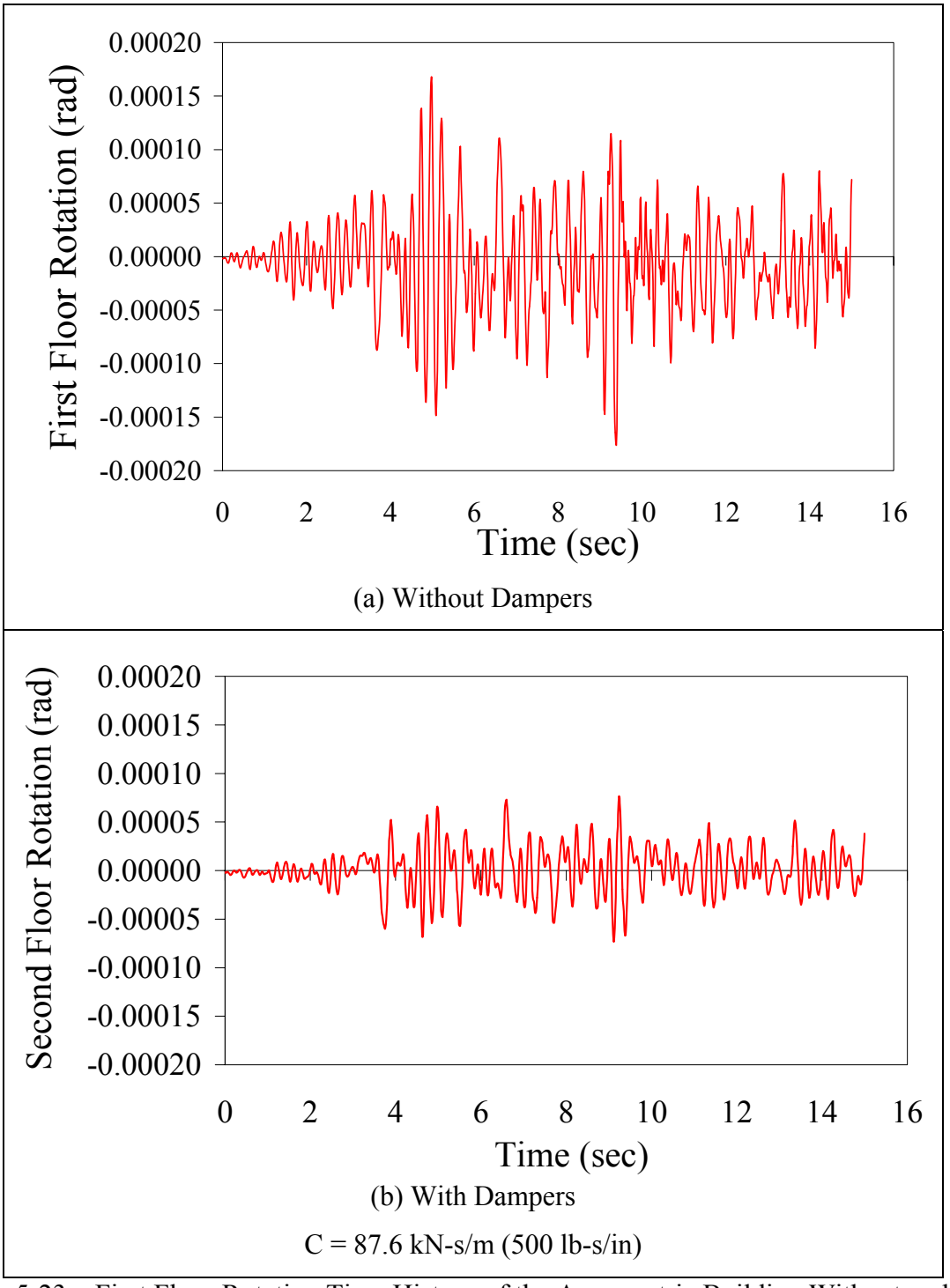

Figure 5-23 – First Floor Rotation Time History of the Asymmetric Building Without and With Dampers Subjected to the Taft Record.

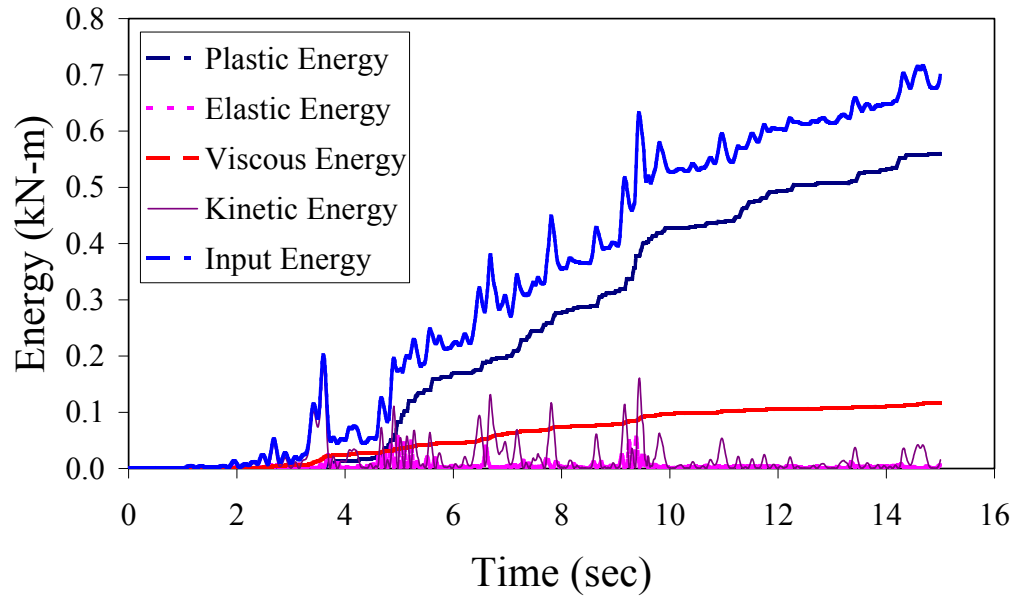

(a) Without Dampers

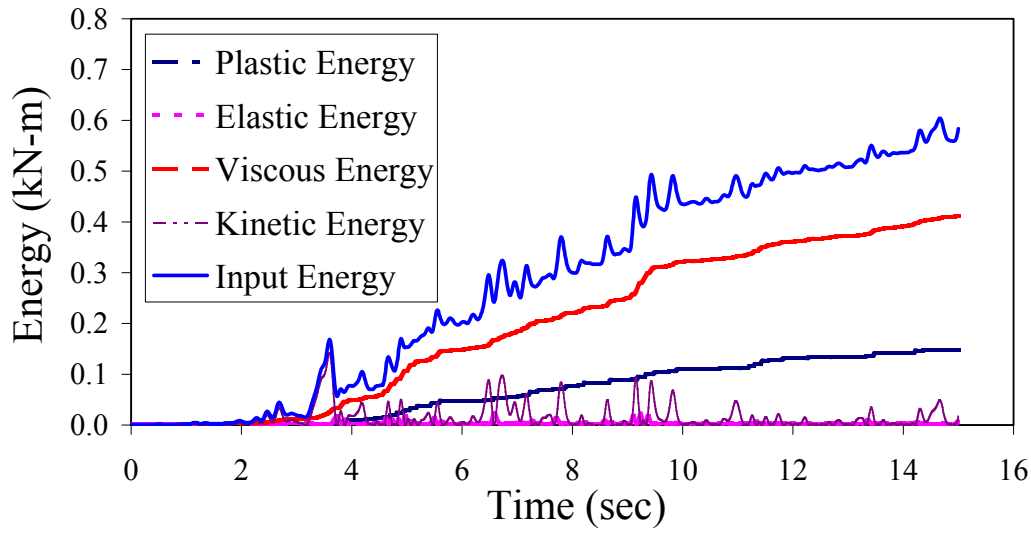

(b) With Dampers

C = 87.6 kN-s/m (500 lb-s/in)

Figure 5-24 - Energy Time History of the Asymmetric Building Without and With Dampers Subjected To the Taft Record.

5.3.3.2 Asymmetric Building Subjected to The Near-Field Earthquake Motion (Newhall Record) – Northridge Earthquake

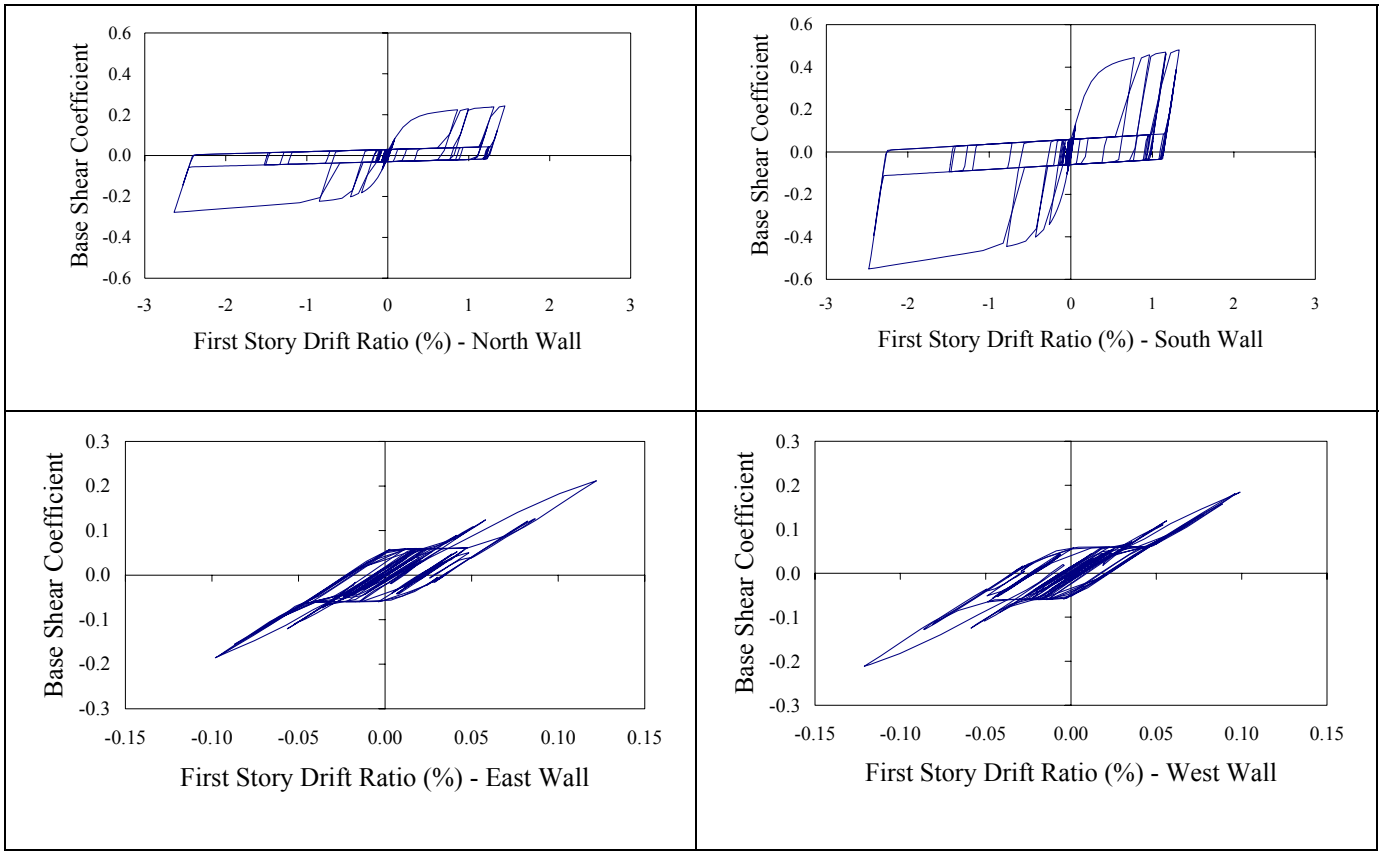

Figure 5-25 – Hysteresis Loops of the Asymmetric Building Without Fluid Dampers Subjected to the Newhall Record.

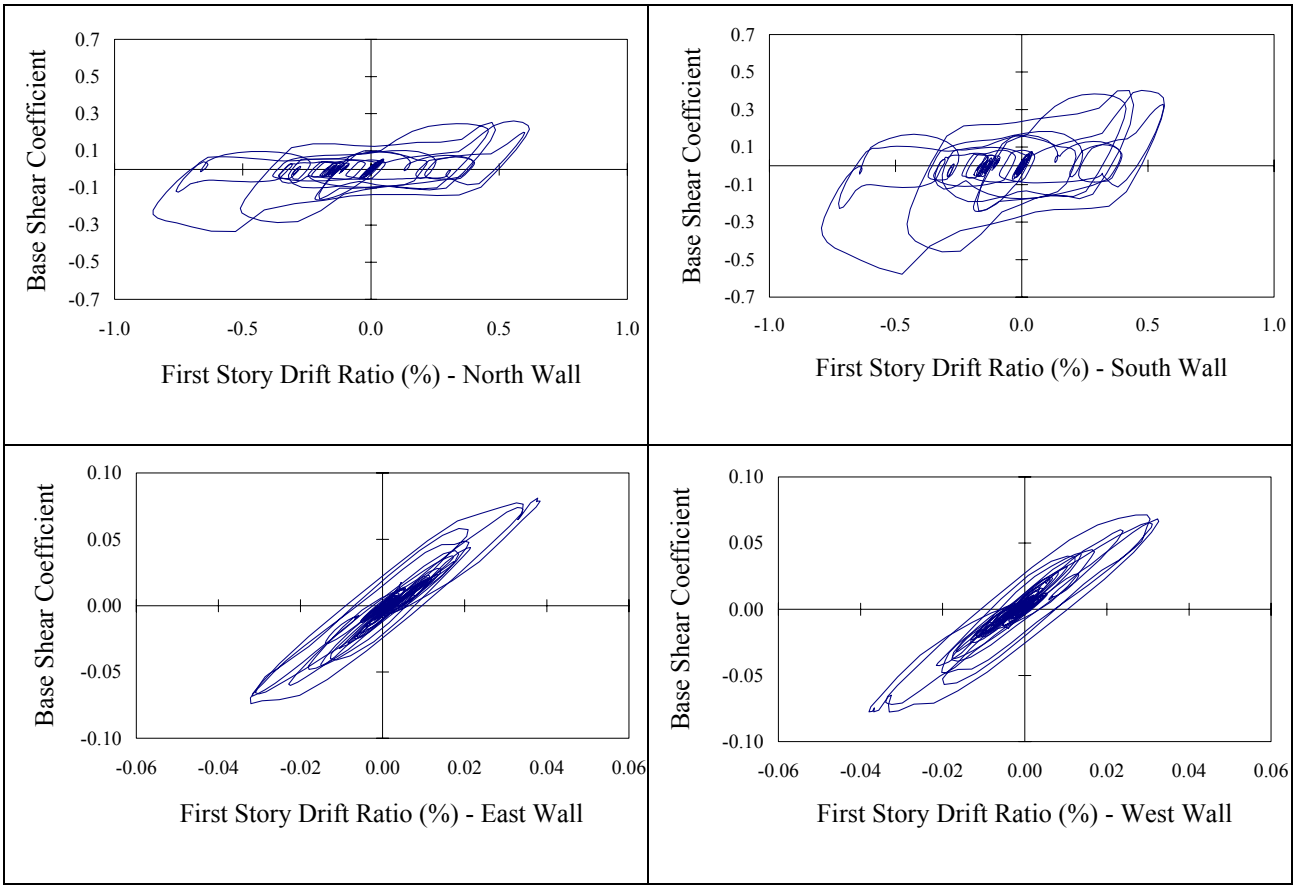

Figure 5-26 - Hysteresis Loops of the Asymmetric Building With Fluid Dampers Subjected to the Newhall Record.

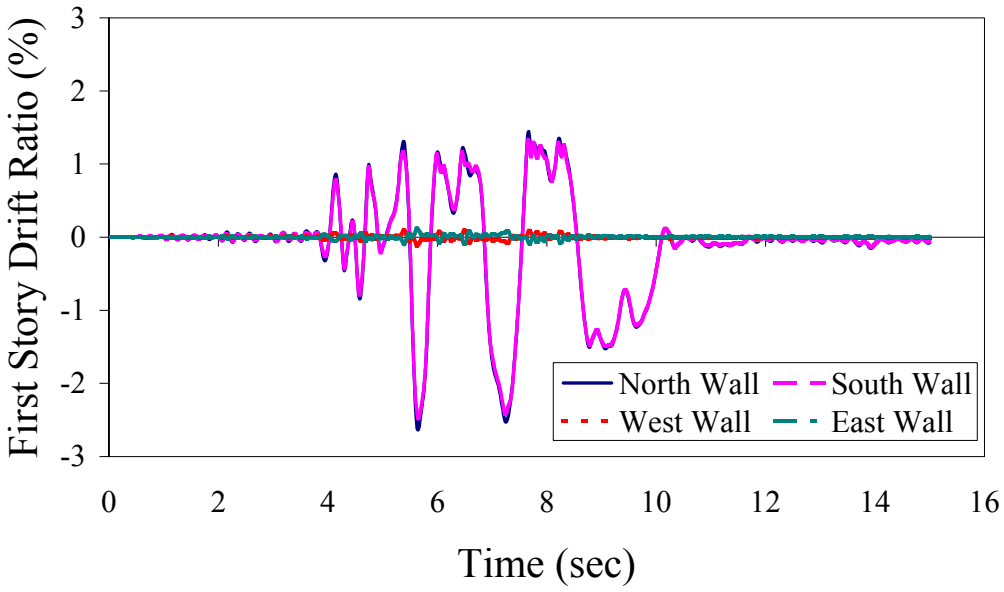

(a) Without Dampers

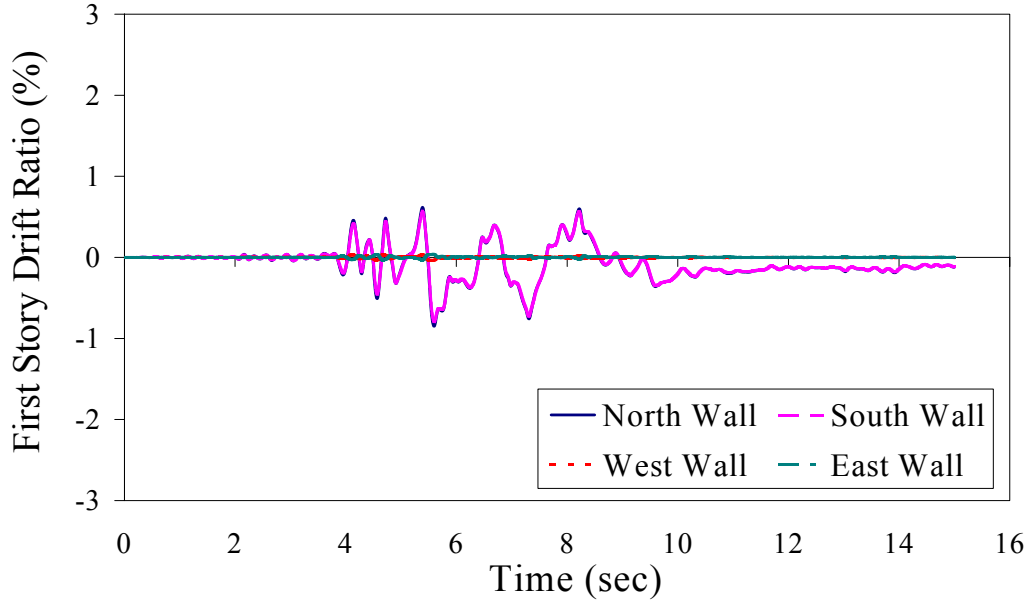

(b) With Dampers

C = 87.6 kN-s/m (500 lb-s/in)

Figure 5-27 – First Story Drift Ratio Time History of the Asymmetric Building Without and With Dampers Subjected To the Newhall Record.

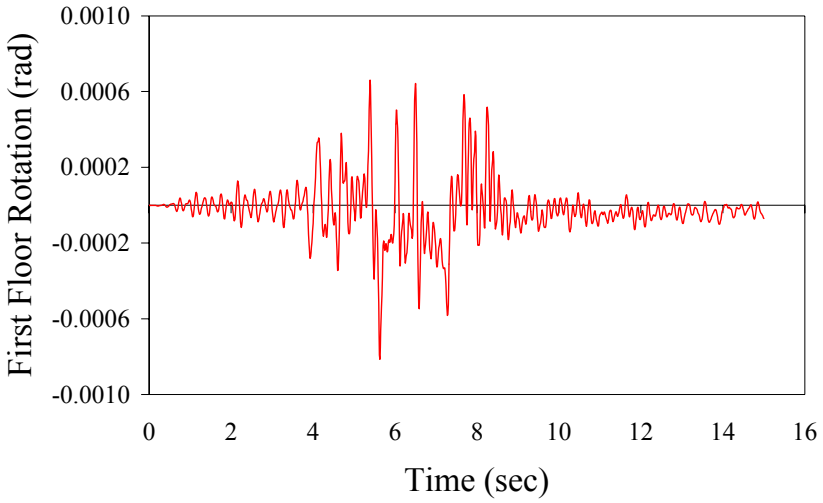

(a) Without Dampers

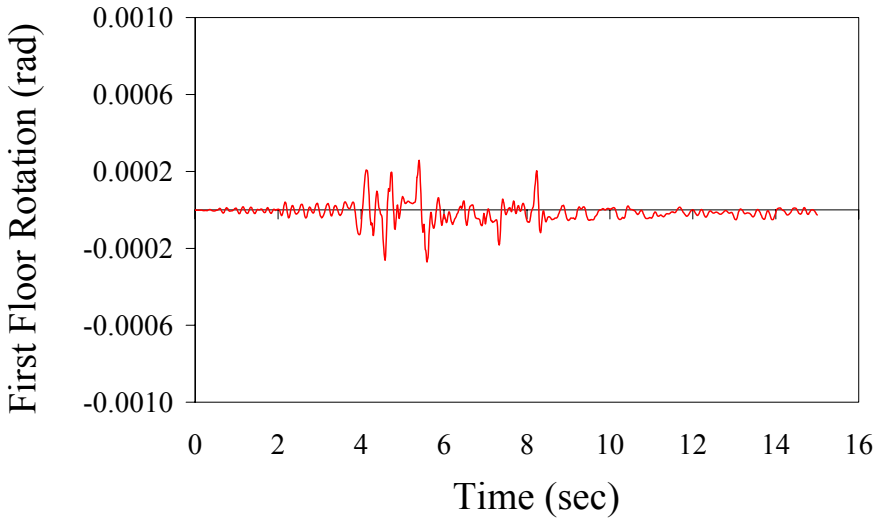

(b) With Dampers

C = 87.6 kN-s/m (500 lb-s/in)

Figure 5-28 – First Floor Rotation Time History of the Asymmetric Building Without and With Dampers Subjected to the Newhall Record.

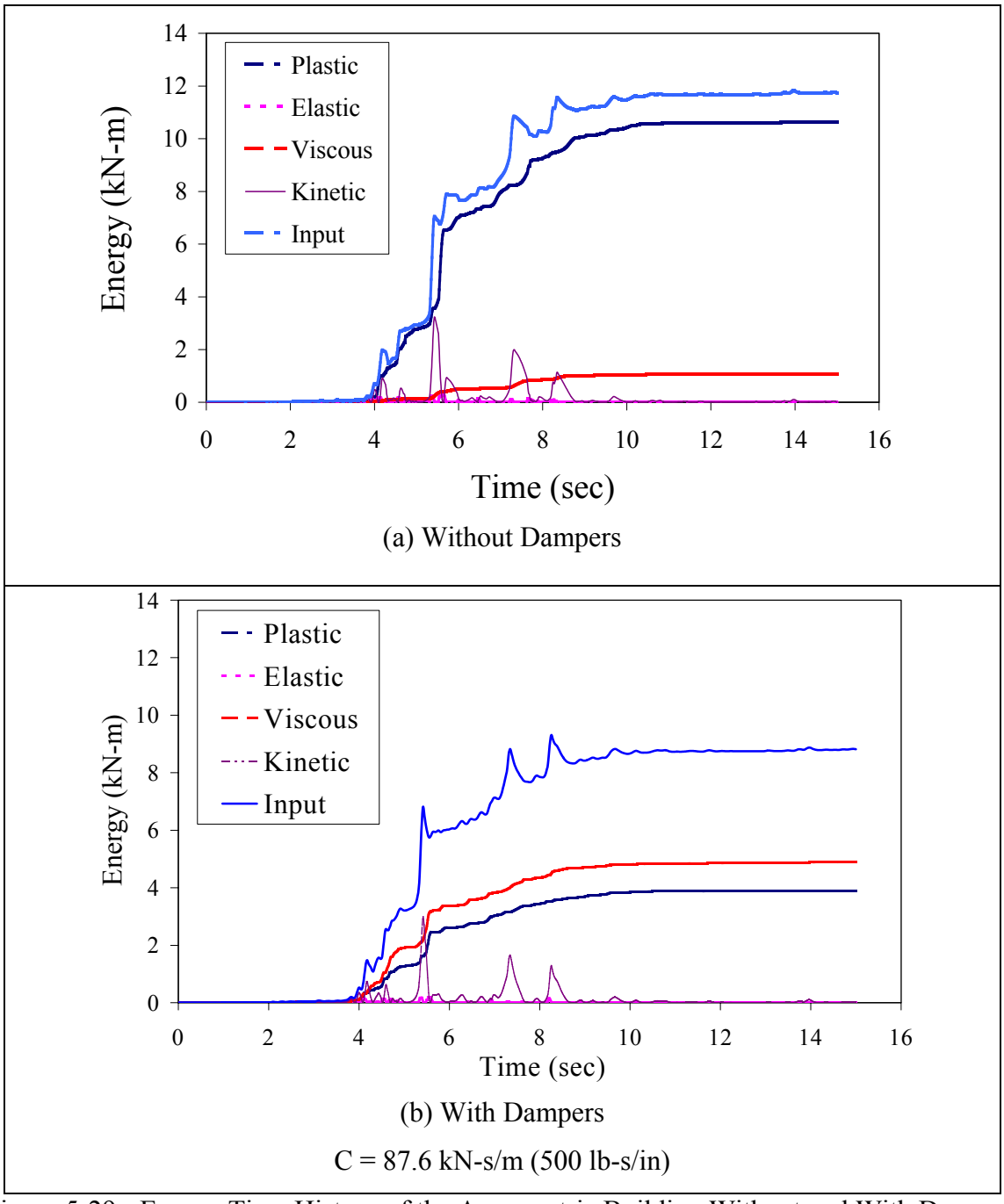

(a) Without Dampers

(b) With Dampers

C = 87.6 kN-s/m (500 lb-s/in)

Figure 5-29 - Energy Time History of the Asymmetric Building Without and With Dampers Subjected To the Newhall Record.

6. Five –Node Model of Wood Framed Shear Wall

6.1 Introduction

In Chapter 4 a successful detailed shear wall model of a standard size 2.4 m (8 ft) x 2.4 (8 ft) was presented. In order to reduce computational requirements, a simplified model with hysteretic cross braces was developed. However, this model requires experimental data of full-size tests to calibrate the properties. Here, a technique is developed to allow simplified models of shear walls. The technique only requires the properties of sheathing-to-frame connections. A user-defined nonlinear element in ABAQUS (1998) called NLDIE (NonLinear Discrete Interface Element) was created to simulate the behavior of a shear wall via a numerical integration method. The method is based on the common acknowledgement that a shear wall is designed to mainly resist lateral loads, such as those from earthquakes, wind, etc. Its overall behavior is primarily controlled by its sheathing-to-framing connections. Therefore, any modeling approach for such walls must be driven by the connections.

6.2 Derivation of User- defined Nonlinear Five-Node Wall Element

The five-node element presented herein has advantages compared to the detailed and the simplified cross-braced wall elements. It uses two-node beam elements to simulate the behavior of studs and sill plates, a rigid panel to represent sheathing, and smeared nonlinear stiffness to represent connections. Figure 6-1 shows that the element has only five nodes with a single node at center representing the panel.

The five-node wall element consists of a four-sided rectangular framing system, sheathing, and discrete elements connecting sheathing and framing members. Framing members are modeled using continuous two-node cubic beam elements. Moment resistance is released at

both ends of each vertical framing member to simulate a racking mechanism. Top and bottom sill plates are considered to be continuous plane frame elements. Small rotations are assumed within this Wall Element. The right-hand rule, associated with a Cartesian coordinate system, is applied in the formulation of the finite element.

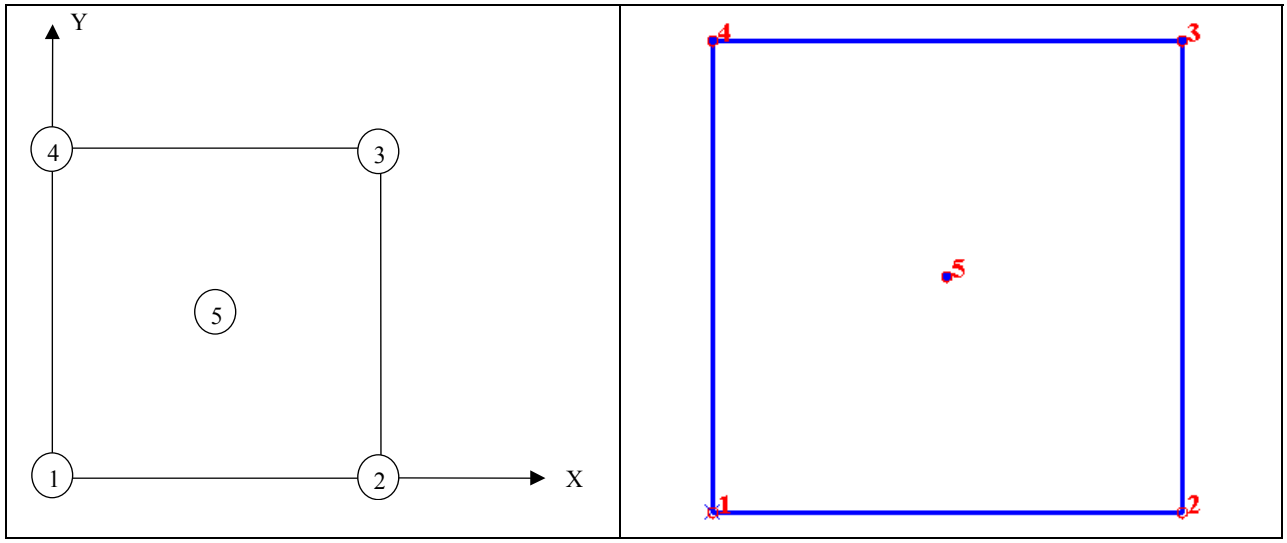

Figure 6-1 - Five Nodes Shear Wall Element in xy local space.

6.2.1 User-Defined Nonlinear Discrete Interface Element (NLDIE)

Nonlinear Discrete Interface Elements are modeled as nonlinear spring elements with three translational d.o.f. in the x, y, and z directions, respectively. It is an isoparametric element. The stretches at any integration point on the wall in the three directions are the differences in displacements at any time between the point on the sheathing and the coincident point before deformation on the framing system. There are five nodes representing the wall system. The middle node represents the sheathing behavior, while the four corner nodes form the framing system. The stiffness of the connectors was formulated by integrating smeared stiffness along

studs. Using the Newton-Cotes method for numerical integration $[K]$ can be numerically evaluated at each integration point along the studs and summed to get the total stiffness of the interface element. A three-integration-point system was used (see Figure 6-2). The smeared stiffness represents the hysteresis behavior of the interface connection. Each node has six d.o.f., so the stiffness matrix of NLDIE is a 30 x 30 matrix.

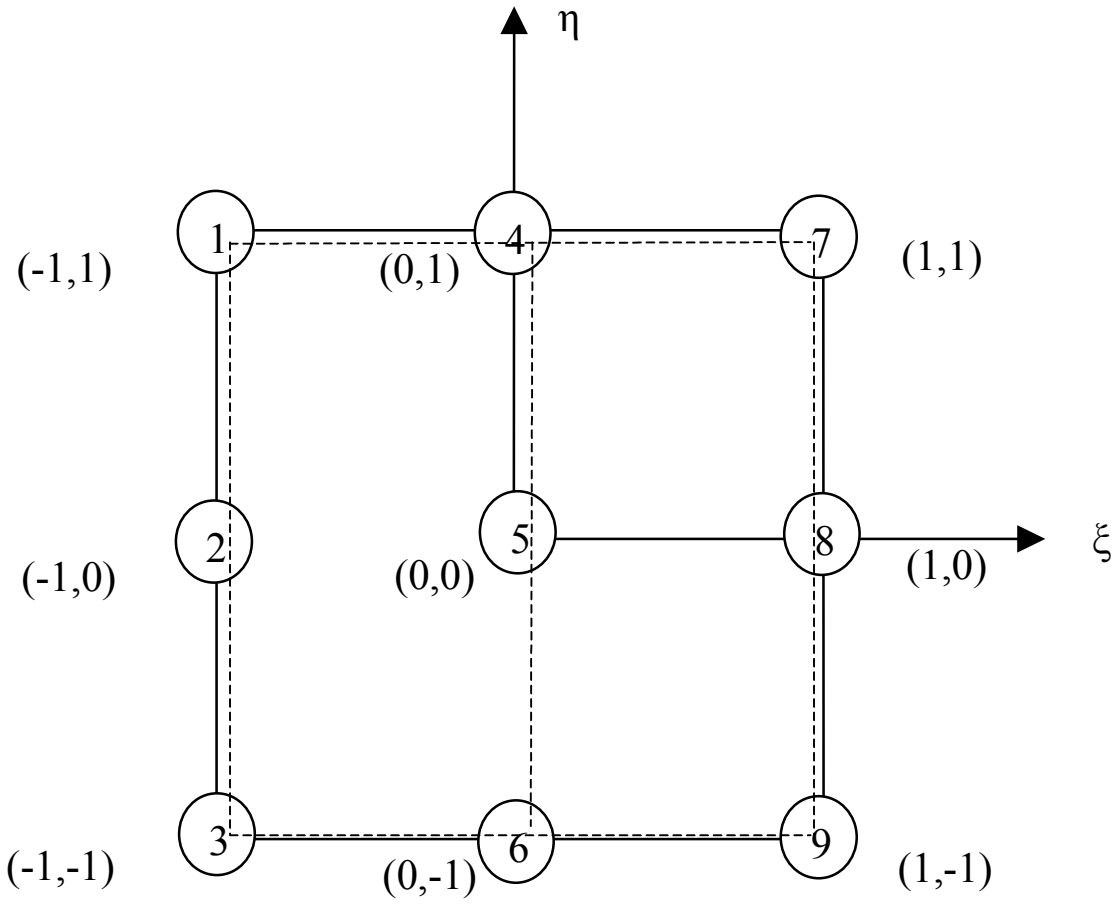

Figure 6-2 – Newton-Cotes Integration Scheme in ξη local space (Dashed lines are lines of integration).

The sheathing panel was assumed to be rigid and restricted to only rotate within the plane of the sheathing itself, with translational d.o.f. in the X and Y directions only. The center point is used to represent the behavior of the sheathing panel. Figure 6-3 shows the rotations of sheathing panel about X, Y, and Z-axis, respectively.

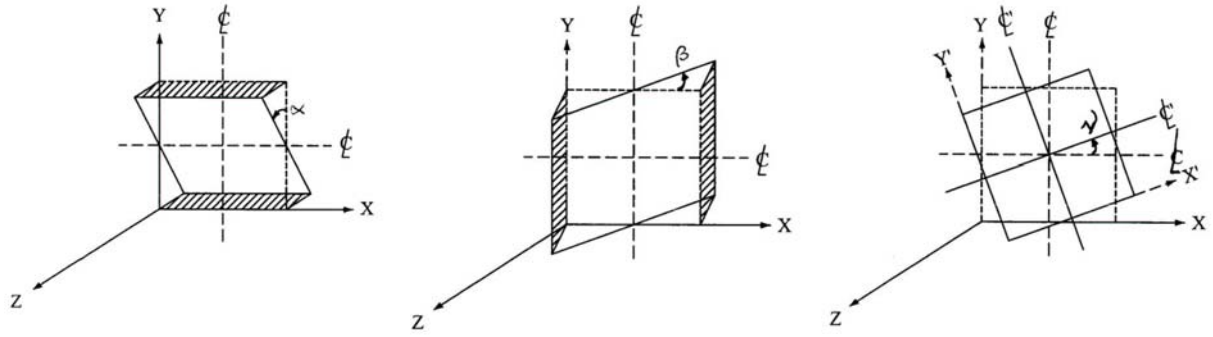

Figure 6-3 – Rotation of the Sheathing Panel

Kinematic relationships are as follows:

$$U_s = U_c - \gamma(y-b) \qquad (6-4)$$

$$V_s = V_c + \gamma(x-a) \qquad (6-5)$$

$$W_s = W_c + \alpha(y-b) - \beta(x-a) \qquad (6-6)$$

$$\xi = \frac{x-a}{a}, \text{ and } x-a = a\xi \quad (-1 \le \xi \le 1) \qquad (6-7)$$

$$\eta = \frac{y-b}{b}, \text{ and } y-b = b\eta \quad (-1 \le \eta \le 1) \qquad (6-8)$$

where U_s, V_s, and W_s = displacements within the panel in the X, Y and Z directions, respectively;

U_c, V_c, and W_c = displacements of sheathing center point in the X, Y and Z directions, respectively;

α, β, γ = rotations of sheathing panel center point;

ξ and η = natural coordinates ($-1 \le \xi \le 1$; $-1 \le \eta \le 1$);

a and b = half the width and height of the wall.

Substituting equations 6-7 and 6-8 into equations 6-4, 6-5 and 6-6 results

$$U_s = U_c - \gamma b \eta \qquad (6-9)$$

$$V_s = V_c + \gamma a \xi \qquad (6-10)$$

$$W_s = W_c + \alpha b \eta - \beta a \xi \qquad (6-11)$$

The Frame system consists of four edge members. Frame elements are used to simulate the members. Each of the nodes at the four corners has six d.o.f. They are three translational and three rotational d.o.fs.

$$U_f = \begin{pmatrix} N_1 & N_2 & N_3 & N_4 \end{pmatrix} \begin{Bmatrix} u_1 \\ u_2 \\ u_3 \\ u_4 \end{Bmatrix} \qquad (6-12)$$

$$V_f = \begin{pmatrix} N_1 & N_2 & N_3 & N_4 \end{pmatrix} \begin{Bmatrix} v_1 \\ v_2 \\ v_3 \\ v_4 \end{Bmatrix} \qquad (6-13)$$

$$W_f = \begin{pmatrix} N_1 & N_2 & N_3 & N_4 \end{pmatrix} \begin{Bmatrix} w_1 \\ w_2 \\ w_3 \\ w_4 \end{Bmatrix} \qquad (6-14)$$

where:

U_f, V_f and W_f = displacements of integration points on the framing system in X, Y, and Z directions.

U_1, u_2, u_3, u_4 = nodal displacements in X-direction.

v_1, v_2, v_3, v_4 = nodal displacements in Y-direction.

w_1, w_2, w_3, w_4 = nodal displacements in Z-direction.

Shape functions N_1, N_2, N_3, and N_4 can be expressed as:

$$\begin{aligned} N_1 &= \frac{(1-\xi)(1-\eta)}{4} \\ N_2 &= \frac{(1+\xi)(1-\eta)}{4} \\ N_3 &= \frac{(1+\xi)(1+\eta)}{4} \\ N_4 &= \frac{(1-\xi)(1+\eta)}{4} \end{aligned} \qquad (6-15)$$

Subtracting the displacements of a point on the sheathing from the displacements of the identical point on the framing system, the stretches in three directions can be expressed as follows:

$$U_n = U_f - U_s = \begin{bmatrix} N_1 & N_2 & N_3 & N_4 \end{bmatrix} \begin{Bmatrix} u_1 \\ u_2 \\ u_3 \\ u_4 \end{Bmatrix} - U_c + \gamma b \eta \qquad (6-16)$$

$$V_n = V_f - V_s = \begin{bmatrix} N_1 & N_2 & N_3 & N_4 \end{bmatrix} \begin{Bmatrix} v_1 \\ v_2 \\ v_3 \\ v_4 \end{Bmatrix} - V_c - \gamma a \xi \qquad (6-17)$$

$$W_n = W_f - W_s = \begin{bmatrix} N_1 & N_2 & N_3 & N_4 \end{bmatrix} \begin{Bmatrix} w_1 \\ w_2 \\ w_3 \\ w_4 \end{Bmatrix} - W_c - \alpha b \eta + \beta a \xi \qquad (6-18)$$

Expanding equations 6-16, 6-17, and 6-18 results in

$$U_n = N_1 u_1 + N_2 u_2 + N_3 u_3 + N_4 u_4 - U_c + \gamma b \eta \qquad (6-19)$$

$$V_n = N_1 v_1 + N_2 v_2 + N_3 v_3 + N_4 v_4 - V_c - \gamma a \xi \qquad (6-20)$$

$$W_n = N_1 w_1 + N_2 w_2 + N_3 w_3 + N_4 w_4 - W_c - \alpha b \eta + \beta a \xi \qquad (6-21)$$

where U_n, V_n, and W_n are stretches at any integration point. Rewriting in matrix form and adding all rotational variables at each corner nodes yield:

$$\begin{Bmatrix} U_n \\ V_n \\ W_n \end{Bmatrix} = B * d \qquad (6-22)$$

Where:

$$[B] = \begin{bmatrix} N1 & 0 & 0 & 0 & 0 & 0 & N2 & 0 & 0 & 0 & 0 & 0 & N3 & 0 & 0 & 0 & 0 & 0 & N4 & 0 & 0 & 0 & 0 & 0 & -1 & 0 & 0 & 0 & 0 & b\eta \\ 0 & N1 & 0 & 0 & 0 & 0 & 0 & N2 & 0 & 0 & 0 & 0 & 0 & N3 & 0 & 0 & 0 & 0 & 0 & N4 & 0 & 0 & 0 & 0 & 0 & -1 & 0 & 0 & 0 & -a\xi \\ 0 & 0 & N1 & 0 & 0 & 0 & 0 & 0 & N2 & 0 & 0 & 0 & 0 & 0 & N3 & 0 & 0 & 0 & 0 & 0 & N4 & 0 & 0 & 0 & 0 & 0 & -1 & -b\eta & a\xi & 0 \end{bmatrix}$$

(6-23)

Here $[B]$ is the stretch - displacement matrix and $\{d\}$ is the nodal displacement vector for the shear wall.

$$\{d\} = \begin{Bmatrix} u_1 \\ v_1 \\ w_1 \\ \theta_{11} \\ \theta_{12} \\ \theta_{13} \\ u_2 \\ v_2 \\ w_2 \\ \theta_{21} \\ \theta_{22} \\ \theta_{23} \\ u_3 \\ v_3 \\ w_3 \\ \theta_{31} \\ \theta_{32} \\ \theta_{33} \\ u_4 \\ v_4 \\ w_4 \\ \theta_{41} \\ \theta_{42} \\ \theta_{43} \\ u_c \\ v_c \\ w_c \\ \alpha \\ \beta \\ \gamma \end{Bmatrix} \qquad (6-24)$$

The element stiffness $[K]$ is defined as:

$$[K]=\int_0^{2b}[B]^T\begin{bmatrix}k_{xi} & 0 & 0\\ 0 & k_{yi} & 0\\ 0 & 0 & k_{zi}\end{bmatrix}[B]dy=\int_{-1}^{1}[B]^T\begin{bmatrix}k_{xi} & 0 & 0\\ 0 & k_{yi} & 0\\ 0 & 0 & k_{zi}\end{bmatrix}[B]Jd\eta \tag{6-25}$$

Using the Newton-Cotes method, $[K]$ can be numerically evaluated at each integration point along the studs and summed to get the total stiffness of the element. Here, [K] is obtained by integrating stiffness at each integration point along three integration lines of connectors, as shown in Figure 6-2. Table 6-1 lists the three integration point values and the corresponding weight factors.

$$[K]=\sum_{i=1}^{n}[B]_i^T\begin{bmatrix}k_{x_i} & 0 & 0\\ 0 & k_{y_i} & 0\\ 0 & 0 & k_{z_i}\end{bmatrix}[B]_i w_i J \tag{6-26}$$

Where, n = total number of integration points along the line of connectors;

i = represents each integration point;

k_{xi}, k_{yi}, k_{zi} = distributed tangent stiffness at each integration point;

w_i = weight factor of each integration point;

J = b, where b is half the height of the wall.

Table 6-1 Newton-Cotes Numerical Integration

Location η_i	-1	0	1
w_i	$\frac{1}{3}$	$\frac{4}{3}$	$\frac{1}{3}$

Figure 6-4 is the flow chart demonstrating the formulation of NLDIE. See Appendix A for procedures for obtaining parameters to define the five-node shear wall model.

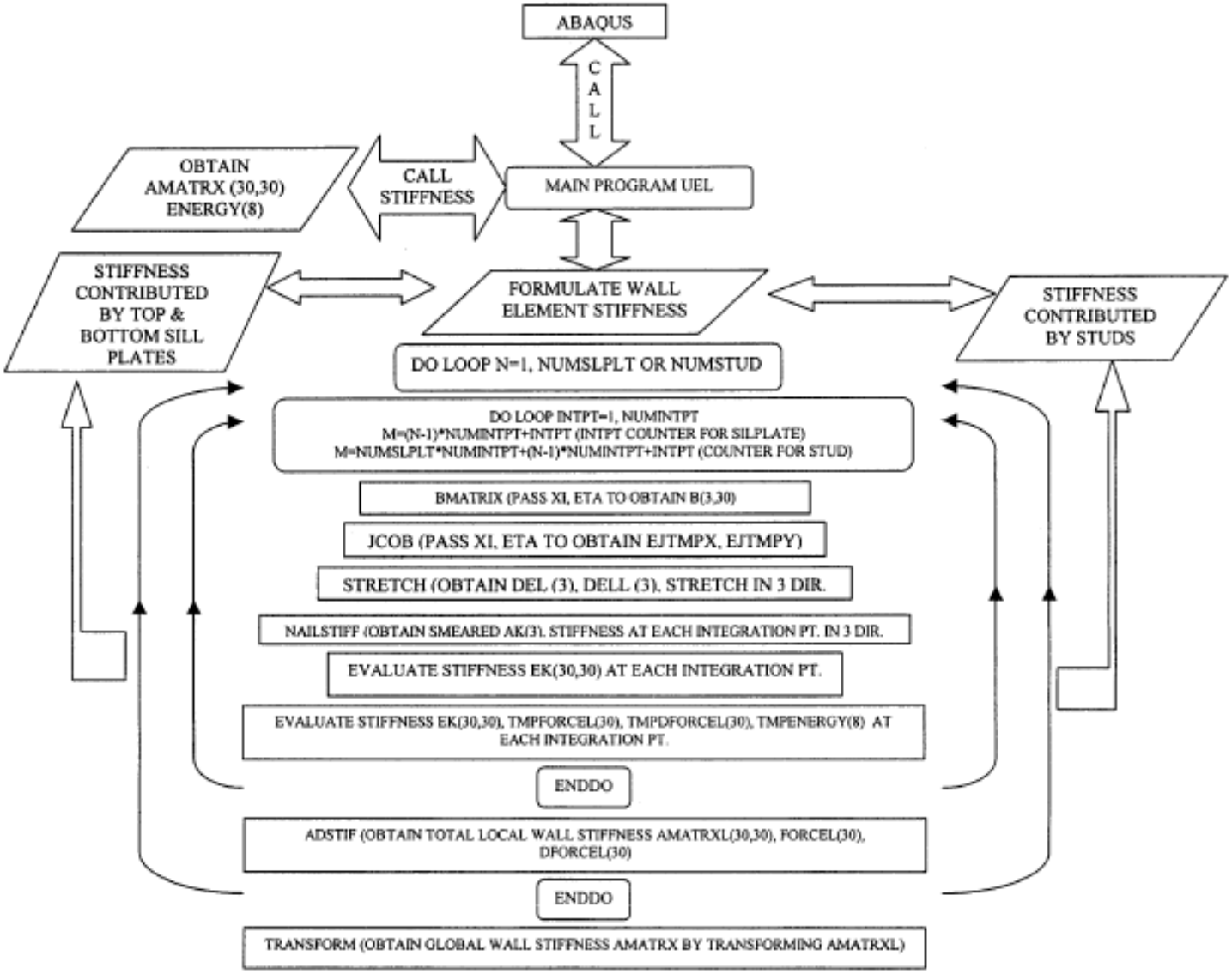

Figure 6-4 – Flow Chart of the Formulation of The NLDIE.

7. Static and Dynamic Response of the Five-Node Wood Frame Shear Wall Model

7.1 Introduction

The general five-node wood shear wall finite element was developed to simulate the behavior of a wood framed shear wall under static and dynamic loads with relatively few degrees of freedom. In order to verify the accuracy of the wall model, static and dynamic simulations were conducted and the results were compared with those of the detailed wall model presented in Chapter 4 and with those of the walls tested by Dolan (1989). Promising results were achieved, given the fact that this model was formulated without calibration procedures. That is, only connector properties and material properties are required to define the model. This data is readily available to engineers and designers.

The element formulation is designed to emphasize the connection properties. Owing to the simplicity of the model, significantly less computer storage is required and significantly less computing time is used when compared to the detailed wall model. Thus, the modeling of complex full-scale houses under different loading conditions is achievable.

7.2 Static Monotonic Response

The static monotonic test protocol is the same as that presented in Figure 4-3 of Chapter 4. Figure 7-1 shows the undeformed shape of the wall with boundary and loading conditions. Transverse load is applied equally to the top nodes while the bottom nodes are constrained against translation. Node 5, which represents the sheathing panel, is constrained against out of plane movement. A comparison of the static monotonic response from the calibrated detailed model presented in Chapter 4, the Five-Node FE Wall Model, and experimental data is shown in

Figure 7-2. The curves have shapes that are quite similar and load capacity levels from the three models are very close. Values of load capacity for the three models are compared in Table 7-1.

The curves show that, initially, the finite element models are both stiffer than the actual wall. At the yield point, the stiffness of the models reduces abruptly, resulting in a close comparison of ultimate strength. The response of the actual wall is smooth, with no definite yield point.

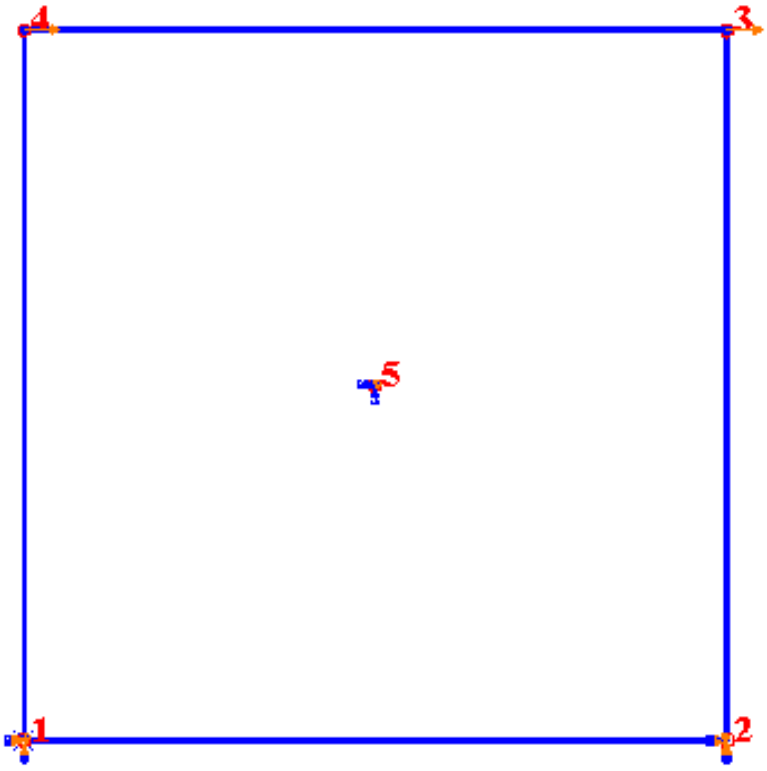

Figure 7-1 – Static Pushover Analysis of the Five-Node Wall Element – Undeformed Shape With Boundary Conditions and Load Shown.

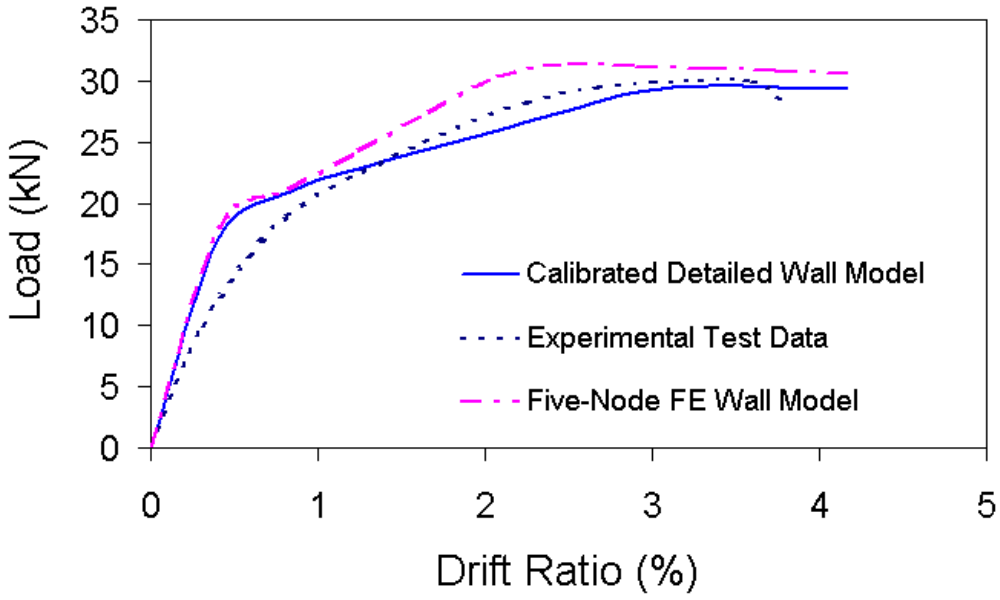

Figure 7-2 – Static Monotonic Response of the Shear Wall without P-Delta Effect: Force vs. Drift Ratio (Experimental test data taken from Dolan (1989)).

Table 7-1 Load Capacity Comparison (Static Monotonic Test)

	Calibrated Detailed Wall Model	Five-Node Wall Mode	Experimental Test (Dolan, 1989)
Load Capacity (kN / lb)	29.6 / 6654.3	31.4 / 7058.5	30.0 / 6744.3

7.3 Static Cyclic Response of the Five-Node Wall Model

The static cyclic test was performed using a similar protocol to the one used in testing the detailed wall model presented in Figure 4-4 (a) of Chapter 4. The hysteresis loops from the Five-

Node model and the calibrated detailed wall model are presented in Figure 7-3 (a). The hysteresis loop from the experiment (Dolan, 1989) is presented in Figure 7-3 (b). The hysteresis loop of the five-node wall model indicates that it resulted in similar load capacity and drift ratio values as those of the detailed wall model and the experiment (Dolan, 1989). The initial stiffness values of both the detailed and the five-node wall models are larger than that from the experiment. This indicates that both the five-node wall model and the detailed wall model have greater initial stiffness in shear than that of the actual shear wall tested by Dolan. This can be seen in static monotonic test shown in Figure 7-2.

The difference in initial stiffness is caused by the procedure of calibration. In order to reach the proper combination of load capacity and drift ratio, three of the seven parameters that define the backbone curve were adjusted. As noted earlier, the finite element models thus exhibit a higher initial stiffness and a much more definite yield point than did the actual wall. However, the initial elastic behavior of shear walls in seismic analysis is of much less importance than other characteristics, such as inelastic characteristics, stiffness degradation, strength degradation, and hysteretic behavior with a pinching zone. The static cyclic result of the five-node wall element reflects all of these properties, as shown in Figure 7-3. Therefore, the five-node model is considered satisfactory in modeling the cyclic behavior of shear walls.

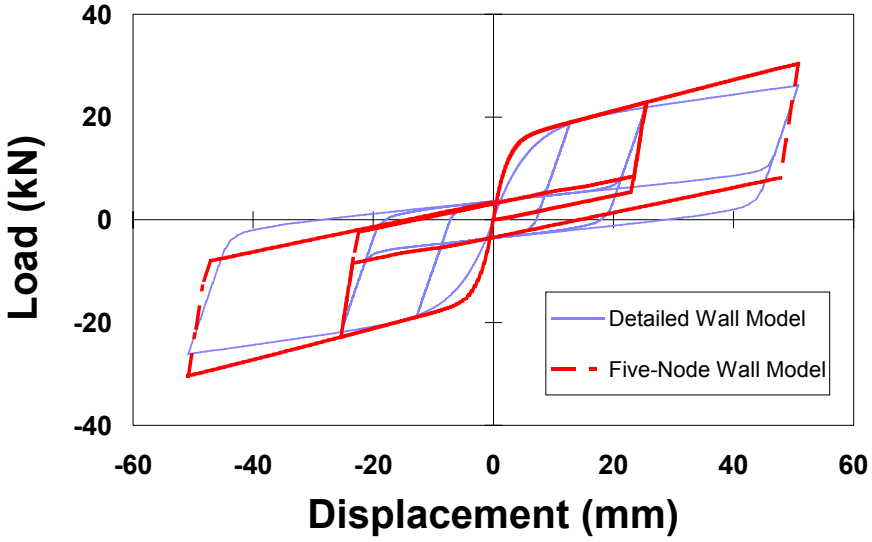

(a)

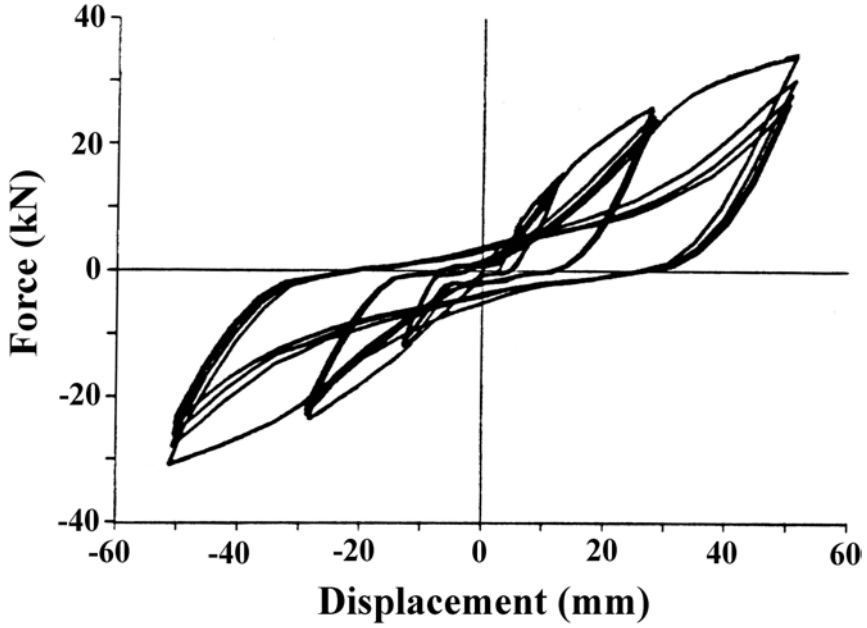

(b)

Figure 7-3 – Static Cyclic Response of the Five-Node Shear Wall: (a) Hysteresis Loop; and (b) Experimental Hysteresis Loop (adapted from Dolan (1989)).

7.4 Dynamic Response of the Five-Node Wall Model

The dynamic analysis was performed by applying the Taft earthquake record to the bottom of the wall. Figure 7- 4 shows the undeformed shape of the five-node shear wall with boundary and loading conditions shown. In addition to mass from self-weight, lumped masses were added to the top two nodes to match the test specimen. The earthquake acceleration record was applied to the bottom two nodes, which were constrained in translational movement.

The Drift Ratio vs. the Base Shear Coefficient loops from the five-node wall model, the detailed calibrated wall model, and the simplified wall model were plotted and shown in Figure 7-5. A comparison was made with the results of the same analysis from the wall models mentioned above. The Taft earthquake record is presented in Figure 4-11 of Chapter 4.

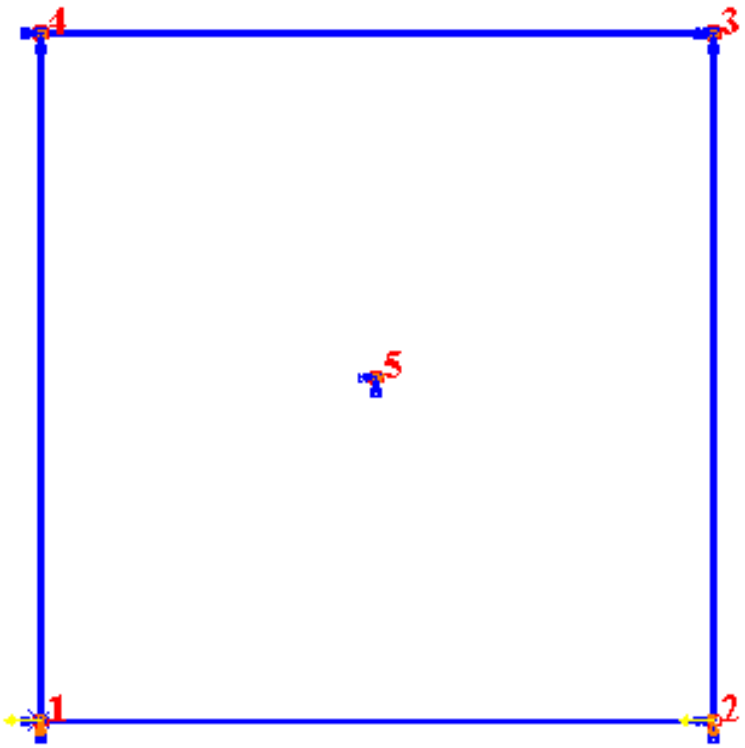

Figure 7-4 –The Undeformed Shape of the Five-Node Shear Wall Model With Boundary and Loading Conditions Shown In Dynamic Analysis.

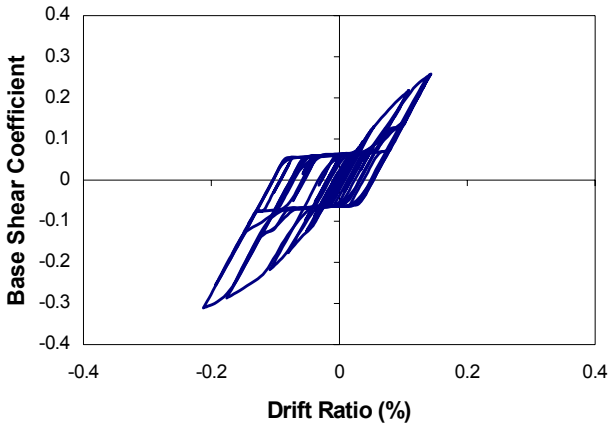

(a)

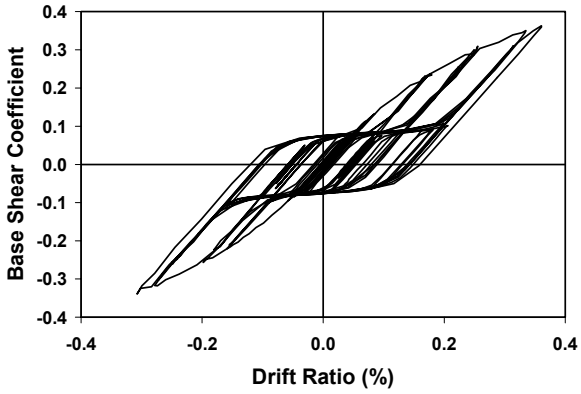

(b)

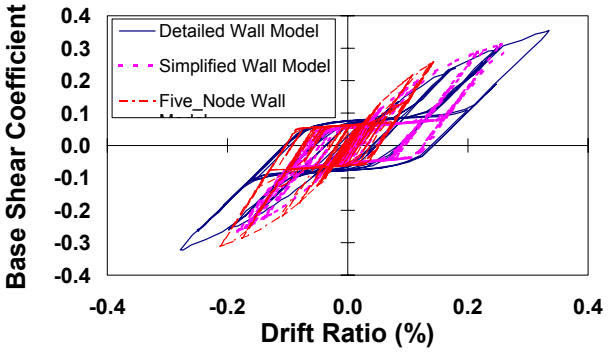

(c)

Figure 7-5- Hysteresis Loop of the Shear Wall Models Subjected to the Taft Record: (a) Five-Node Shear Wall; (b) Calibrated Detailed Shear Wall; (c) Comparison of the Hysteresis Loop of the Three Walls – Detailed, Simplified, and Five-Node Wall Models.

The hysteresis loop of the five-node wall model shown in Figure 7-5 (a) has a shape that is similar to that of the detailed wall model when both were subjected to the Taft record, and the drift ratio levels are reasonably close. The load capacity level is about the same as the detailed wall model in the compression zone, but it has a slightly lower load capacity in the tension zone as compared to the detailed and the simplified wall models. The reason is that the solution failed to converge prior to the final hysteresis loop for the five-node element model.

The weakness in strength of the five-node wall results from the fact that the five-node model only has nine integration points. Each integration point has a significant impact on the integrity of the system as far as strength is concerned. In the detailed wall model, which has 415 nodes and 126 connector elements, however, each connector's failure does not have as significant an impact on the system as that of each integration point in the five-node wall model. Once failure has occurred at an integration point in the five-node wall model, the strength of the wall starts to reduce at a relatively higher rate, leading to a lack of convergence in the nonlinear solution process.

This effect mentioned above is even more apparent in the seismic analysis using the Newhall record, as seen in Figure 7-6. Up to 0.3% of the drift ratio, the shape of hysteretic loops for both the detailed wall model and the five-node wall model were similar and the load capacity was very close. At that point, there was a very large spike in the earthquake (see Figure 4-11 (b)) that caused significant yielding in many connectors. The solution failed for the five-node model (see Figure 7-6 (a)), while that of the detailed model continued for several cycles more (see Figure 7-6 (c)). As mentioned above, once the critical point at the corners of the wall started

degrading in strength, the strength of the entire wall also decreased. Thus, the reason that the difference in drift ratio capacity between the five-node model and the detailed model is so large in this analysis compared to the one using the Taft record is the fact that the Newhall record has a peak acceleration of 0.6g compared to 0.18g for the Taft record. This indicates that the Northridge earthquake is much more intense. To mitigate the apparent abruptness of failure in the five-node element model, the removal of softening in the response could be considered. Such adjustments are items of future research.

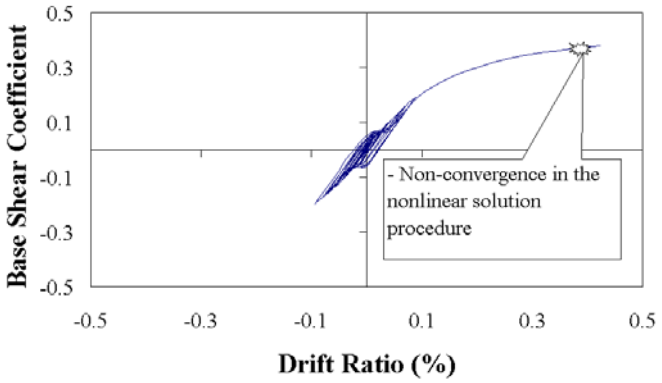

(a) Five-Node Shear Wall Model (up to 0.3% drift ratio)

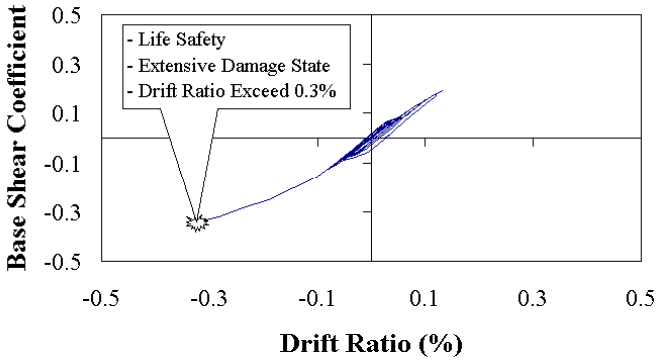

(b) Calibrated Detailed Shear Wall Model (up to 0.3% drift ratio)

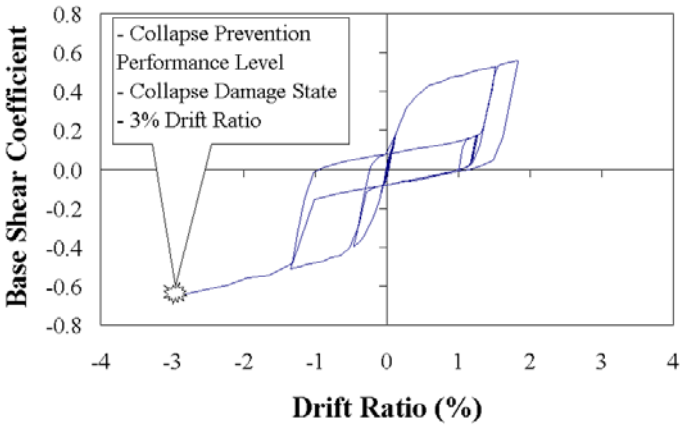

(c) Calibrated Detailed Shear Wall Model (failure occurred)

Figure 7-6 – A comparison of Hysteresis Loops of the Five-Node Model and the Detailed Model Subjected to the Newhall Record.

8. Conclusions and Recommendations

A new finite element shear wall modeling technique was developed. The five-node shear wall model developed using such a technique successfully predicted the load capacity and drift ratio observed in experiments and those resulting from a detailed calibrated shear wall model and a simplified braced wall model presented in this dissertation. The analytical modeling of the wall was developed within the commercially available finite element software, ABAQUS.

An analytical study was performed to evaluate the effect of the addition of viscous fluid dampers on the performance of shear walls and two-story buildings using actual ground motions, scaled to represent both code anticipated ground motion levels and more frequent events. A detailed nonlinear shear wall model and a two-story building model with symmetric and asymmetric configurations were used for cases with and without fluid dampers to evaluate their effect on performance. The study shows significant effectiveness of fluid dampers in dissipating energy, reducing drift, and increasing strength in both shear walls and buildings when subjected to earthquakes. The results from the application of a damper with a damping coefficient of 87.6 kN-s/m (500 lb-s/in) were presented. This type of damper with damping coefficient of 87.6 kN-s/m (500 lb-s/in) was identified as a device that could be readily manufactured.

The results from the above study led to the following conclusions and recommendations:

1. Comparison of the three shear wall models

   In the detailed shear wall model, each sheathing fastener was modeled using an element with pinching and degrading stiffness behavior defined by the modified Stewart-Dolan connector model. Reloading and unloading behavior was assumed to

be linear to facilitate numerical convergence. This detailed model was able to accurately predict the load capacity and stiffness in static monotonic, static cyclic, and nonlinear seismic analyses when compared to experiment. Since a total of 415 nodes were used to define this model, however, the analyses required large amounts of storage and hours of computing time.

The simplified braced shear wall was modeled using double nonlinear hysteretic cross brace elements connecting the diagonals of the wall framing. The nonlinear hysteretic cross brace element, while capturing the hysteresis behavior of the dominant sheathing-to-frame connectors, required experimental data from full-scale shear walls to calibrate the properties of the wall.

The five-node shear wall element has advantages compared to the detailed and the simplified cross-braced wall elements. It was created to simulate the behavior of shear walls via a numerical integration technique for the connectors without the need for experimental data from full-scale shear walls. The total stiffness of the wall contributed by the connections was formulated by integrating smeared stiffness along lines of framing members. A total of five nodes were used to define the element. The hysteretic behavior and the strength of the five-node element in static monotonic, static cyclic, and dynamic tests were in close agreement with the data from experiment and the detailed and simplified braced wall models. Both the static and dynamic analyses required much less computer storage and computing time compared with the detailed model. The fewer degrees of freedom make the modeling of complete structures practical in a reasonable time, with minimal storage requirements.

2. Conclusions on the study of the effectiveness of fluid dampers in light-framed structures.

   Finite element models of a shear wall and a two-story wood structure were used to evaluate the effectiveness of embedded fluid dampers in reducing the structural demand from earthquakes. The models were subjected to two earthquake acceleration records, the 1952 Kern County Earthquake Taft Record, and the 1994 Northridge Earthquake Newhall Record. The Taft record has a peak ground acceleration of 0.18g, and the Newhall record has a peak ground acceleration of 0.60g. The hysteresis loop for analysis of the shear wall element when subjected to the Taft record indicated a reduction in peak drift ratio from approximately 0.35 percent without the damper to 0.15 percent with the damper. The hysteresis loop for analysis of the wall when subjected to the Newhall record indicated a reduction in the peak drift ratio from approximately 4.5 percent without a damper to 0.37 percent with the damper.

   The analysis of the symmetric two-story building subjected to the Newhall record with no dampers yielded failure at a 3 percent drift ratio in the first story and a 0.45 percent drift ratio in the second story. When dampers were installed, the analysis yielded peak drifts of 1.3 percent in the first story and 0.5 percent in the second story. Similar improvements were observed in the asymmetric building.

3. Recommendations and future research

   The shear wall model and the two-story full-scale building used in the analysis consisted of only structural elements. Finishing materials and partitions were not

included in either model. Finishing materials are important in identifying system properties, however. For the analysis of complete structures, including nonstructural components would be necessary to fully quantify the structural response. With the five-node element, structures with nonstructural components, such as partition walls, can be modeled if testing is done to determine the properties.

Practical installation procedures for embedded dampers are difficult to achieve. Thus, a detailed study should be undertaken to determine how realistic it is to install such fluid dampers in shear walls and buildings. Once the hardware and the method for installing the dampers in walls become available, shear walls and three-dimensional buildings with dampers can be built and tested to fully evaluate the effect of the fluid dampers in reducing damage and improving wall performance.

Finally, the five-node element needs to be applied to models of full-scale structures. To determine the best modeling procedures, issues of element size (i.e., mesh density), insertion of openings for doors and windows, ways to model roof and floor diaphragms, application of load and boundary conditions, and others need to be considered carefully. The analytical results should then be compared to full-scale tests.

REFERENCES

ABAQUS (1998). Standard User's Manual (Version 5.8), Hibbitt, Karlsson, and Sorenson, Inc., Pawtucket, RI.

ABAQUS (2001). Viewer User's Manual (Version 6.2). Hibbitt, Karlsson, and Sorenson, Inc., Pawtucket, RI.

Ambrose, J. E. and Vergun, D. (1987). Design For Lateral Forces. John Willey & Sons, Inc.

Bodig, J. and Jayne, B.A. (1993). Mechanics of wood and wood composistes. Jrieger Inc., Pawtucket, RI. Publicshing Co.,Mebourne, Fla.

Chui, Y. H., Ni, C. and Jiang, L. (1998). "Finite – Element Model for Nailed Wood Joints Under Reversed Cyclic Load," *Journal of Structural Engineering*, ASCE. Vol. 124, No.1, 96-103.

Comartin, C.D., Niewiarowski, R.W., Freeman, S.A., and Turner, F.M. (2000). " Seismic retrofit and evaluation of concrete buildings: a practical overview of the ATC 40 document," *Earthquake Spectra*, 16(1), 241-262.

Cook, R. D., Malkus, D.S, and Plesha, M. E. (1989). Concepts And Applications Of Finite Element Analysis. John Wiley & Sons.

CUREE Report No. W-03. (2001). "Woodframe Project Testing and Analysis Literature Reviews," Edited by Andre Filiatrault, Consortium of Universities for Research in Earthquake Engineering, pp. 225-246.

Dinehart, D. W. and Shenton, H. W. III. (1998a). "Comparison of Static and Dynamic Response of Timber Shear Walls," *Journal of Structural Engineering*, ASCE. Vol, 124, No.6, 686-695.

DinehaRT, D.W., Shenton, H.W. III, and Elliott, T.E (1999)."The dynamic response of wood-framed shear walls with viscoelastic dampers," *Earthquake Spectra*, Vol. 15, No. 1, 67-86.

Dinehart, D. W. and Sheaton, H. W. III. (2000). " Model for Dynamic Analysis of Wood Frame Shear Walls," *Journal of Engineering Mechanics*, ASCE. Vol. 126, No.9, 899-908.

Dolan, J.D. (1989). "The Dynamic Response of Timber Shear Walls," Ph.D. Dissertation, University of British Columbia, Vancouver, B.C.

Dolan, J. D. and Madsen, B. (1992). "Monotonic and Cyclic Tests of Timber Shear Walls," *Can. J. Civ. Eng*. 19, 415-422.

Easley, J. T., Foomani, M., and Dodds, R. H. (1982). "Formulas for Wood Shear Walls," *Journal of the Structural Division*, *Proceedings of the American Society of Civil Engineers*, ASCE, Vol. 108, No. ST11, 2460 – 2477.

Filiatrault, A. (1990). "Analytical Predictions of the Seismic Response of Friction Damped Timber Shear Walls," *Earthquake Engineering and Structural Dynamics*, John Wiley & Sons, Ltd. Vol. 19, pp. 259-273.

Filiatraut, A. (1995). "Seismic weaknesses of some residential wood framed buildings: confirmations from the 1994 Northridge earthquake," *Canadian Journal of Civil Engineering,* Vol. 22, 403 – 414.

Filiatraut, A. (1995). "Performance of timber structures during the Hyogo-ken Nanbu earthquake of 17 January 1995," *Canadian Journal of Civil Engineering*, Vol. 23, 652 – 664.

Fischer, D., Filiatrault, A., Folz, B., Uang, C-M. and Seible, F. (2001). "Shake Table Tests of a Two-Story Woodframe House," *CUREE Publication No. W-06*, Consortium of Universities for Research in Earthquake Engineering (CUREE), Richmond, CA.

FEMA (1997). *NEHRP Guidelines for the Seismic Rehabilitation of Buildings*, FEMA Report 273, Federal Emergency Management Agency, Washington, D.C.

Foliente, G. C. (1995) " Hysteresis Modeling of Wood Joints and Structural Systems," *Journal of Structural Engineering*, ASCE. Vol. 121, No. 6. 1013-1022.

Forest Products Laboratory (1987). "Wood Hand Book: Wood as an Engineering Material," Agriculture Handbook No. 72, Forest Service, U.S. Department of Agriculture, Washington, DC.

Gatto, K. and Uang, C-M. (2002). "Cyclic Response of Woodframe Shearwalls: Loading Protocol and Rate of Loading Effects," CUREE Publication No. W-13, Consortium of Universities for Research in Earthquake Engineering (CUREE), Richmond, CA.

Gibson, R. F. (1994). Principles of Composite Material Mechanics. McGraw – Hill, Inc., United States of America.

Gibson, L. and Ashby, M. F. (1988). Cellula solids, structure and properties. Pegamon Press, New York, N.Y.

Groom, K. M. and Leichti, R. J. (1992). "Load-Withdrawal Displacement Characteristics of Nails," *Forest Prod. J*. Forest Products Society, J.43(1): 51- 54.

Groom, K. M. and Leichti, R. J. (1994). " Transforming a Corner of a Light-Frame Wood Structure to a Set of Nonlinear Springs," *Wood and Fiber Science*, The Society of Wood Science and Technology, 26(1), 28-35.

Gupta, A. K. and Kuo, G. P. (1985). " Behavior of Wood-Frames Shear Walls," *Journal of Structural Engineering*, ASCE. Vol. 111, No. 8, 1722-1733.

He, M., Lam, F., and Foschi, R.O. (2001). "Modeling Three –Dimensional Timber Light-Frame Buildings," *Journal of Structural Engineering*, ASCE. Vol. 127, No. 8, 0733-9445.

Kasal, B. and Leichti, R. (1992). "Nonlinear Finite Element Model For Light-Frame Stud Walls," *Journal of Structural Engineering*. ASCE. Vol. 118, No. 11, 3122-3135.

Kasal, B., Leichti, R. J., and Itani, R.Y. (1994). "Nonlinear Finite-element Models of Complete Light-Frame Wood Structures," *Journal of Structural Engineering,* ASCE. Vol. 120, No. 1. 100-119.

McCutcheon, W. J. (1985). "Racking Deformation in Wood Shear Walls," *Journal of Structural Engineering*, ASCE. Vol. 111, No.2, 257-269.

Ni, C., Smith, I., and Chui, Y.H. (1993). "A Simplified Approach for Predicting Response of Nailed Wood Joints to reversed Cyclic Loads," *Canadian Society For Civil Engineering Annual Conference, June 8-11. 375-384.*

Paton-Mallory, M., Cramers, S. M., Smith, F. W., and Pellicane, P. J. (1997). "Nonlinear Material Models For Analysis of Bolted Wood Connections," *Journal of Structural Engineering*, ASCE. Vol. 123, No. 8. 1063-1070.

Shenton III, H. W., and Dinehart, D. W., and Elliott, T. E. (1998). "Stiffness and Energy Degradation of Wood Shear Walls," *Civ. J. Civ. Eng.* 25: 412-423.

Smith, I. (1982). "Failure criteria for timber subjected to complex stress states due to short term loading," *Tmber Res. And Devel. Assn. Res. Rep.3/82, High Wycombe, Bucks.*

Stewart, W.G. (1987). "The Seismic Design of Plywood-Sheathed Shearwalls," Ph.D. Dissertation, University of Canterbury, Christchurch, New Zealand.

Symans, M.D., Cofer, W.F., Fridley, K.J. (2002a). "Base Isolation and Supplemental Damping Systems for Seismic Protection of Wood Structures: Literature Review," *Earthquake Spectra*, EERI, **18**(3), 549-572.

Symans, M.D., Cofer, W.F., Du, Y., and Fridley, K.J. (2002b). "Evaluation of Fluid Dampers for Seismic Energy Dissipation of Woodframe Structures," CUREE Report No. W-20, Consortium of Universities for Research in Earthquake Engineering (CUREE), Richmond, CA.

Tarabia, A. and Itani, R. Y. (1997). "Seismic Response of Light-Frame Wood Buildings," *Journal of Structural Engineering*, ASCE. Vol. 123, No. 11, 1470-1477.

Tuomi, R. L. and McCutcheon, W. J. (1978). " Racking Sterngth of Light-Frame Nailed Walls," *Journal of Structural Engineering*, ASCE. Vol. 104, No. 7. 1131-1140.

Uniform Building Code. (1994). International Conference of Building Officials, Whittier, Calif.

White, M. W. and Dolan, J.D. (1995). " Nonlinear Shear-Wall Analysis," *Journal of Structural Engineering*, ASCE. Vol. 121, No. 11. 1629-1635.

APPENDIX A

A. Procedures for obtaining parameters to define the five-node shear wall model.

Parameters defining the hysteretic loop of connectors are defined in section 3.3.2. These parameters are used herein to define similar values for smeared behavior at each integration point. They are obtained by uniformly distributing the properties of connectors over the length of the integration lines, as defined by connector spacing.

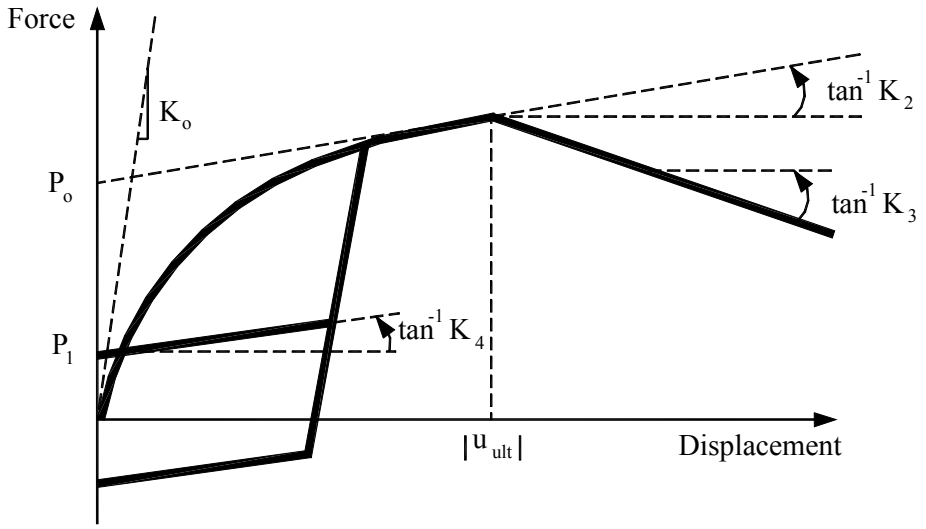

Figure A - 1 - Illustration of sheathing connection parameters defining the monotonic and cyclic load-displacement behavior.

To obtain values of parameters defining properties of integration points, equation (A-1) is used.

$$P_I = \frac{P_C}{s} \times N_{stud} \qquad \text{(A-1)}$$

where: P_I, P_C = parameters defining integration points and sheathing connection, respectively.

s = connector spacing.

N_{stud} = Number of studs within the tributary area of a line of integration.

The following is an example of how to obtain the parameters required to define the five-node shear wall model, given the properties of each sheathing connection.

Step 1: Determine the properties for each sheathing-to-frame connector. Table A-1 lists the values of parameters defining the sheathing connectors used in the analyses of Chapter 4. The sheathing-to-framing-connections consisted of 6.35 cm (2.5 in.) 8d galvanized common nails with field and perimeter nail spacing of 15.24 cm (6 in.). Thus, the connector spacing s in equation A-1 is 15.24 cm (6 in.).

Step 2: Determine the number of studs within the tributary area of a line of integration. There are three integration lines within the panel. For the analyses of Chapter 6, each integration line was equivalent to two lines of studs being placed at a spacing of 40.64 cm (16 in.) on center. Therefore, N_{stud} was given a value of 2.

Step 3: Apply equation A-1 to obtain the values of each parameter defining properties of integration points. Table A-2 lists the values for the analyses of Chapter 7. For example, P_{Io} = P_o/s *N_{stud} = 206 lb / 6.0 in.* 2 = 68.7 lb/in.

Table A -1 - Values of Parameters Defining the Sheathing Connector Model.

P_o	P_1	K_0	K_2	K_3	K_4
915 N (206 lb)	180 N (40 lb)	1320 N/mm (7536 lb/in)	39 N/mm (220lb/in)	-3.0N/mm (-17.1lb/in)	29.5N/mm (168.4lb/in)

Table A -2- Values of Parameters Defining Properties of Integration Points.

P_{Io}	P_{I1}	K_{I0}	K_{I2}	K_{I3}	K_{I4}
12.01 N/mm (68.7 lb/in)	2.33 N/mm (13.3 lb/in)	439 N/mm^2 (2512 lb/in^2)	13 N/mm^2 (73.3 lb/in^2)	-1.0 N/mm^2 (-5.7 lb/in^2)	9.8 N/mm^2 (56.13 lb/in^2)